UNIVERSITA' DEGLI STUDI DI PADOVA IN COLLABORAZIONE CON SAPIENZA UNIVERSITA' DI ROMA

Dipartimento di Ingegneria Industriale DII

Corso di Laurea Magistrale in Energy Engineering

DISTRICT-LEVEL BUILDING DECARBONIZATION THROUGH RENEWABLE TECHNOLOGIES, HEAT PUMP AND ENERGY STORAGE: TECHNo-ECONOMICAL AND ENVIRONMENTAL OPTIMIZATION

Relatore: Prof. Michele De Carli

Ph.D. Miriam Di Matteo

Prof. Andrea Vallati

Simone Gaion 2095669

ACADEMIC YEAR: 2024/2025

Abstract

This master's thesis investigates the technical and environmental optimization of district-scale building decarbonization by integrating renewable technologies, heat pumps, and energy storage. This thesis' work focuses on an archetype of mass housing, where current heating and electricity demand is met by natural gas boilers and grid power. The research starts from detailed building load profiles and implements dynamic energy system models in MATLAB/Simulink. Nine scenarios are considered: a baseline (gas boiler plus grid) and combinations of photovoltaic (PV) or photovoltaic-thermal (PVT) panels with various heating systems (hybrid, air-source, and water-source heat pumps). Key performance indicators—such as renewable fraction, self-consumption, self-sufficiency, primary energy savings, and cost indices—are computed for each scenario. The analysis demonstrates that integrating heat pumps and PV/PVT significantly reduces primary energy use and CO_2 emissions while increasing renewable self-consumption. The thesis provides guidelines for balancing environmental benefits and economic viability in district energy communities, aligning with European decarbonization targets.

Abstract italian version

Questa tesi magistrale esamina l'ottimizzazione tecnica e ambientale della decarbonizzazione di edifici a livello distrettuale tramite l'uso combinato di tecnologie rinnovabili, pompe di calore e sistemi di accumulo. Lo studio esamina un archetipo di edificio di massa, i cui carichi termici ed elettrici sono attualmente soddisfatti da caldaie a gas naturale e rete elettrica nazionale. Il lavoro parte da profili di carico e implementa modelli dinamici energetici in MATLAB/Simulink. Vengono confrontati nove scenari: uno base (caldaia a gas più rete) e combinazioni di pannelli fotovoltaici (PV) o fotovoltaici-termici (PVT) con sistemi di riscaldamento quali pompe di calore ibride, pompe di calore aria-acqua e acqua-acqua. Per ogni scenario si calcolano indicatori di prestazione come frazione rinnovabile, autoconsumo, autosufficienza, risparmio di energia primaria e indici economici. L'analisi mostra che l'integrazione di pompe di calore e di produzione locale (PV/PVT) riduce significativamente il consumo di energia

primaria e le emissioni di CO_2, aumentando l'autoconsumo. La tesi offre raccomandazioni su come bilanciare benefici ambientali ed economici nelle comunità energetiche di distrettuali, in linea con gli obiettivi di decarbonizzazione europei.

Table of contents

I. Chapter I – Introduction

I.1. Worldwide energetic and climatic crisis

The climatic crisis is by now confirmed by strong scientific evidence: the medium global surface temperature raised by more than 1°C with respect to pre-industrial era[1], and 2023 was the warmest year ever registered (+1,2°C with respect to the average of 1951-1980); frequency and intensity of extreme meteorological events (heatwaves, droughts, fires, floods) increased, pointing out the climatic crisis status. This global warming is due to the increase of greenhous gas concentration: in 2024 atmospheric CO2 reached 422,5 ppm (around 50% more than pre industrial levels) [3].

The strong interconnection between climate change, greenhouse gas emissions, and energy consumption lies at the heart of the current environmental crisis. The energy sector, heavily reliant on fossil fuels, is the primary source of anthropogenic CO_2 emissions. As energy demand continues to grow—driven by electrification trends, industrial development, and population growth—the carbon intensity of the global energy mix becomes a crucial factor. Without a structural transformation of energy production and use, the increase in consumption inevitably translates into higher emissions, amplifying global warming and its consequences. Addressing this linkage is therefore essential to formulate effective mitigation strategies and accelerate the transition towards a low-carbon energy system.

The situation is critical from the energetic point of view too. In 2024 the global demand for primary energy rose by 2,2% with respect to the previous year, reaching almost 650 EJ. Most of this growth was driven by the electric demand: +4,3%, much greater than the growth of PIL worldwide, +3,2% [1]. Consequently, the emissions of CO_2 from the energy sector worldwide reached a new historical maximum of 37,8 Gt in 2024: +0,8% with respect to 2023. These peaks of consumptions and emissions, together with the geopolitical uncertainties, for example the european gas crisis starting from 2022, show the fragilities of a system based on fossil fuels.[2]

I.2. Urgency of the decarbonization

The climatic and energetic context outlined requires us to act urgently on decarbonization. IPCC (Intergovernmental Panel on Climate Change) estimates that to have at least a 50% probability of limiting global warming to +1,5°C, the residual budget of CO_2 from 2020 on amounts to only 500 $GtCO_2$ [3]. With the current rate of emissions, this budget would be exhausted within few decades, with serious and irreversible consequences for ecosystems, societies and critical infrastructures. To respect the goals of the Paris Agreement (limiting net warming to 1,5-2°C), it's therefore compulsory to drastically reduce global emissions of greenhouse gases within the next decade.

This necessity reflects on regulatory constraints. In Europe the legislation aims at reducing net emissions by at least 55% within 2030 with respect to 1990 (Green Deal [4]) and to reach climatic neutrality by 2050. The international tendency towards low-carbon energy scenarios consolidates: investments and strategies are increasingly adressing the expansion of renewable energy and energy efficiency. Moreover, decarbonization reinforces energetic security: a european study indicates that thermal renovation and electrification of residential buildings could reduce by 25% the import to UE of russian gas by 2030, saving around 15 billions of euros yearly [5]. In other words, the ecological energy transition is also a strategical lever to reduce dependency from imported fossil fuels and mitigate the risks of energetic shocks.

I.3. The building sector as priority of intervention

The building sector emerges as crucial in the decarbonization process. Globally, the construction industry (including heating/cooling, lighting, appliances and construction materials) emitted around 12 $GtCO_2$. In terms of energy, buildings absorb around 1/3 of global demand: in 2019 the final consumption of energy in buildings reached 128,8 EJ (31% of total consumption) [3].

In Europe the relevance of this sector is even more pronounced. AEA energy states that in 2022 the building sector in UE contributed to around 34% of greenhouse gas emissions related to energy; buildings consume almost 40% of the european total energy. To meet the target of the Green Deal, the Commision assesses that

the sector must reduce its emissions by 60% within 2030 and completely decarbonize within 2050 [5].

Consequently, european policies (Green Deal, Renovation Wave, revision of EPBD) pose great emphasis on the improvement of energy efficiency, electrification of consumptions and use of renewable sources in buildings [5].

The choice of focusing on buildings is furthermore justified by the wide potential of mitigation available. Literature highlights that interventions in the sector (avanced cohibentation, high efficiency heat pumps, integrated solar systems, ecc.) allow significative emission reductions [3]. In Europe, for example, efficiency and decarbonization measures already adopted let the emissions from the building sector decrease by 34% between 2005 and 2022 [1].

Further accelerations – through deep renovations and integrative legislations – are considered essential to reach goals in 2030 and 2050 [6].

In summary, data and studies confirm that the building sector, due to the relevant weight on energy consumption and total emissions, represents a strategical lever for decarbonization. The focus on targeted interventions – from energy efficiency to shifting to low carbon heating – is therefore considered the priority to respect international climatic commitment, grant energy security and increase the global sustainability of the building heritage [7].

I.4. The role of energy communities in this context

Renewable Energy Communities (RECs) represent a powerful strategy for accelerating the decarbonization of buildings at district level. These communities allow groups of citizens, businesses, and public bodies to jointly produce, share, and consume renewable energy within a defined geographical area. Introduced into Italian legislation via the "Milleproroghe" Decree [8] and aligned with the EU RED II directive [9], RECs facilitate the deployment of distributed energy resources (DERs), such as rooftop PV systems and heat pumps, in a cooperative and localized manner.

In this context, RECs contribute to three major goals:

1. Decentralized decarbonization: By promoting local generation and consumption of renewable energy, RECs reduce reliance on fossil fuels and

grid-supplied electricity, thereby cutting CO_2 emissions at neighbourhood scale.

2. Increased energy self-consumption and self-sufficiency: Through smart energy sharing mechanisms, communities can optimize the use of locally produced electricity. For example, surplus energy generated by one building during the day can be consumed by another, avoiding curtailment and enhancing overall system efficiency.
3. Improved integration of renewable technologies: RECs offer an ideal framework for combining various technologies—PV, PVT, HPs, batteries, thermal storage—under a shared infrastructure. This integration not only improves energy autonomy but also ensures better alignment with user demand profiles, especially in mixed-use districts.

Recent studies and pilot projects in Italy and across Europe confirm the effectiveness of RECs in reducing energy consumption and CO_2 emissions. Simulations show that combining PV systems with heat pumps in community-based setups can result in primary energy savings of up to 30–40% and significant reductions in annual emissions [10]. Additionally, economic benefits such as lower energy bills and faster payback periods can be achieved when incentives and net metering are applied.

From a policy perspective, RECs are increasingly supported by national and EU frameworks. They are recognized as essential tools to meet the EU Green Deal's decarbonization targets—at least −55% emissions by 2030 and full climate neutrality by 2050 [11]. Incentive schemes, such as feed-in tariffs for shared energy, tax deductions for renewable installations, and dedicated EU funding (e.g., from the Recovery Plan and PNRR in Italy), further enhance the feasibility of these projects [12].

In summary, RECs enable a paradigm shift from centralized to distributed energy systems. They empower local actors, reduce systemic energy losses, and represent a scalable model for climate-neutral neighbourhoods. Their role is therefore central to the successful electrification and decarbonization of the building stock in line with EU and national goals.

I.5. Literature review

This section provides an analysis of the literature on district energy and heat pump systems, as well as the policy context for building decarbonisation. The following paragraphs analyse the individual technologies and the relevant literature.

In the current years many studies have been conducted to increase localized production and consumption. Shafiei et al. [13] developed a novel multi-objective optimization framework that simulates an IEEE standard electrical test system incorporating multiple load types—including residential, commercial, and industrial consumers—within a local energy system. It simultaneously minimizes power loss, greenhouse gas emissions, and operational costs while maximizing system resilience and flexibility in the presence of renewable energy sources (RES). Integrated RES and BESS reduced total energy generation needs by up to 10.8%. DRPs reduced the daily peak load by 45%, enabling more stable grid operation.

A study conducted by the University of Naples "Parthenope" [14] aimed at evaluating and comparing Power-to-X strategies (specifically Power-to-Heat, Power-to-Gas, and Power-to-Power) to improve the energy efficiency, environmental sustainability, and energy independence of a new renewable energy community in an area with high geothermal potential. Power-to-Power (battery-based) increased self-consumption by 54%. Power-to-Gas enabled energy storage over longer time scales and increased self-consumption by 33%.

Gomes et al. [15] conducted a study focusing on Corvo Island (Azores, Portugal), a small and isolated island, to design and optimize a 100% renewable energy community that ensures complete autonomy by integrating electricity, heating, and freshwater production through renewable sources. The optimized system with solar thermal heating was the most cost-effective solution for achieving complete decarbonization.

Calise et al. [16] focused on a residential district in Naples, Southern Italy, composed of 60 multi-apartment buildings with low thermal insulation and various user types (families, young adults, elderly). The objective of the study was to investigate and compare different layouts of renewable energy communities (RECs) aimed at reducing both electricity and space heating demands, with a focus on integrating district heating networks (DHN) and Power-to-Heat (P2H)

strategies while avoiding major refurbishments inside apartments. The approach demonstrated high profitability and feasibility for existing residential districts without major internal renovations. The innovative REC layout combining DHN and P2H achieved the best results, with a payback period of 2.2 years, Primary Energy Savings equal to 38% and self-consumed electricity increase by 15% compared to the conventional REC

In Los Angeles a high-resolution techno-economic analysis has been conducted regarding four electrification upgrade scenarios at different efficiency levels, focusing on equity implications and energy burden for vulnerable households [17]. Various electric technologies for space and water heating have been considered, including high-efficiency heat pumps. Analyses included capital costs, energy burden, and electricity demand. Major barriers to equitable adoption are high upfront costs, rate structures, and installation challenges (physical and cultural).

Electrified homes enhance demand-side flexibility and integration with DER (Distributed Energy Resources)/microgrids, offering benefits like pre-heating/cooling and thermal storage. Achieving equitable and beneficial electrification requires high-efficiency technologies supported by strong policy and utility actions.

Khosravani et al. [18] analyzed a city-scale building electrification in Salt Lake County, USA, excluding industrial facilities (approximately 380,000 buildings categorized into 10 types), through EnergyPlus, OpenStudio and Homer Pro. The objective was to assess the techno-economic viability of city-scale building electrification integrated with hybrid renewable energy systems (HRESs) by comparing a base case with conventional HVAC to an electrified scenario with heat pumps. Results show that an optimal renewable fraction between 80% and 90% balances CO2 reduction and economic viability; the cost of carbon emission reduction is minimized with renewable fractions between 70% and 85%.

Yang et al. [19] carried out an analysis of a prototype U.S. single-family detached house in four diverse locations: Tampa, FL; San Diego, CA; Denver, CO; and Great Falls, MT.

The goal of the study was to assess the long-term impacts of energy efficiency retrofits (EER) and electrification on decarbonization and household economics (energy burden and payback period) across different climates and with increasing

grid clean energy penetration. Electrification can reduce long-term emissions with increased clean energy but doesn't always guarantee decarbonization due to mismatches between clean energy availability and demand. This suggests that simply switching from fossil fuel heating to electric heating in colder climates, without significant improvements in building efficiency or changes in how electricity is generated and used, could lead to higher costs for homeowners and put more strain on the electricity grid during winter.

The study points out that combining electrification with energy efficiency retrofits can help mitigate some of these negative economic impacts. Additionally, the increasing penetration of clean energy on the grid could eventually lower the carbon emissions associated with this increased electricity demand.

Decarbonizing buildings is now at the core of EU and global climate policy. According to IPCC AR6 report (2022), the global building sector in 2019 accounted for about 12 $GtCO_2e$ (≈21% of world Greenhouse Gases (GHG) and ≈31% of CO_2 emissions) [20]. This underscores that retrofitting and electrifying buildings is critical to meet the Paris goals. The IPCC highlights the growing scientific evidence of the sector's mitigation potential, noting that energy efficiency improvements and electrification (e.g. widespread heat pump adoption) are among the most effective strategies.

On the international front, organizations like the IEA stress that achieving a 1.5 °C trajectory requires very rapid uptake of heat pumps, solar PV, and related technologies. The IEA's Net Zero Roadmap (2023) projects that global electricity demand will rise as heating is electrified and calls for a steep decline in fossil fuels this decade. In essence, if countries fail to scale building electrification and renewables, they cannot meet their net-zero objectives [21].

The EU policy framework has become correspondingly stringent. The recent EPBD recast (Directive EU/2024/1275) decrees that all new buildings must be zero-emission by 2028 (public buildings) and 2030 (other buildings) [22]. A "zero-emission building" is defined as one with no on-site fossil fuel CO_2 emissions and very high performance. This is a major tightening from the prior "nearly zero-energy" standard and is explicitly aligned with the EU's 2050 climate-neutrality goal. Complementary directives (e.g. the revised Energy Efficiency Directive 2023)

also demand deep renovation of existing buildings and integration of renewables [23].

At the governance level, the EU's *Governance Regulation* (2018/1999, updated for the Fit-for-55 package) sets compulsory 2030 targets (e.g. –55% GHG, ≥42.5% renewable energy) and requires member states to align national plans accordingly [24].

In summary, both EU legislation (EPBD, Energy Governance, RED III, etc.) and international assessments (IPCC, IEA) converge on the imperative of building electrification and renewable integration. These policies create the context for any technical solution: district heating networks, heat pumps and PV systems must be evaluated in a scenario of nearly-zero targets and emissions limits.

I.6. Purpose of the work

This thesis aims at evaluating and comparing district-level energy configurations that combine renewable energy production, heat pump technologies and storage systems, focusing on their techno-economic and environmental performance. The goal is to identify solutions that can optimize energy efficiency, reduce greenhouse gas emissions, and increase the energy self-sufficiency of urban areas—particularly within the framework of energy communities.

The core objective is to simulate and assess different energy supply scenarios for a district-level residential building located in Rome. The analysis investigates how various combinations of renewable energy technologies—photovoltaic (PV), photovoltaic-thermal (PVT) panels—and different types of heat pumps (Air Source, Water Source, and Hybrid Heat Pumps) can improve system sustainability. The study also evaluates the role of storage systems (both electrical and thermal) and energy management strategies in enhancing performance and flexibility.

The thesis employs a dynamic modeling approach using MATLAB/Simulink for simulating energy flows under different configurations. These tools allow for detailed, time-resolved simulations that reflect real climatic conditions and use patterns. Nine distinct scenarios are analyzed, ranging from a baseline using a natural gas boiler to advanced configurations that fully integrate renewable energy systems. Key performance indicators (KPIs)—including renewable fraction, self-

consumption, self-sufficiency, primary energy savings, CO_2 emissions, and economic metrics such as Decarbonization Cost and payback time—are used to assess and compare the scenarios.

The analysis highlights trade-offs between environmental and economic performance and identifies optimal configurations for different building types and usage patterns. The outcomes are intended to support policymakers, engineers, and planners in making informed decisions for the energy transition in the building sector. Ultimately, the thesis contributes to the growing body of knowledge on how integrated renewable and electrification technologies can be effectively applied at the community level to achieve decarbonization goals.

I. Chapter II - Technology overview

This section describes the technologies implemented in the configurations.

I.1. Natural Gas Boiler

Traditional NGBs burn natural gas to heat water for heating and disperse their combustion fumes in the environment, leading to thermal loss. Condensing boilers, on the other hand, recover part of this heat by cooling them and condensing the water vapor.

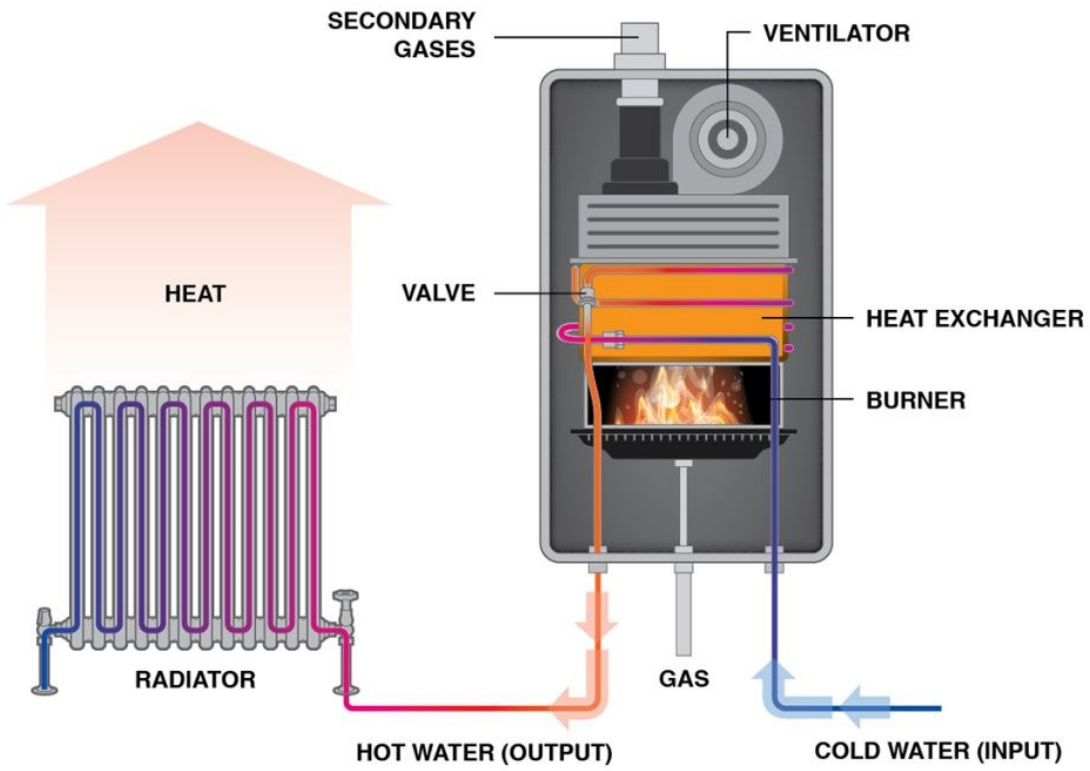

Figure 1: NGB working principle [25]

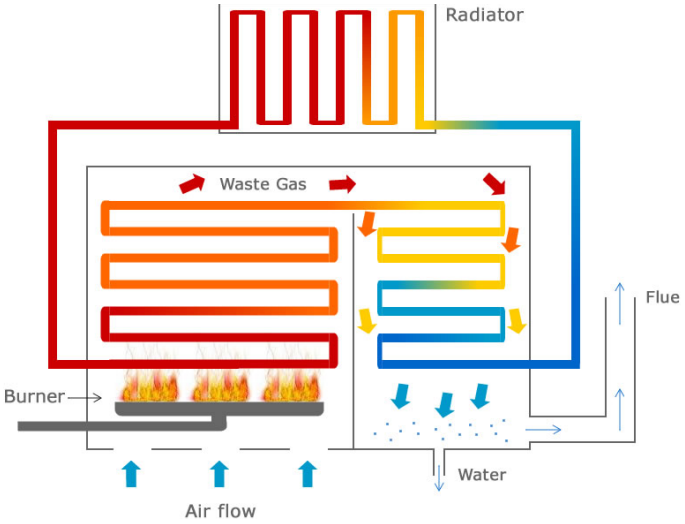

Figure 2: condensing NGB. The condensed particles from the waste gas are collected ("water" in the picture) [26]

This allows for better efficiency, achieving reductions in Natural Gas consumption up to 14% [27].

This is why, in Italy, a 65% detraction of the expenses can be requested when an old heating plant is substituted by a condensing boiler[28]. These are often chosen to work in integration with a Heat Pump (Hybrid Heat Pump) because of their higher thermal efficiency compared with traditional ones, particularly at low temperatures.

The price of Natural Gas has increased in the recent years, especially because of war in Ukraine. Arera [29] states that, in 2022, the price for NGB increased by more than 70% with respect to 2021. This made Natural Gas-powered technologies less competitive than other more efficient alternatives like Heat Pumps.

I.2. Photovoltaic Panel

The PV effect allows to transform solar energy into electrical energy: PV modules are composed of photovoltaic cells, usually made of Silicium, and when radiation hits a cell electrons are excited and they generate a continuous current (DC). This current flows into an inverter and is transformed into alternating current (AC) compatible with the electric grid and domestic or industrial uses. The produced energy can be:

- Self-consumed in real time;
- Stored in batteries;
- Injected into the grid.

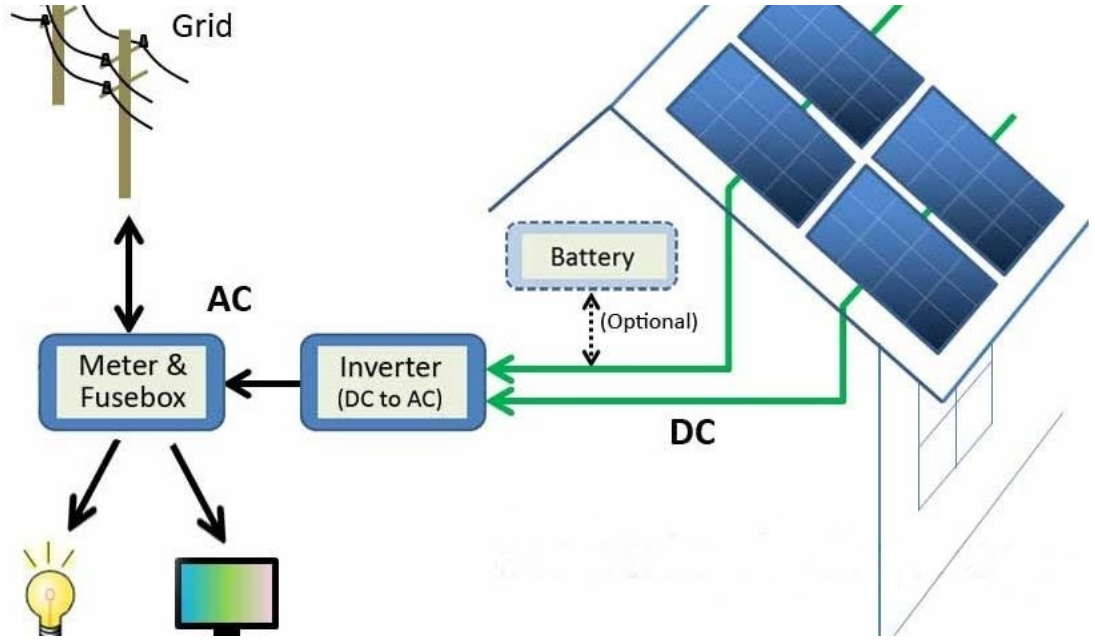

Figure 3: PV system configuration [30]

This is the first technology to be integrated in the model, and it is the most common way to use solar power nowadays thus playing a crucial role in generating clean energy and decreasing carbon emissions. The importance of adressing the growing global demand for power is highlighted by its expected increase by 30 % within 2030 [31]. Solar technologies are foreseen to play a major share in the net-zero emissions scenario [32].

Photovoltaic (PV) technology for electricity generation has become a promising method for electricity generation owing to its increasingly competitive commercial costs . The International Energy Agency Photovoltaic Power Systems (IEA PVPS) states that the worldwide capacity of photovoltaic systems achieved a significant milestone in 2023, reaching 1600 GW [33]. This impressive number underscores the continuous growth and extensive use of PV technology across the globe. It is projected that by 2050, energy generated by PV panels will account for 25% of the total energy production of the world [34].[34].

I.3. Photovoltaic Thermal Panel

The PVT system integrates electric and thermal production into a single collector. It's composed of a photovoltaic module coupled with a heat exchanger on the back side.

During operation:

- Solar radiation is absorbed by the PV panel and generates electricity;
- Part of solar energy is transformed into heat, which would normally cause an increase in the panel temperature and a reduction of its electrical efficiency;
- This heat is recovered through the heat exchanger and is used for heating, DHW or integration with existing thermal systems;
- The thermal recovery cools the PV cells and allows them to better exploit the solar irradiation, increasing the energetic global efficiency;
- The working fluid of the heat exchanger is typically a mixture of water and glycol or propylene, which circulates through embedded channels or serpentine-shaped pipes behind the photovoltaic module.

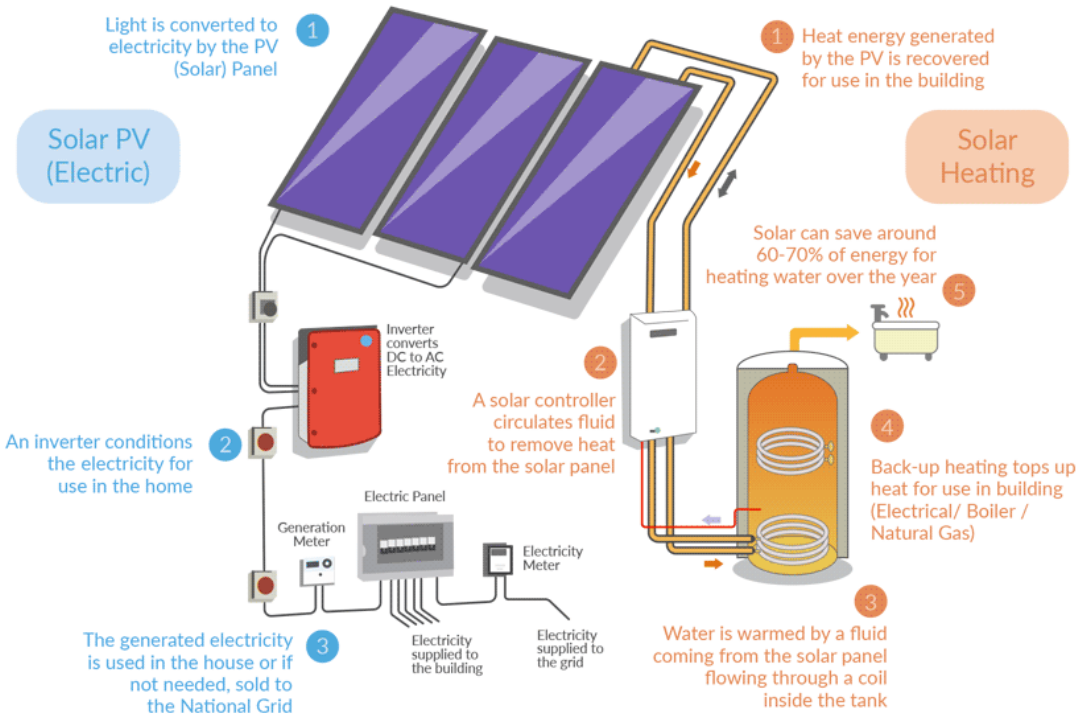

Figure 4: PVT functioning scheme [35]

The integration of energy storage technologies with renewable energy systems is crucial for maximizing the efficient use of solar energy, ensuring a stable and continuous energy supply, and advancing the goal of achieving net-zero energy buildings. Assareh et al. [36] studied the use of Phase Change Materials (PCM), assessing the enormous improvements they could bring to energy systems. Ma et al. [37] studied the modular configuration of PVT systems, which facilitate seamless integration into a diverse array of applications, making them a compelling alternative to conventional solar energy systems. Debbarma et al. [38] analysis covers thermal modeling, energy and exergy considerations about the BIPVT (Building Integrated Photovoltaic Thermal) leading to the determination that the system's maximum thermal efficiency is 53 %. Hamzat et al. [39] focus on the advancement of PV and PVT cooling technology, highlighting the remarkable potential of nanofluids in PVT systems, which can enhance PV thermal efficiency by over 60 %.

I.4.Heat Pumps

Heat Pumps are devices able to transfer heat from a low-temperature source (air, water or the ground) to a high temperature sink by using electricity. The working principle is based on an inverse thermodynamic cycle (usually Carnot cycle or the vapor-compression refrigeration cycle). The system is mainly composed of:

- Evaporator: here the refrigerant fluid absorbs heat from the external source, evaporating;
- Compressor: electrically powered, it compresses the refrigerant increasing temperature and pressure;
- Condenser: the fluid rejects heat to the internal ambient (ie. Building), condensing;
- Expansion valve: reduces pressure and temperature of the refrigerant fluid, closing the cycle.

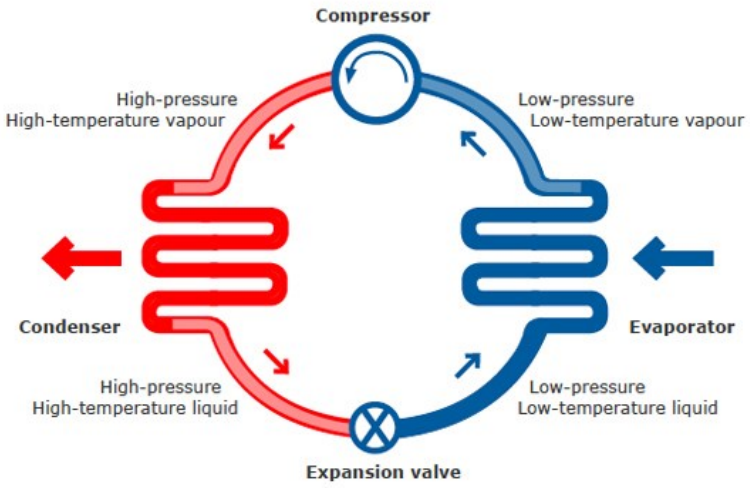

Figure 5: thermodynamic cycle working a heat pump [40]

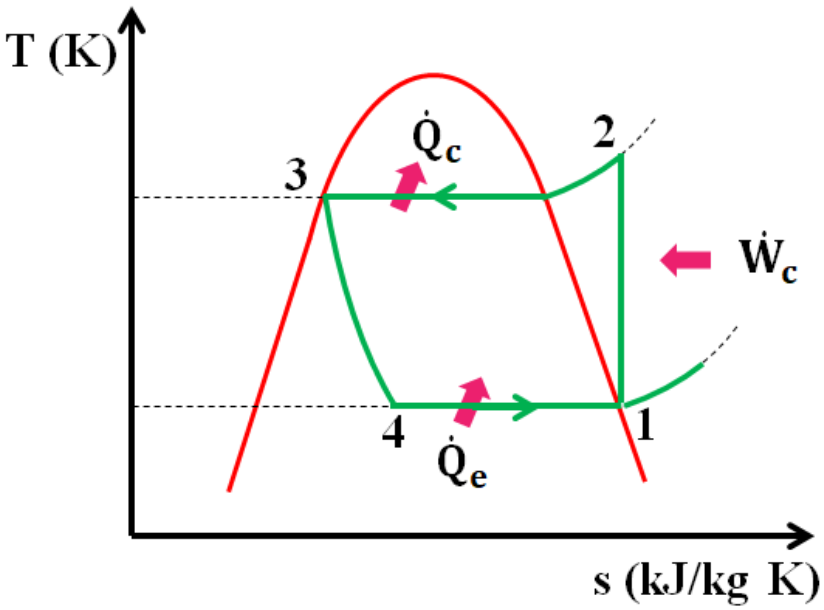

Figure 6: temperature-entropy ideal graph of the thermodynamic cycle in a heat pump [41]

The performance of a heat pump is expressed through the Coefficient of Prestation COP, defined as the ratio of useful heating or cooling provided to work (energy) required. Higher COPs means higher efficiency, lower electricity

consumption and lower operating costs. The COP, especially in heat pumps, exceeds 1 since in addition to just converting work to heat, it pumps additional heat from the source to the sink. Most air conditioners have a COP between 3.5 and 5 [42] indicating that they provide more heating or cooling energy than the electricity consumed and that they are a more cost-effective and environmentally friendly option for conditioning indoor spaces [43].
Almost all new air conditioning units have heating and cooling functions. These units are called reverse cycle units.

An inverter air conditioning system adjusts the speed of the compressor, providing precise cooling or heating as needed. Essentially, it operates as a variable-speed motor, with the inverter controlling the compressor's rotation speed by regulating the frequency and voltage of its power supply. This variable speed compressor makes them very energy efficient.

To make the use of HP significant in the context of heating, Fan Coil (FC) terminal units or radiant floors may be adopted, as they bring a much better efficiency than coupling HPs with radiators would.

Heat pumps are distincted based on their heat source/sink. In this work Hybrid, Air Source and Water Source Heat Pumps were analyzed:

I.4.1. Hybrid Heat Pump

The HHP combines in a single plant a Heat Pump and an NGB, exploiting the advantages of both technologies to grant efficiency, flexibility and continuity of service.

During operation in favorable climatic conditions (external temperatures are moderate), the electric compressor of the Heat Pump covers the thermal load, offering great efficiency thanks to the high Coefficient of Performance. When external air temperature decreases under a certain limit or when thermal loads increase (ie. high-temperature demand), the NGB starts working, alternated or simultaneously with the HP

The system can be managed by a smart control system, which chooses real-time the most convenient source based on:

- The istantaneous efficiency of each generator;

- Price of electricity and gas;
- Climatic conditions;
- User needs.

It may be fit especially for regions with significant seasonal temperature variations.

Being able to switch to gas boiler mode when HP efficiency drops, under optimal conditions HHP demonstrates better seasonal performance than monovalent heat pumps [44]. Bagarella et al. [45] carried out an annual simulation and an energy-economic analysis of hybrid heat pump systems for residential buildings. The maximum *SPF* of the on–off system was obtained with the heat pump unit sized to satisfy between 59% and 72% of the building peak load, which allows to meet about 95%–98% of the annual heating demand.

Nicoletti et al. [46] studied the optimized strategy for hybrid systems with heat pumps, boilers, PV and battery storage. Results indicate up to 19% cost savings in colder cities, a 12% reduction in CO_2 emissions, and a 3% decrease in primary energy consumption. This approach holds significant potential for enhancing the integration of renewable energy sources, contributing to long-term sustainability goals.

I.4.2. Air Source Heat Pump

Air-source heat pumps are innovative and energy-efficient systems used for both cooling and heating in residential and commercial buildings.

Air is inexhaustible and not limited by geographical conditions, so, compared to other heat pumps, it has obvious advantages and broad development prospects. The efficiency of these systems depends highly on the external air temperature.

In heating mode, air-source heat pumps draw heat from the outside air, even in cold climates, using a refrigerant that remains effective at low temperatures. The refrigerant absorbs heat from the outdoor air and, through compression, its temperature increases. This heat is then released inside the building, warming the indoor space. In cooling mode, the process is reversed, and air-source heat pumps function similarly to traditional air conditioners: they absorb heat from the indoor air, releasing it to outdoor air through a refrigeration cycle. The refrigerant, in a gaseous state, absorbs heat from the indoor air as it evaporates into a low-

pressure, low-temperature vapor. The vapor is then compressed, increasing its temperature and pressure, and this heat is expelled to the outside environment as the refrigerant condenses back into a liquid state [47] .

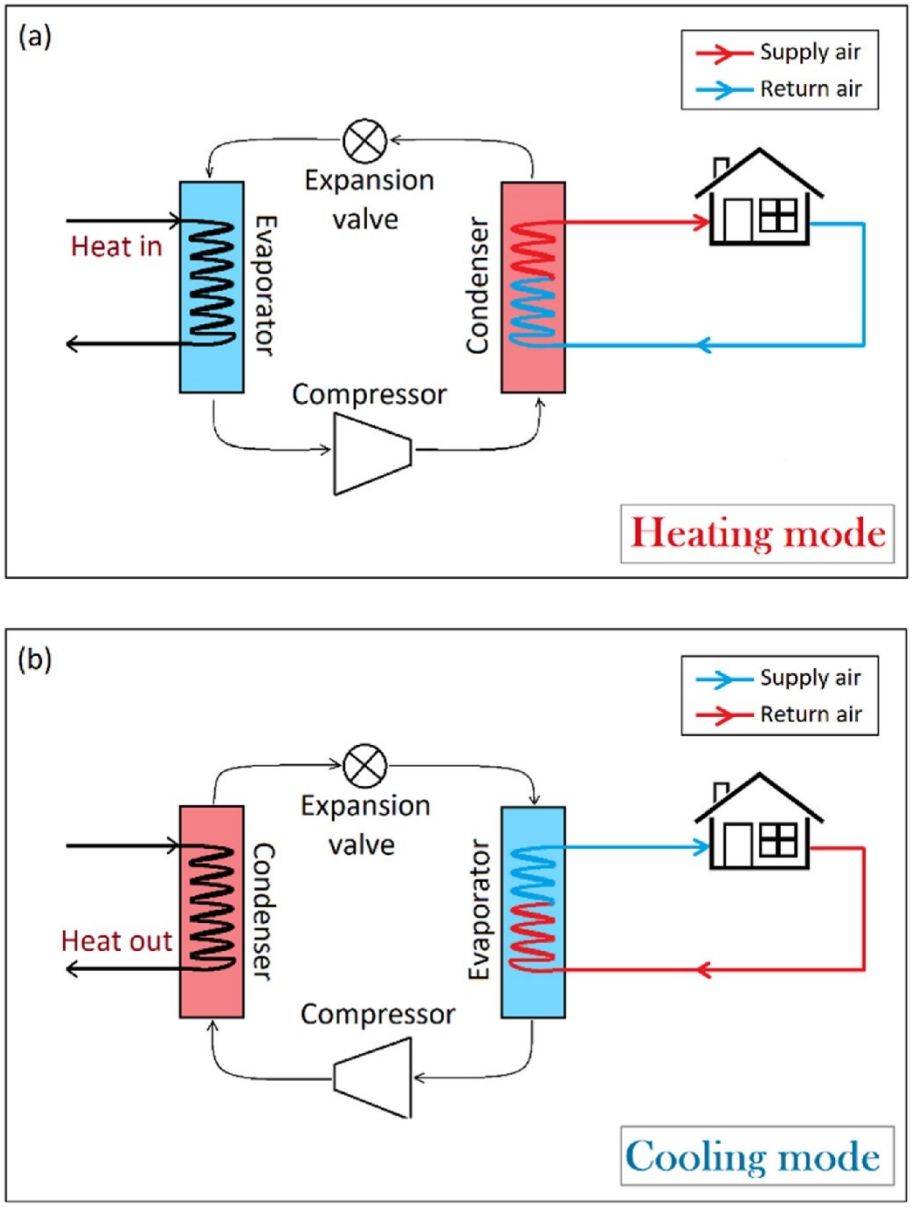

Figure 7 a): air source heat pump in cooling mode. b: air source heat pump in heating mode [48]

Overall, air-source heat pumps offer a promising solution for sustainable and efficient indoor climate control, combining cooling and heating functions to create a comfortable environment [49].

Li et al. [50] analyzed the performance of ASHPs in more than 270 cities in China, with a focus on extreme temperatures and different altitudes, to explore their

potential to curb carbon emissions in the context of fluctuating carbon emission factors for electricity. ASHPs have demonstrated significant benefits as a low-carbon heating solution in specific regions and are increasingly compatible with the evolving green grid adapting well to different environments.

Bae et al.'s [51] study devised an integrated PVT–air source heat pump (ASHP) system that allows installation in a limited space and reduces the initial cost. Particularly, a real-scale experimental plant was constructed based on a small-scale building to evaluate the performance of the PVT–ASHP system. The average heating and cooling COPs of the PVT–ASHP system were 3.54 and 3.31 respectively, increasing by approximately 52% compared to the ASHP. The PVT module could offset approximately 18% in winter and 27% in summer of the total power consumption of the PVT–ASHP system.

Carella et al.[52] propose the replacement of existing boilers for heating and domestic hot water (DHW) production systems, with air / water heat pumps, as an intervention to improve urban air quality. The researchers analyzed the replacement scenarios, within the entire residential building stock in the Municipality of Rome. Results showed a reduction of total primary energy demand by 26% and CO2 emission by 30%. The authors found out that a storage system is a key to smooth down the load volatility introduced by the air-water HPs. The replacement would eliminate the individual localized emission sources, concentrating the emissions at a thermoelectric plant, located in peripheral areas, characterized by the highest generation efficiency and equipped with pollutant abatement systems.

Wang et al. [53] investigated the operational performance of a solar coupled air source heat pump heating system integrated with two-stage phase change heat storage in severe cold regions. By comparing heating systems with different structures, it was found that preheating outdoor air with two-stage phase change heat storage devices in severe cold regions can improve COP of the air source heat pump and reduce system energy consumption.

By optimizing system parameters and leveraging staged heat storage, the system maximizes solar energy utilization while minimizing reliance on auxiliary heating sources.

Although Water Source Heat Pumps (WSHP) and Solar-Assisted Heat Pumps (SAHP) were considered of high interest during the initial literature review phase, they were not implemented in the present work. These technologies were thoroughly examined to inform the development of the study; however, their integration into the simulation model was ultimately excluded in order to maintain computational feasibility.

I.4.3. Water Source Heat Pump

WSHPs exploit thermal energy from groundwater: an aspiration unit pumps water from an extraction sink and exchanges heat which is used for heating/cooling (thanks to the fixed groundwater temperature) or DHW. Then, water returns to the ground and the cycle starts again.The quantity and quality of groundwater must be controlled; the annual medium groundwater temperature is 10°C, granting maximum efficiency to HPs.

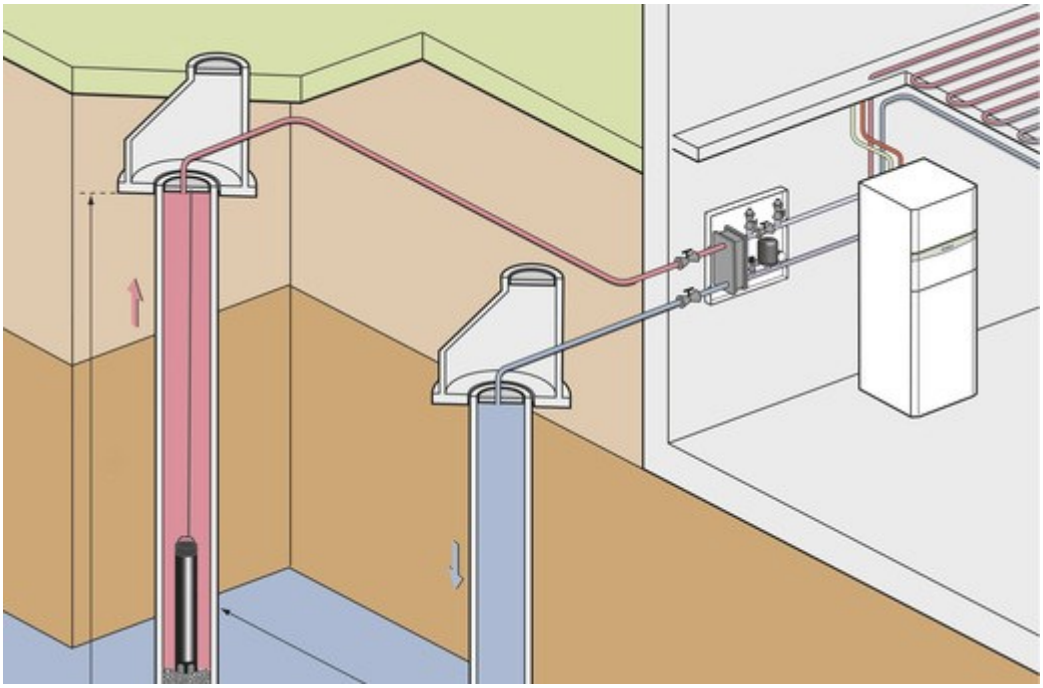

Figure 8: water source heat pump coupled with radiant floor [54]

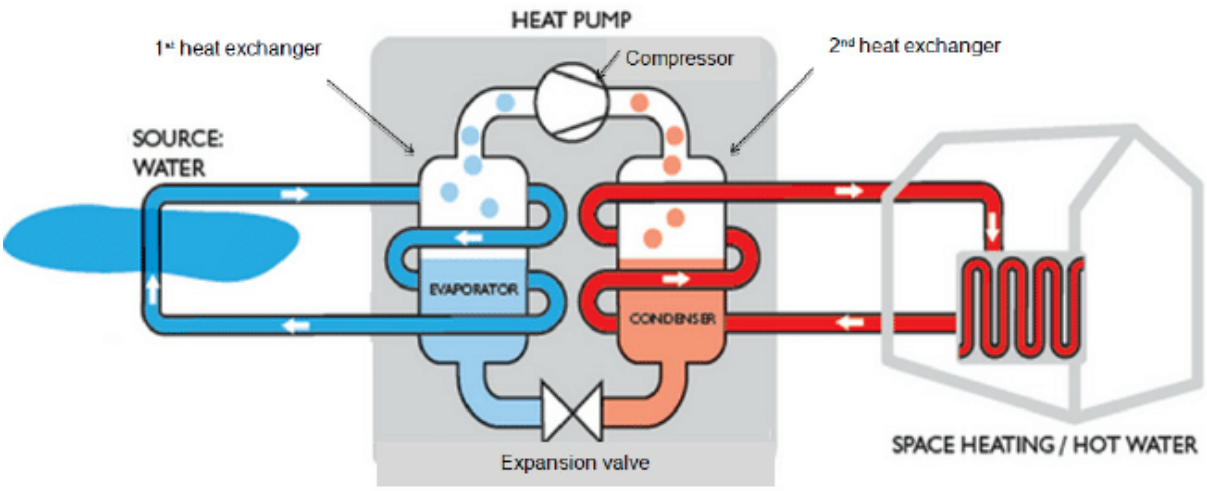

Figure 9: water source heat pump coupled with radiators [55]

The working fluid inside the HP can exchange heat with water for DHW or with water+glycole for heating.

The energy performance is constant and better than air-source, but the availability is variable. Wells are needed for injection and production and regulatory constraints must be met.

Shin et al. [56] examined a Surface Water Source Heat Pump (SWHP) system which works by recovering the solar energy stored naturally in river water, open water or the sea. The study proposed and evaluated optimal partial-load operation strategies for SWHPs integrated with TESs to enhance energy efficiency and reduce operating costs in large office buildings. TES-based strategies exhibit superior cooling performance in large office buildings.

The optimized strategy reduces operating costs by 16.8% over the full-load strategy.

Recent studies emphasize ambient-temperature loop systems, where a near-ambient water network links multiple buildings with individual water-source heat pumps (WSHP). For example, an NREL analysis notes that district loops allow sharing of a high-cost thermal resource (e.g. a geothermal borehole field) across many users, reducing each user's costs and energy bills [57]. Early deployments (e.g. Whisper Valley, USA [58]) and designs (e.g. GreenSCIES in London [59]) leverage low-grade water loops and heat pumps in each building. The London New River GreenSCIES project alone is projected to supply >10,000 residents (3,500

homes + schools/businesses) with low-carbon heat, saving ~5,000 tCO_2/year and reducing emissions by up to 80% versus conventional heating [60]. Such systems boost self-sufficiency by exchanging thermal energy among heating and cooling loads via bidirectional warm/cold pipes

The Queen's Quay (Clydebank, Scotland) development is Europe's largest industrial-scale river-source district heating systems. It will use two 2.6 MW WSHP units drawing heat from the River Clyde to serve a new housing estate, college, and local businesses. This project is expected to cut the local carbon footprint by roughly 60% compared to gas boilers [61]. In the design, a thermal storage absorbs excess WSHP heat for later use, and gas boilers provide peaking capacity: since the boilers run only ~25 hours/year, for the larger amount of the time the system will produce no local carbon [62]. This case highlights how a WSHP-based district scheme can dramatically decarbonize heating even when backup is mantained for rare peaks.

I.4.4. Solar-Assisted Heat Pumps (SAHP)

Although not directly simulated in this study, SAHPs represent an interesting variant of heat pump systems, particularly relevant in climates with high solar irradiance, such as Rome.

Solar-assisted heat pumps (SAHP) can operate using either direct expansion (DX) or indirect expansion. In a direct expansion system, the refrigerant flows directly through the solar thermal (or hybrid) collector, which acts as the evaporator of the heat pump.

Essentially, the solar collector becomes an integral part of the refrigeration cycle, with the refrigerant evaporating inside it due to solar heat. In contrast, in an indirect system, a heat transfer fluid (typically water or a water-glycol mixture) absorbs heat from the solar collector and delivers it to the heat pump's standard evaporator. Here, the solar collector acts as a hydraulic heat exchanger, while the actual evaporator remains within the heat pump unit.

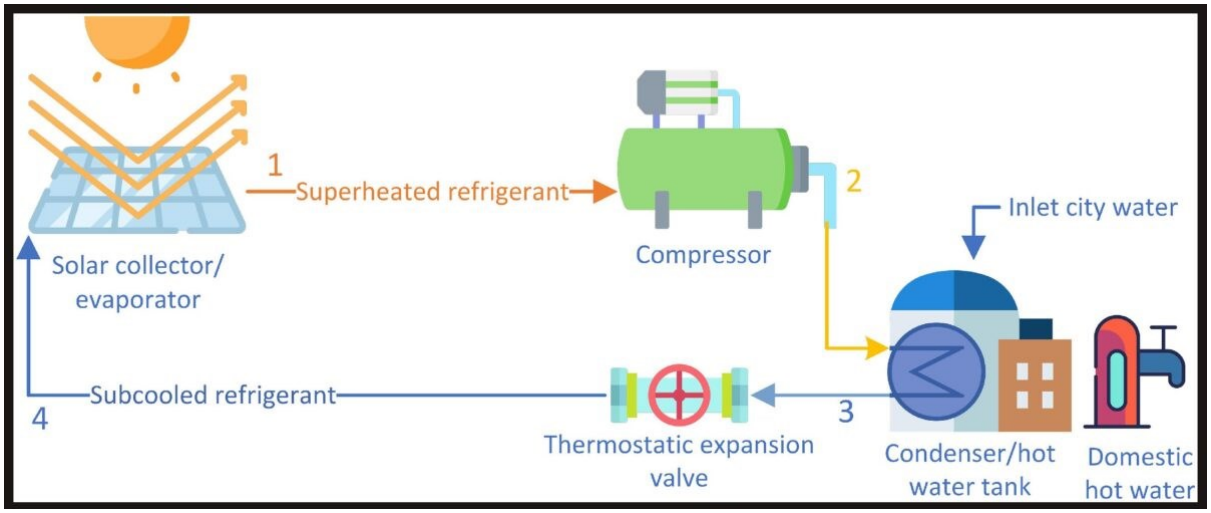

Figure 10: direct expansion Solar Assisted Heat Pump [63]

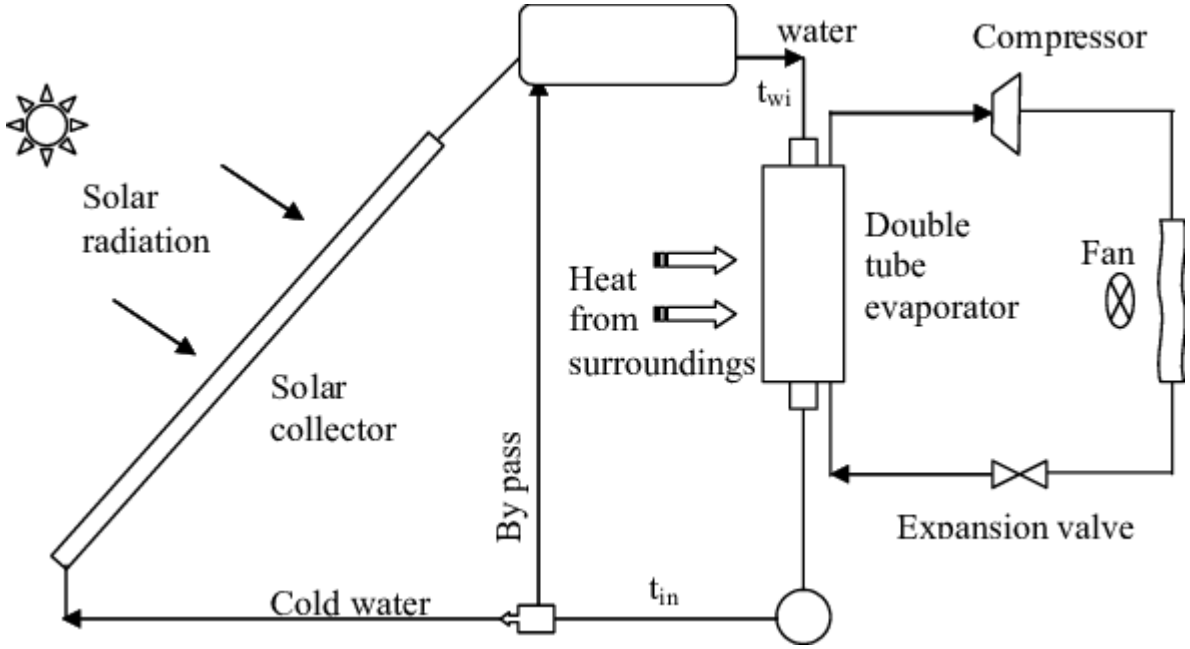

Figure 11: indirect expansion Solar Assisted Heat Pump [64]

This difference affects thermal efficiency, system complexity, and typical applications. Direct expansion systems usually achieve more efficient heat transfer, as they eliminate the intermediate heat exchange with the secondary fluid. As a result, they generally achieve a higher COP, thanks to uniform collector temperature and the absence of intermediate thermal losses. Recent studies confirm that integrating the refrigerant directly into the solar collector improves overall system performance compared to the indirect layout. However, direct

expansion systems are more technically demanding: they require specialized collectors (e.g., refrigerant-based or hybrid PVT panels) and a sealed refrigerant loop, involving more careful design considerations. On the other hand, indirect expansion systems use conventional hydraulic solar collectors and a water circuit with additional pumps and heat exchangers. This simplifies implementation in existing installations (e.g., integration with storage tanks or boilers), but slightly reduces efficiency due to the added heat exchange step.

This distinction between direct and indirect expansion applies to all types of heat pumps, not just SAHPs. In general, direct expansion systems deliver better performance when the thermal source (air, ground, or solar) is utilized without intermediaries. Conversely, indirect systems are more versatile and easier to integrate into existing hydraulic systems, at the cost of a slight drop in performance.

In summary, the choice between direct and indirect expansion involves a trade-off between efficiency and system complexity: direct expansion aims for maximum COP with dedicated components, while indirect expansion offers more flexible implementation at the cost of a slight efficiency penalty.

II. Chapter III – Methodology

This chapter has described the scenarios analysed and the methodology adopted for this purpose. It has also described the KPIs selected for this analysis and the mathematical models implemented in the Simulink environment.

II.1. Object of study

The main goal of this work is to evaluate and optimize the behaviour of a district-level building from the energetic, environmental and economic point of view, focusing on self-sufficiency and self-consumption, thus reducing the environmental impact.

The condominium is hypothesized by employing representative building archetypes derived from the Urbem dataset. The simulation considers a residential building modeled in Simulink to reflect energy demand patterns and construction characteristics.

The residential building considered in this study is located in the Tor Bella Monaca district of Rome, an emblematic example of Italian mass housing developed between the 1960s and 1980s under Law 167/62 and the PEEP program (Piani di Edilizia Economica e Popolare). The building typology is characterized by high residential density and standardized construction methods typical of post-war urban planning paradigms.

The specific case analyzed is the R5 linear multi-storey block, comprising approximately 1,266 apartments, with a net floor area of 93,331 m^2. The average wall transmittance (U-value) is 0.665 W/m^2K. The building is part of a larger megastructure originally designed to accommodate up to 27,000 residents.

The building archetype used in this study was developed by Vallati et al.[65], who conducted a comprehensive data-driven process to construct a representative model of Italian public housing. This process included:

- On-site measurements (e.g., wall heat transfer via TESTO 635-2 sensors),
- Energy audits (thermal and electrical load profiles, occupancy patterns),

- Document reviews and site surveys to collect architectural and mechanical data,
- Statistical analysis, including regression and cluster analysis, to identify the most recurring design and energy characteristics among similar buildings.

Based on these steps, a validated archetype was created and compared with the TABULA model, demonstrating higher energy efficiency due to more detailed characterization of energy systems and user behavior. The archetype was modeled using UMI (Urban Modeling Interface), and energy loads were simulated at the hourly level. The data were exported per service type (e.g., heating, electricity), with an average simulation error of less than 4.7%, making the results robust and reliable.

A 3D model of the district was developed using GIS, Rhinoceros, and Grasshopper scripts to extrude building volumes and apply energy-related templates across the area.

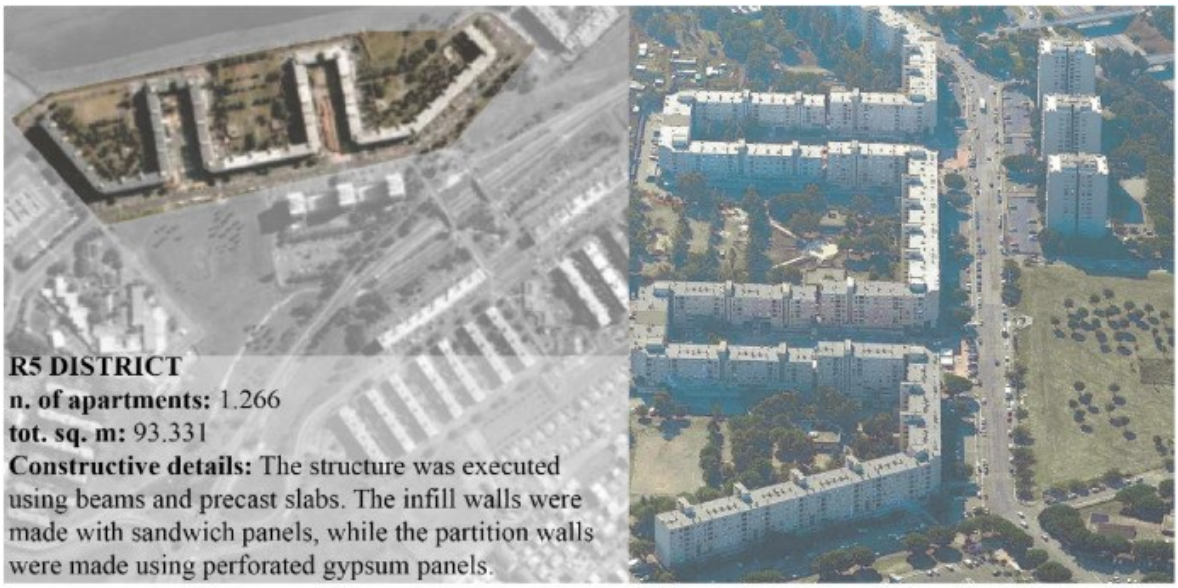

Figure 12: the R5 district in the Tor Bella Monaca district [65]

It is important to highlight that the data collection, archetype development, and validation work—including the use of UMI, GIS, and Grasshopper—were conducted by Vallati et al. as part of the referenced research. In this thesis, the validated archetype and its datasets were used as a basis for Simulink-based simulations, focusing on evaluating different energy system configurations.

II.2. Scenario descriptions

To assess the impact of different heating technologies on energy efficiency and sustainability, the scenarios are categorized into four groups, arranged by increasing technological complexity.

Scenario S0 represents the baseline, relying solely on a traditional Natural Gas Boiler (NGB), while scenarios S1, S2, and S3 explore progressively more advanced systems that combine the NGB with renewable thermal energy sources: S0: Natural Gas Boiler (NGB), S1: Hybrid Heat Pump (HHP), combining a heat pump and NGB in an integrated system and S2: Air Source Heat Pump (ASHP), using ambient air as a renewable heat source

These configurations allow for a comparative analysis of performance, environmental impact, and compatibility with decarbonization goals.

The scenarios are formed as a combination between these different heat sources and the adoption of PV/PVT systems.

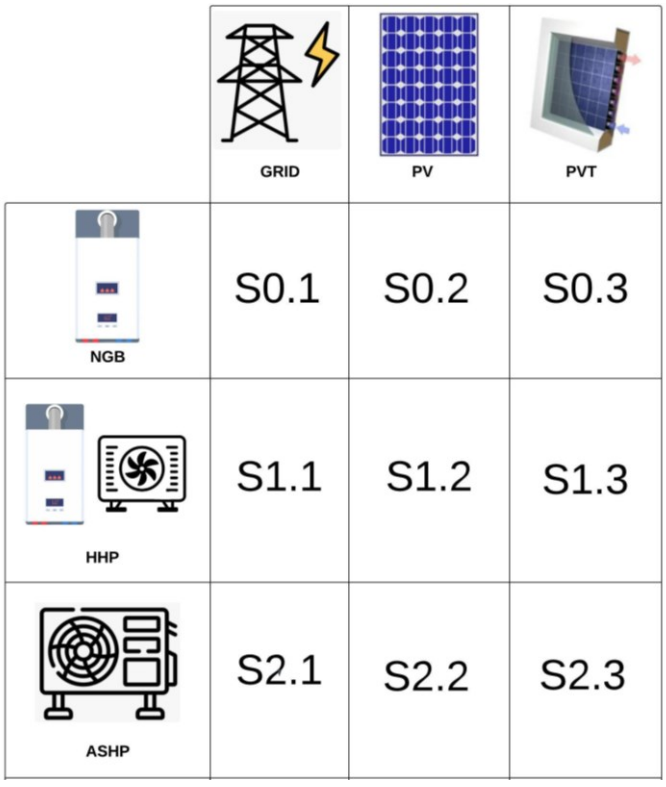

Figure 13. scenarios overview

- **S0.1**: Baseline scenario. Heating is provided by a Natural Gas Boiler (NGB) and all electricity is drawn from the national grid. This configuration is representative of the majority of residential buildings in Italy today and serves as the reference point for comparative analysis.
- **S0.2**: Identical to S0.1 in terms of heating (NGB) but includes photovoltaic (PV) panels to meet part of the electric demand. This allows for an initial evaluation of self-production benefits.
- **S0.3**: Maintains the NGB for heating but integrates Photovoltaic-Thermal (PVT) panels to supply both electricity and thermal energy. This configuration enables a more advanced coupling of renewable resources.
- **S1.1**: Introduces a Hybrid Heat Pump (HHP) system, which operates in combination with the NGB, while relying on grid electricity. It represents a transitional solution between traditional and renewable heating systems.
- **S1.2**: Same heating configuration as S1.1 (HHP), but powered by PV electricity, increasing the share of renewable energy and reducing dependency on the grid.
- **S1.3**: Combines the HHP with a PVT system, aiming to optimize both electrical and thermal contributions from renewable sources.
- **S2.1**: Replaces the HHP with an Air Source Heat Pump (ASHP), fully powered by electricity from the grid. This scenario evaluates the impact of fully electrified heating using ambient air as the renewable source.
- **S2.2**: ASHP supported by PV electricity. This configuration is more sustainable than S2.1 and contributes to decarbonization goals through local energy generation.
- **S2.3**: Uses a PVT system to supply electricity and heat to the ASHP. It represents a highly integrated renewable energy system with potential for high efficiency and autonomy.

In the proposed energy system, thermal energy recovered from the photovoltaic-thermal (PVT) panels is characterized by relatively low temperatures. As a result, this low-grade heat is not suitable for space heating via traditional radiators, which require higher supply temperatures to ensure thermal comfort. Instead, the recovered thermal energy is more efficiently allocated to domestic hot water (DHW) production, where lower temperature levels are sufficient and advantageous from an energy efficiency standpoint.

The baseline scenario (S0.1) assumes the presence of traditional split air conditioners for summer cooling, powered exclusively by electricity from the grid. This configuration is extended to scenarios S0.2 and S0.3, where the electricity demand is partially or fully met by photovoltaic (PV) or photovoltaic-thermal (PVT) systems, respectively. The most significant changes across scenarios will therefore be observed in the heating sector, where the impact of different technologies and energy management strategies is evaluated in detail.

The scope of this modelling effort is to explore how different combinations of renewable energy systems (photovoltaic and photovoltaic-thermal panels), heat pump technologies (air-source, water-source, and hybrid systems), and storage can be deployed to meet its demands, currently satisfied through Natural Gas Boilers (NGBs) and electricity from the grid. The configuration is not intended to reflect a real-world pilot, but rather to serve as a generalizable and modular simulation environment for evaluating the energy, environmental, and economic implications of various decarbonization strategies at the district scale.

The analysis focuses on testing the effectiveness of these tecnhological implementations through mathematical modeling, operating on Matlab/Simulink. This software was chosen for its flexibility in modifying inputs and outputs, enabling the creation of different scenarios that can be directly compared. The understanding of energy retrofit concept was also supported by reviewing relevant literature, real-world applications, and current policies, providing a comprehensive background to the study.

Two parts of the work can be identified:

- Part 1 – Modeling the building: inserting the provided data, checking the results of simulations, working on adjustment factors.
- Part 2 – Intervention scenarios: testing scenario results and analyzing their environmental, energetic and economic outcomes to identify the most efficient interventions.

To develop the simulation models, we started from existing Simulink frameworks previously developed by a PhD student at Sapienza University as part of earlier studies in the Tor Bella Monaca district. Together, we revised and extended these models to adapt them to the objectives of this research. This work involved the

implementation of multiple configurations representing different technological mixes, ranging from conventional systems to advanced renewable energy-based solutions. The adaptation process required a thorough restructuring of the original models, including the integration of additional components, control logic, and performance tracking tools suitable for comparative analysis.

The load profiles were used as inputs in the Simulink simulations, allowing us to study the response of each scenario to a variety of demand conditions. This approach enabled a better understanding of how energy communities can manage heterogeneous energy needs and how the selected technologies perform under different load patterns.

With the customized Simulink models, the study provides a detailed performance evaluation of the proposed scenarios in terms of energy efficiency, emissions, and economic returns.

II.3. Simulation tools and modeling environment

MATLAB (Matrix Laboratory) is a high-level numerical computing environment with extensive toolboxes for control design, optimization and data analysis [66]. Its integrated Simulink platform is a graphical block-diagram environment for modeling and simulating dynamic multi-domain systems. In the context of building energy engineering, MATLAB/Simulink is widely used to develop energy management and control strategies – for example, MathWorks notes that one can "model, simulate, and design optimal EMS control strategies for scheduling power systems and HVAC systems operations" using these tools [67]. These capabilities made MATLAB/Simulink a natural choice for this thesis: it was used to implement the control algorithms and to perform any required optimization or data processing.

The combined MATLAB/Simulink approach ensured that the thesis could accurately simulate the dynamic building physics while simultaneously designing and testing advanced control strategies, in line with best practices in building energy modeling and control.

The following sections describe the mathematical models relating to the main plant components.

II.3.1.1. Condensing natural gas boiler

Natural Gas Boiler (NGB) supplying both space heating and domestic hot water (DHW) for the building. The model calculates thermal energy needs and regulates the operation of the boiler to satisfy these demands.

The model processes the operational parameters of the boiler and estimates the consumption and pollutant emissions. It considers the load conditions, fuel flow, and boiler efficiency to compute emission quantities. The model allows estimate of environmental impact. Then the outputs include the thermal output, the fuel flow rate, the efficiency and emissions such as the gCO grams of carbon monoxide emitted, gCO2 grams of carbon dioxide emitted, gNOx grams of nitrogen oxides emitted and mgNOx milligrams of NO_x.

I know the thermal load of the building at each time step, which was set equal to the energy supplied by the heat generator. The partial load ratio (PLR) was then calculated as the ratio of the maximum power of the machine to the power delivered at the specific time step.

$$PLR = \frac{\dot{Q}_{need}}{\dot{Q}_{max}}$$

So, it is possible evaluate all other output. The fuel consumption will depend on the energy required and the efficiency supplied to the type. $\dot{Q}_{fuel}$ is expressed in kJ/s, to estimate the fuel consumption in m3 (e.g. of methane) it will be necessary to divide by the lower heating value (LHV).

$$\dot{Q}_{fuel} = \frac{\dot{Q}_{need}}{\eta_{boiler}}$$

An important output is the actual fluid outlet temperature.

$$T_{out} = T_{in} + \frac{\dot{Q}_{max}}{\dot{m}_{fluid} Cp_{fluid}}$$

Finally, knowing the burner efficiency and $\dot{Q}_{fuel}$, it is possible to calculate energy exhausted from the boiler through the combustion stack or chimney ($\dot{Q}_{exhaust}$) and combustion energy losses ($\dot{Q}_{loss}$).

$$\dot{Q}_{exhaust} = \dot{Q}_{fuel}(1 - \eta_{combustion})$$

$$\dot{Q}_{loss} = \dot{Q}_{fuel} - \dot{Q}_{exhaust}$$

II.3.1.2. Air source heat pump (ASHP)

The Air Source Heat Pump (ASHP) subsystem simulates the dynamic thermal behavior of an air-source heat pump. It receives as inputs the outdoor temperature, the thermal load to be covered, and the design supply water temperature, and it calculates the thermal power delivered and the electrical power consumed. It also estimates the Coefficient of Performance (COP) under both nominal and partial load conditions.

Inside the ASHP block, the main functional block is labeled 'Calcolo Funzionamento a carico parziale', which handles performance modulation under partial load operation. It adjusts the nominal COP and electrical/thermal power values based on current boundary conditions and load fraction.

The heat pump model was based on the MAP methodology/HP mapping curves as per the manufacturer's data sheet.

Given the operating conditions of the heat pump, it is possible to go and calculate the nominal performance of the machine, in particular note output temperature required at HP ($T_{w,set,HP}$) and outside air temperature (T_{ext}) it is possible to derive by interpolation of the curves in Figure 1 the nominal heat capacity, electrical power input and COP at those given conditions.

$$P_{th,HP,rt} = f\left(T_{w,set,HP}, T_{ext}\right)$$

$$P_{el,HP,rt} = f\left(T_{w,set,HP}, T_{ext}\right)$$

$$COP_{rt} = f\left(T_{w,set,HP}, T_{ext}\right)$$

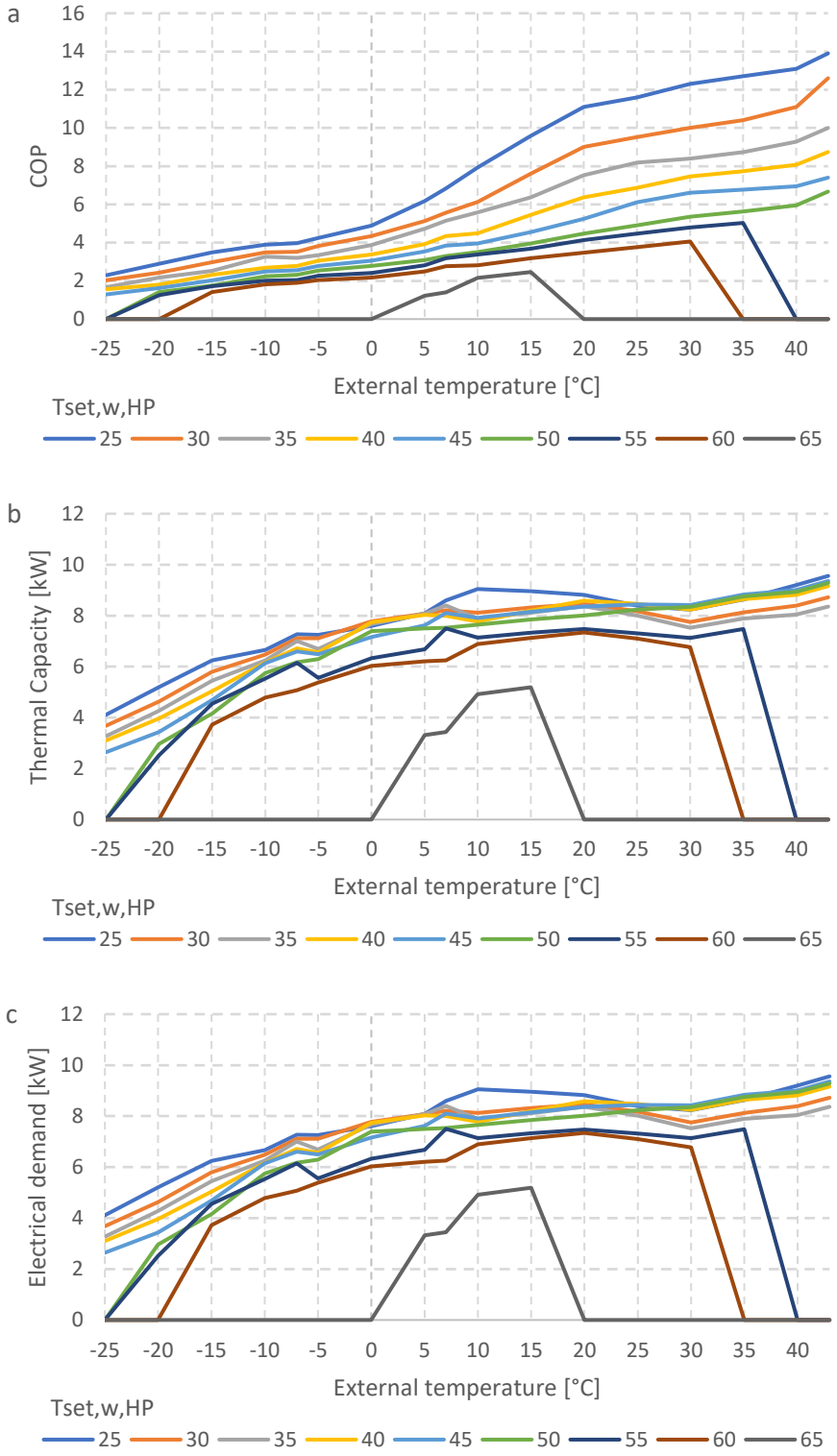

Figure II-14. Air source heat pump Heatin capacity (a), electrical power (b) and COP (c) MAP.

Inputs:

- T_ext [°C]: External air temperature
- Tw.supply.design [°C]: Design temperature of the water to be supplied
- Pth.load: Required thermal load [kW]
- on-off_HP: Binary signal indicating whether the HP is active (1) or not (0)

A correction factor Fp,COP based on the ratio between the actual and nominal thermal power:

$$F_{p,COP} = f\left(P_{th,load}/P_{th,nom}\right)F_{p,COP} = fP_{th,load}/P_{th,nom}$$

This factor adjusts the nominal COP to obtain the effective COP:

$$COP_{eff} = COP_{nom} * F_{p,COP}$$

The effective electrical power is:

$$P_{el,eff} = P_{th.load}/COP_{eff}$$

The final electrical consumption is:

$$P_{el,HP,eff} = P_{el,eff} * (on - off_{HP})$$

Outputs:

- Pth,HP,t: Thermal power required by the load [kW]
- HP_COPeff: Effective Coefficient of Performance
- Pel_HP,eff: Effective electric consumption of the heat pump [kW]

This subsystem allows the model to:

- Evaluate dynamic performance of the HP depending on real operating conditions
- Correct COP and power values under non-nominal conditions
- Distinguish between nominal and part-load behavior, ensuring higher

In cooling condition a fixed COP of 3.5 has been assumed for the air-source heat pump representing a performance unit under standard European conditions, as reported by the European Commission's JRC report on heat pump efficiency [70].

II.3.1.3. Climatic Compensation and set point temperature

The subsystem named "KT" represents a temperature-based control logic used to compute a control parameter denoted as K, which likely acts as a climatic compensation factor or gain based on supply and external air temperatures. The model performs a series of arithmetic operations to dynamically compute the value of K based on design and environmental conditions.

The mine inputs and constants are:

- T_sup_d: Design supply temperature (e.g., desired flow temperature in a heating system).
- T_shift: A constant shift temperature, here fixed to 30°C.
- T_ext_min: Minimum external air temperature for which the system is designed, set to 0°C.
- 20: A constant representing the base internal design temperature (in °C).

The first block computes the numerator of the final expression:

$Numerator = T_{sup} - T_{shift}$

This calculates the difference between the design supply temperature and the shift temperature.

The second part computes the denominator using the expression:

$Denominator = T_{base} - T_{ext\_min} = 20 - 0 = 20$

This represents the total temperature range between internal comfort temperature and the minimum external temperature.

The result K is then calculated as:

$$K = \frac{T_{sup} - T_{shift}}{T_{base} - T_{ext,min}} = \frac{T_{sup} - 30}{20}$$

This quotient represents a linear gain factor for adjusting heating setpoints or control strategies based on external temperatures, commonly used in heating curve logic. It's a normalized temperature-dependent factor.

This KT block implements a linear temperature compensation logic, where the output value K varies proportionally with the design supply temperature. This type of calculation is typical in climatic control systems for HVAC or heating applications, particularly for determining control gains or slopes of heating curves.

The “climat straight” subsystem defines a temperature-dependent control strategy commonly used in climate compensation logic, particularly in heating systems. Its purpose is to dynamically compute the supply setpoint temperature (T_{supply}) based on the external air temperature (T_{amb}) using a linear control law governed by the slope K, which is provided by the previously defined KT block.

The subsystem computes T_{supply} using the following formula:

$$T_{supply} = -K \cdot (T_{amb} - 20) + 30$$

This can be interpreted as a linear heating curve, where:

- As T_{amb} decreases below 20°C, T_{supply} increases linearly.
- As Tamb increases above 20°C, T_{supply} decreases.
- At T_{amb} = 20°C, the system delivers exactly 30°C as the supply temperature.

The output passes through a saturation block, which limits T_{supply} within minimum and maximum operational bounds, ensuring system safety and efficiency.

By adjusting T_{supply} based on real-time ambient conditions, the system maintains thermal comfort while optimizing energy efficiency.

The K value is calculated based on design parameters (T_{sup_d}, T_{shift}, and T_{ext_min}) using the K block.

- This creates a flexible and parametric model where the slope of the heating curve adapts to different building designs or climate zones.

II.3.1.4. Photovoltaic panel

The core of the photovoltaic (PV) subsystem is responsible for calculating the real-time electrical efficiency, the instantaneous electric power, and the operating cell temperature of a photovoltaic panel, based on environmental and module-specific parameters.

The PV model begins by estimating the cell temperature (T_PV_cell), a critical factor influencing the module's electrical efficiency. This is calculated using the NOCT (Nominal Operating Cell Temperature) model, which relates the ambient temperature (T_amb) and incident solar irradiance (G_solar) to the cell operating temperature. The temperature deviation from standard test conditions (STC) is computed as follows:

$$T_{pv,\,cell} = T_{amb} + \left(NOCT - T_{ref}\right) \cdot \frac{G_{solar}}{G_{ref}}$$

where:
T_ref is 20°C (reference ambient temperature), G_ref is 1000 W/m^2 (reference solar irradiance), NOCT is the panel-specific nominal operating temperature.

With the actual cell temperature determined, the model adjusts the electrical efficiency (η_el) to reflect temperature effects. This is done through a linear correction:

$$\eta_{el} = \eta_{el,std} + P_{el,coeff} \cdot \left(T_{cell,std} - T_{PV,cell}\right)$$

where:
η_el_std is the electrical efficiency at STC; P_el_coeff is the temperature coefficient (negative, indicating performance drops with rising temperature), T_cell_std is the cell temperature at STC (25°C).

Once the real-time efficiency is known, the instantaneous electrical power output (P_el) is calculated:

$$P_{el} = \eta_{el} \cdot G_{solar} \cdot A_{surf}$$

With - G_solar: solar irradiance [W/m^2]; - A_surf: surface area of the PV module.

The outputs from this subsystem are: η_el: instantaneous module efficiency [%], P_el: electric power produced by a single module [W], T_PV_cell: cell operating temperature [°C].

The PV - Production block integrates the PV MODULE into the larger simulation framework to compute the total system power and energy output.

The outputs from the PV MODULE are used as follows:

1. Electric Power Output Scaling:The single-module power output P_el is converted from watts to kilowatts.It is then multiplied by the number of PV modules in the system (n_pv0), resulting in the total PV power output P_el_tot in kilowatts.

2. Energy Calculation: The total power P_el_tot is integrated over time (via a 1/s block) to compute the total energy produced E_el_tot in kilowatt-hours (kWh).

3. Monitoring and Export: Additional outputs are extracted for system analysis and data logging: η_el: PV efficiency (for performance monitoring); Prod_el_tot: total power produced; E_el_PV_tot: total energy produced.

In summary, this PV subsystem effectively models the dynamic behavior of a photovoltaic panel under varying environmental conditions. It accounts for real-time temperature-dependent efficiency changes and accurately computes the power and energy output of the entire PV system. The modular structure allows for scalability and precise performance analysis.

II.3.1.5. Photovoltaic Thermal Panel

The PVT MODULE subsystem extends the modeling of traditional photovoltaic panels by including the thermal dynamics of hybrid photovoltaic-thermal (PVT) collectors. Unlike the PV MODULE, which focuses solely on electrical performance, this model computes both electrical and thermal outputs, simulating the energy conversion process of a PVT system under varying environmental conditions.

The subsystem receives three inputs: T_w,in: inlet water temperature [°C], T_amb: ambient temperature [°C], G_solar: incident solar radiation [W/m^2].

It produces the following outputs: η_el: electrical efficiency [%], P_el: instantaneous electric power output [W], - T_PV_cell: PV cell operating temperature [°C], T_w_out: outlet water temperature [°C], P_th: thermal power output [W], η_th: thermal efficiency [%]

The thermal power extracted by the working fluid (water) is calculated using a first-law energy balance over the fluid:

$$P_{th} = m_w \cdot c_{p,w} \cdot \left(T_{w,out} - T_{W,in}\right)$$

Where: m_w: mass flow rate of water [kg/h], c_p,w: specific heat of water [kJ/kg·K], T_w_out: outlet temperature, T_w_in: inlet temperature, Internally, time unit conversion blocks (hour-to-second) are included to ensure consistency with SI units.

The outlet water temperature is derived by inverting the thermal balance:

$$T_{w,out} = \frac{P_{th}}{m_w \cdot c_{p,w}} + T_{w,in}$$

Thermal losses to the environment are modeled through the overall heat loss coefficient U_L, with a heat loss term proportional to the temperature difference between the absorber plate and the ambient:

$$Q_{loss} = U_l \cdot \left(T_{PV,cell} - T_{amb}\right) \cdot A_{surf}$$

However, instead of computing losses explicitly, the absorbed thermal power is estimated:

$$P_{th} = A_{surf} \cdot FR \cdot \left[\tau \cdot \alpha \cdot G_{solar} - U_l \cdot \left(T_{w,in} - T_{amb}\right)\right]$$

Where: F_R: heat removal factor τ: transmittance, α: absorptance

The thermal efficiency is then calculated as the ratio of thermal power to incident solar power:

$$\eta_{th} = P_{th} \cdot \left(G_{solar} \cdot A_{surf}\right)$$

This allows the model to dynamically assess the collector's thermal performance under changing solar and thermal boundary conditions.

In the higher-level Solar Array Model, the PVT MODULE is repated five times, each representing an individual collector. This modular replication enables scalability of the simulation, allowing the full system thermal and electrical behavior to be studied as the sum of each module's outputs.

Each PVT module is evaluated independently using its respective environmental inputs and flow conditions, and the aggregated output is then used in the larger energy system model to compute total energy balances, performance metrics, and emission reduction potentials.

II.3.1.6. Electrical Storage System

The Electrical Storage block represents the top-level control logic of the Battery Energy Storage System (BESS), integrating all electrical flows between renewable sources (PV or PVT), storage systems, and the utility grid. The subsystem receives two main inputs:

- Cons_el_tot: total electrical demand of the system [kW]

- Prod_el_tot: total renewable electrical production [kW]

These two signals are fed into the central energy balance module, which evaluates the power flow conditions and determines the routing logic across various components. The core output variables include:

- P_el_Rbattery_1: power drawn from the battery to meet electrical demand

- P_el_Rgrid_2: power required from the grid (when battery and RES are insufficient)

- P_el_SCd_1, P_el_SCd_2: power that is directly self-consumed

- P_el_Dgrid_1: power injected into the grid due to surplus generation

This structure acts as the control center for dispatching electrical flows according to priority rules and storage availability. Internally, the Electrical Storage block includes several nested subsystems, the first of which is the Pel,excess evaluation unit.

Pel,excess Evaluation – Energy Balance for Storage Management

The Pel,excess evaluation subsystem performs the fundamental balance between the total electrical production and the electric demand of the building or system. Its purpose is to determine whether there is a surplus of electricity, and, if so, how to allocate it—either toward storage or as direct export to the grid.

This value is processed through a logical structure that classifies it as either Pel_excess (surplus electricity) or Pel_grid (energy drawn from the grid). The output variable Pel_excess is routed toward the battery management system, where it will either be stored (if capacity is available) or exported to the grid.

Key outputs include:

- Pel_SCd_1: part of the energy directly self-consumed

- Pel_Rbattery_1: energy required from the battery when demand exceeds production

- Pel_excess2: residual energy to be stored or exported to the grid

This subsystem defines the boundaries of battery usage and sets the basis for efficiency analysis and self-consumption calculations.

The first layer of the battery management subsystem orchestrates the interface between system-level control and the actual battery logic. It receives operational inputs and computes intermediate energy quantities for charge/discharge management and state tracking.

Inputs:

- Pel_st_max: Maximum allowable charge/discharge power, based on installed battery capacity

- Pel_st_in (Pex): Electrical power available for charging the battery

- Pel_Rbattery_1: Energy demand to be covered by battery discharge

Outputs:

- E_el,stored: Total electrical energy currently stored in the battery [kWh]

- Pel_charge,t: Power charged into the battery [kW]

- Pel_discharge,t: Power discharged from the battery for self-consumption [kW]

- SOC: State of charge of the battery, expressed as percentage

- Pel_st_battery, P_el_discharge, Pel_st_out: Control and monitoring signals used for system-level energy routing and tracking

This internal layer handles the core energy balance logic for battery operation, including charge, discharge, energy update, and SOC calculation. The model ensures energy conservation and feasibility through prioritization and constraint logic. Charge and discharge processes are mutually exclusive and based on minimum selection across:

- Available excess energy

- Battery’s available capacity (or energy that can be removed during discharge)

- Maximum allowed charge/discharge rates

Energy charged or discharged in each timestep is integrated to update the stored energy value. The model prevents overcharging and deep discharges by applying conditional constraints on energy availability and required load. The discharged energy is primarily directed to local self-consumption rather than grid export, and is subtracted accordingly from the SOC.

The SOC is computed as a normalized ratio between stored energy and maximum battery capacity. This parameter governs system-level decisions and prevents operation beyond physical or safety limits.

The subsystem is responsible for classifying the final electrical flows from the system and quantifying how the generated or stored energy is either consumed on-site or exported to the grid. It operates after the main battery charge/discharge evaluation, acting as a post-processing stage for energy routing.

This subsystem compares the following quantities: Pel_Rbattery_1: electrical demand from the system that could be supplied by the battery, P_el_discharge: actual power discharged from the battery, Pel_excess: residual energy available from the PV/PVT generation, Pel_st_battery: power that could still be stored in the battery (i.e., unused storage margin)

Two core evaluations are performed:

1. Grid Import Condition: If the electrical demand exceeds the battery discharge availability, the difference is counted as grid import.

2. Grid Export Condition: If the PV excess power exceeds what the battery can still absorb, the surplus is exported to the grid.

The outputs of this logic are:

- Pel_to_Grid2: power exported to the grid due to battery saturation
- Pel_demand_to_Grid2: power imported from the grid due to insufficient RES and battery
- SC_direct1: locally self-consumed electricity (PV to load, without battery mediation)

II.3.1.7. Thermal Energy Storage (TES)

The Thermal Energy Storage (TES) system is modeled through a modular approach, combining different subsystems that handle specific control and thermal dynamics. The overall TES configuration is split into two main parts:

Tank–PVT Control: manages the interaction between the PVT collectors and the storage system, including switching logic and auxiliary heating control.

Buffer Tank: simulates the dynamic thermal behavior of the water storage vessel, accounting for heat inputs, losses, and demand.

In the following sections, each part of the TES system will be described in detail to illustrate its role and implementation within the broader energy system model.

The Tank–PVT control module regulates the thermal interaction between the photovoltaic-thermal (PVT) panel and the domestic hot water (DHW) storage tank. It ensures that the PVT unit contributes to the DHW load only when the temperature conditions are favorable, and it manages the activation of auxiliary heating sources as needed.

The system is composed of two subsystems:

- A Differential Thermostat Controller, which controls the heat transfer from the PVT to the storage tank
- An Auxiliary Control Logic, which manages the request for backup thermal energy if the PVT contribution is insufficient

Differential Thermostat Controller block evaluates the temperature differential between:

- T_out_SF: the fluid outlet temperature from the PVT collector
- T_top: the temperature at the top of the DHW storage tank

Using a differential setpoint (DeltaT_diff_set), the controller determines whether the temperature difference is sufficient to justify heat transfer.

The output is a binary PVT switch signal:

- ON (1) if $T_{out\_PVT} - T_{top} \geq \Delta T_{set}$
- OFF (0) otherwise

This ensures that heat is only injected into the tank when it would result in a beneficial increase in storage temperature.

The Aux control block handles the backup thermal energy management. It compares:

- Ttop: actual top tank temperature
- T_desgn_DHW: the design DHW temperature setpoint
- Pth_DHW_demand: required thermal power for DHW
- Pth_PVT: actual PVT thermal contribution

Two main outputs are computed:

- Pth_aux: the power required from the auxiliary system
- DHW_backup_request: a binary signal indicating the need for backup

The control logic activates the auxiliary system if:

- The top tank temperature is below the DHW design threshold
- And/or the thermal power delivered by the PVT is insufficient to meet the demand

The auxiliary power is calculated as the difference between demand and PVT supply, and activated only when this difference is positive.

II.3.1.8. Buffer Tank

The Buffer Tank block acts as the integration interface for the domestic hot water (DHW) thermal storage system, managing all thermal inputs and outputs relevant to the vessel.

The following signals enter the subsystem:

- `P_th_PVT_eff`: effective thermal power from the PVT collector [kW]
- `P_th_DHW_demand`: thermal power demand from the domestic users [kW]
- `P_th_aux`: auxiliary backup power input [kW]
- `T_w_in_DCW`: cold water inlet temperature [°C]
- `T_out_SF`: temperature at the solar field outlet [°C]
- `T_ext`: ambient external temperature [°C]
- `Vessel_volume`: volume of the storage tank [m^3]

From the buffer tank, several quantities are monitored and passed to other systems:

- `T_avg_vessel`: average tank water temperature [°C]
- `T_top`: temperature at the top of the tank [°C]
- `P_th_out_BT`: power delivered by the buffer tank to meet DHW demand [kW]
- `P_th_DHW_demand`: forwarded to other systems for load calculation
- `P_th_PVT`: passed to control blocks
- `P_th_aux`: passed to auxiliary logic
- `T_out_SF`: exported to average temperature calculation

The core subsystem is the block HOT_WATER_STORAGE, which simulates the thermal and dynamic behavior of the water inside the tank.

This level simulates the thermal dynamics of the vessel through a simplified energy balance, accounting for energy inputs, losses, and the thermal inertia of the system.

The vessel temperature is computed using a first-order differential equation derived from the conservation of energy:

$$\frac{dT_{vessel}}{dT} = \frac{1}{m \cdot c_p} \cdot \left(P_{th,in} - P_{th,out} - Q_{loss}\right)$$

- *Pth,in*: total thermal power input from PVT and auxiliary sources [kW]
- *Pth,out*: thermal power withdrawn by DHW demand [kW]
- *Qloss*: thermal power loss to the ambient [kW]

The term $\frac{1}{m \cdot c_p}$ represents the inverse of the thermal capacity of the water, where:

- $m = \rho \cdot Vm$, with water density $\rho = 1000\ kg/m3;$
- $c_p = 4.1869\ kJ/kg.$

Losses are modeled via a conduction equation using the surface area and insulation quality of the tank:

$$Q_{loss} = U \cdot A \cdot (T_{vessel} - T_{outdoor})$$

- *U*: insulation value [W/m^{2}K]
- *A*: surface area of the vessel [m^2]
- *Toutdoor*: ambient air temperature

These losses are also accumulated over time to compute energy lost in [MWh].

Computed Outputs are:

- T_vessel_avg: current average temperature of the vessel water [°C]
- T_top: temperature at the top of the tank [°C], extracted for controller logic
- Thermal losses: real-time and cumulative thermal losses [kW and MWh]
- Time constant: calculated from the water mass and heat capacity, used in the differential system dynamics

This subsystem dynamically simulates the tank's thermal response to load and input fluctuations over time, making it suitable for yearly simulations with hourly or sub-hourly resolution.

This subsystem implements the thermal dynamic model of the buffer tank using a physical energy balance approach, combining thermal inputs, water mass properties, and heat losses to ambient.

The mine inputs used are:

- `P_th_PVT`: thermal power from PVT collectors [kW]
- `P_th_aux`: thermal power from the auxiliary system [kW]
- `P_th_DHW_demand`: thermal power withdrawn by domestic hot water load [kW]
- `T_ext`: outdoor temperature [°C]
- `Vessel_volume`: water volume in the tank [m^3]
- `T_w_in_DCW`: cold water inlet temperature [°C]

Mass and Thermal Capacity Calculation: The water mass is calculated as:

$m = \rho \cdot V_m$

where ρ=1000kg/m^3 and V is the tank volume.

The thermal capacity is then:

$C = m \cdot c_p$

with c_p =4.186kJ/kg. This defines the time constant of the system.

Energy Balance: The vessel temperature is updated based on the net power input:

$$dT = C \cdot P_{net}$$

where:

$$P_{net} = P_{th,PVT} + P_{th,aux} - P_{th,DHW} - Q_{loss}$$

Heat Loss Calculation: Heat loss to the ambient is computed as:

$$Q_{loss} = U \cdot A \cdot (T_{vessel} - T_{ext})$$

where A is the surface area (computed from volume), and U is a fixed insulation parameter.

Integration Block: The vessel temperature is updated using a Simulink integrator that solves the differential equation above at each timestep.

II.3.2. Control Logic for Power Flow Management

The control diagram defines the energy management logic based on the balance between electrical production and demand. The difference between produced and demanded electrical power (Pel,prod - Pel,dem) is the key control variable.

- When demand exceeds production (Pel,prod - Pel,dem < 0), the system first draws electricity from the battery (BESS). If the BESS cannot supply the required energy—e.g., due to reaching its minimum state of charge—the remaining demand is covered by the grid.
- When production exceeds demand (Pel,prod - Pel,dem > 0), the surplus electricity is first used to charge the BESS. Any additional excess is directed to the heat pump to generate thermal energy (power-to-heat). If neither electrical storage nor thermal storage capacity is available, the residual electricity is injected into the grid.

This hierarchical structure ensures local optimization: prioritizing self-consumption, storing excess energy, and minimizing grid exchange.

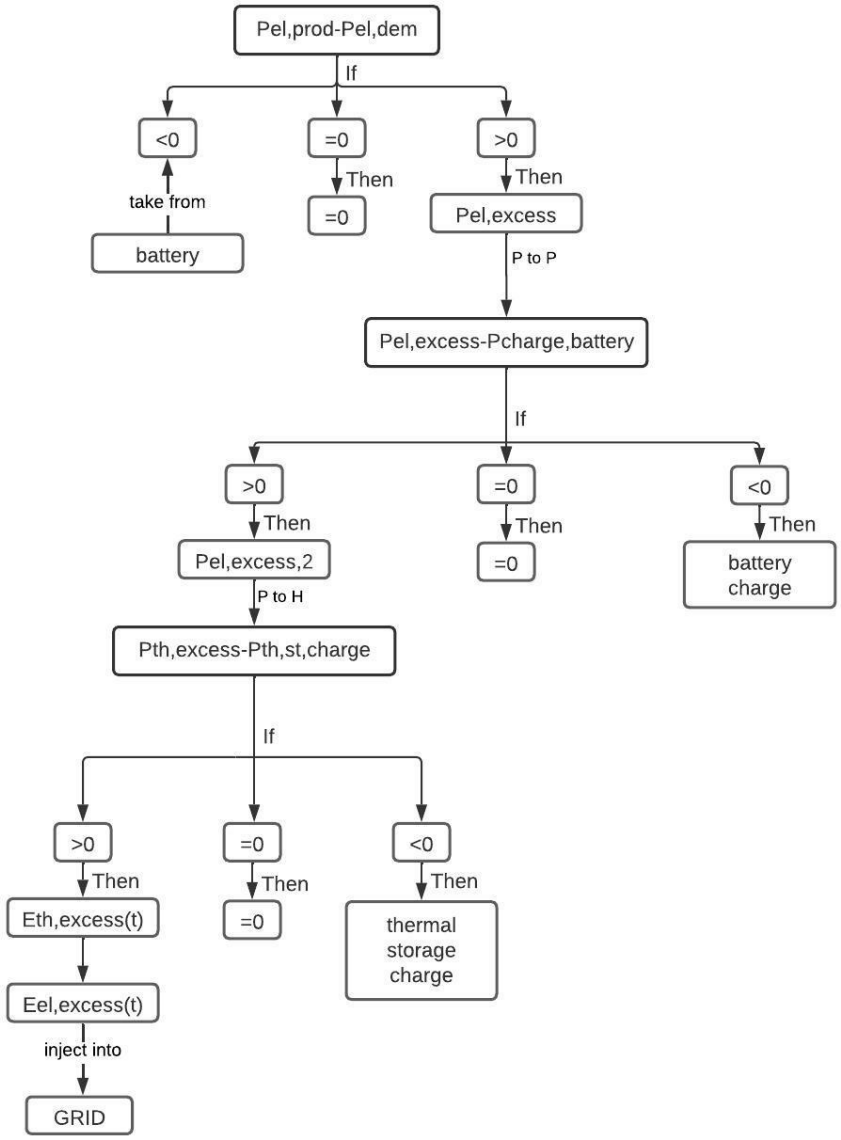

It is important to distinguish between meeting thermal demand and managing thermal storage. Thermal demand is typically met directly by heat pumps (HPs) during PV generation, when electricity is available in real time. This allows for efficient use of renewable electricity for thermal production.

Thermal Energy Storage (TES) is used primarily to shift thermal supply in time, making previously stored thermal energy available during periods when PV production is unavailable or inefficient (e.g., at night or during low solar irradiation). In the absence of PV production, thermal demand is met according to the following hierarchical order:

- TES (discharging previously stored thermal energy);
- BESS (providing electricity to operate the HP);
- Grid (as a last resort, to supply electricity to the HP).

  This logic ensures that local and renewable resources are prioritized, while maintaining supply continuity and minimizing grid dependency.

II.4. Key Performance Indicators

The different Key Performance Indicators (KPI) used are described in the following graph:

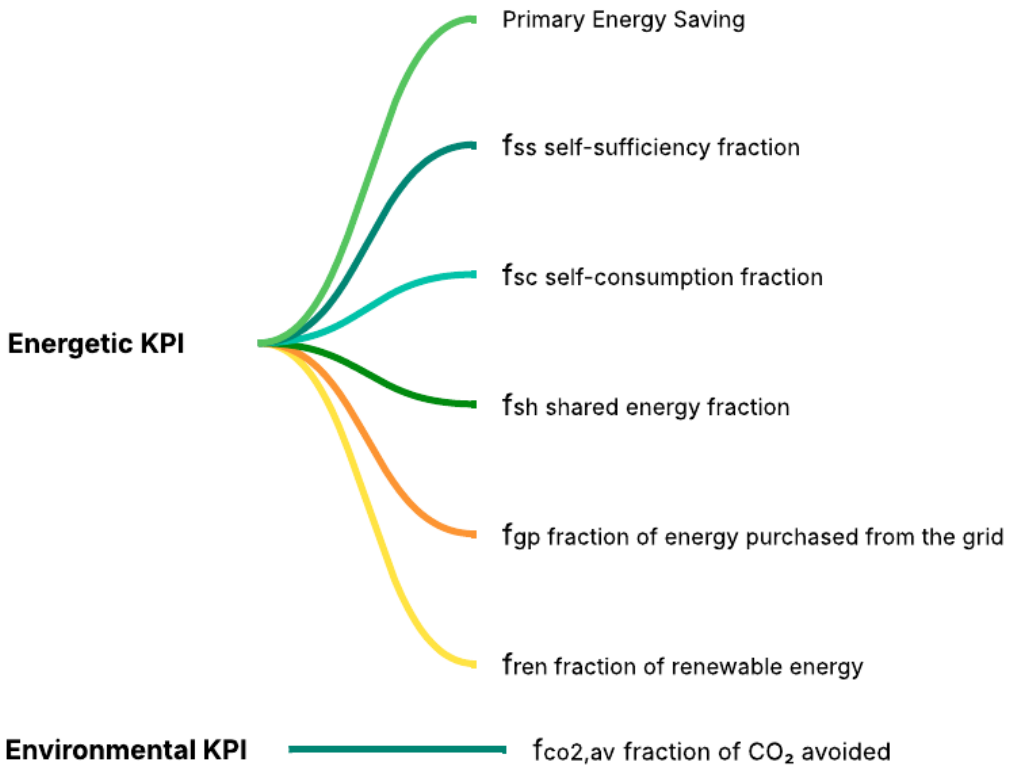

Nine Key Perfomax Indexes (KPI) were evaluated to compare the six scenarios, offering a complete evaluation from energetic and environmental perspectives.

Inside an Energy Community, the electrical energy generated by PV panels is primarily destined to self consumption by prosumers; eventual exceedings can be exploited by other members of the community or fed into the grid.

Starting from data related to energy demand and solar production, the self consumption achievable in every configuration was calculated and defined through the self-consumption index f_{sc}, found through the ratio between renewable electricity locally consumed and yearly photovoltaic production.

$$f_{SC} = \frac{E_{el,SC}}{E_{el,PVT}}$$

In parallel a calculation was made finding the quantity of exceeding energy that wasn't consumed but shared with other members of the community:

$$E_{el,sh,excess} = E_{el,PVT} - E_{el,SC}$$

On this basis, the energy sharing factor is defined (f_{sh}) wich is the ratio of energy actuallky shared and absorbed by the community members to photovoltaic production:

$$f_{SH} = \frac{E_{el,SH}}{E_{el,PVT}}$$

To complete the energy balance, the amount of energy fed to the national grid is evaluated, too. This is the energy that is not self-consumed nor shared:

$$E_{el,PV,grid} = E_{el,PVT} - E_{el,SC} - E_{el,sh}$$

A further indicator is the electrical self-sufficiency index (f_{ss}), wich represents the global capacity of the EC to meet its electrical needs through renewable self-produced energy. It is found as the ratio of total self-consumption and shared energy to the global yearly consumption:

$$f_{ss} = \frac{E_{el,SC} + E_{el,SH}}{E_{el,load}}$$

From the environmental perspective, the benefit is evaluated through the Primary Energy Saving (PES), comparing every improved scenario with the base-case scenario with no interventions applied (S0):

$$PES = \frac{PE_{nREN,i}}{PE_{nREN,S0}}$$

Furthermore, other useful parameters were considered to complete the energetuic-environmental evaluation of the analysed configurations. For what regards electrical energy:

- f_{gi} fraction of energy taken by the grid with respect to total electrical consumption:

$f_{gi} = \frac{E_{el,from\ grid}}{Eel,load}$

- f_{gd} fraction of energy fed to the grid with respect to total electrical consumption:

$$f_{gd} = \frac{E_{el,to\ grid}}{Eel,load}$$

These two indexes are inversely proportional to the efficiency and autonomy of the community: high values mean a suboptimal use of energy and a higher environmental impact.

To estimate the global environmental impact, were also considered:

- The CO_2 emissions associated with the electrical energy consumption from the grid, calculated by the medium national emission factor ($f_{CO2,el}$, expressed in gCO_2/kWh):

$$gCO_{2,el} = f_{CO2,el} \cdot E_{el,from\ grid}$$

- The CO_2 emissions due to consumption of natural gas in the methane gas grid:

$$gCO_{2,fuel} = f_{CO2,el} \cdot E_{th,comb}$$

Finally, the net environmental benefit is evaluated through the calculation of the avoided CO_2, considering:

- The fewer energy taken from the grid thanks to renewable self-consumption;
- The reduced use of fossil fuels.

The avoided CO_2 index is calculated as:

$$f_{CO2,avoided} = 1 - \frac{gCO_{2,s1}}{gCO_{2,s0}}$$

Maximizing the renewable fraction (the share of demand met by local renewables) is a natural goal for decarbonization, but it does not always line up with maximal CO_2 reduction or the best economics. Several trade-offs and counterintuitive outcomes arise in district energy planning:

- **Temporal mismatch and system integration limits:** Pushing for maximum renewable fraction—especially through extensive PV deployment—can lead to mismatches between generation and demand. Most PV output occurs at midday, while peak heating demand often arises in the early morning or evening. Without adequate storage or flexible loads, this surplus production may be underutilized (curtailed), offering limited additional CO_2 savings [71]. At the same time, increasing PV capacity does not proportionally reduce emissions if the local grid is already decarbonized during peak solar hours. In such cases, integrating more PV leads to diminishing returns, both environmentally and economically [72]. A better-aligned design—possibly with smaller PV systems but better storage or load-shifting strategies—may achieve comparable CO_2 reductions while avoiding inefficiencies.

- **Economic vs. environmental optimization:** Systems aiming purely for maximum renewables often incur high capital costs (oversized PV/batteries, etc.) with long payback times. In many cases, the least-cost solution (highest ROI Return On Investment) uses a mix of renewables and conventional supply. For instance, the Queen's Quay system uses modest gas boilers for rare peaks so that for the larger amount of time the system will produce no local carbon [73], instead of achieving 100% on-site generation at much higher cost. In general, adding the last increments of renewable capacity means decreasing fuel savings per euro invested. Economic KPIs (LCOE Levelized cost of electricity, NPV Net Present Cost, ROI) often improve by accepting a lower renewable fraction or by using dispatchable backup, rather than pushing to the technical limit [74]. Moreover, scenarios with high shares of on-site renewables may depend heavily on storage, smart inverters, or predictive load management. These elements increase system sophistication and introduce new failure points, maintenance needs, and coordination challenges. Conversely, hybrid systems that rely partially on grid imports or dispatchable generation may offer simpler, more robust operation with only marginal sacrifices in sustainability. This trade-off between technical simplicity and maximal environmental performance is often overlooked but can significantly impact real-world feasibility and reliability [75].

- **Load-profile and technology interactions:** Different scenarios can invert expected outcomes. A summer-oriented PV installation may deliver a very high renewables share in July but rely on fossil energy in winter, whereas a balanced mix (e.g. including WSHP or wind) might give more stable decarbonization.

In regions with a low-carbon grid, maximizing renewables adds little benefit, while in carbon-intensive grids it is critical. Optimization studies confirm such trade-offs: for example, one case found that the renewable penetration in a hybrid district system increased significantly only when a high carbon price was applied [76]. Without that incentive, the minimal cost design accepted a moderate renewables share.

In summary, the optimal design depends on multi-objective balance. A scenario that maximizes the renewable fraction (e.g. 100% PV+storage) may not minimize lifecycle CO_2 or maximize ROI if it leads to overinvestment or suboptimal dispatch. Therefore, interpreting KPIs requires attention: high renewable fraction is necessary but not a guarantee of best performance. Often, the configuration with slightly lower renewables but better grid interaction and lower costs can take to equal or better CO_2 savings per euro spent. Understanding these trade-offs is essential for assessing district energy scenarios: it guides decision-makers to recognize that “more renewables” is not the sole objective but must be weighed against economic viability and actual emission reductions.

III. Results

The following section presents and discusses the graphical results of the three main configurations investigated in this work: Scenarios S0, S1, and S2. Each scenario explores a different system configuration aimed at satisfying the building's space heating and domestic hot water (DHW) needs through increasingly advanced technologies. In Scenario S0.1 electricital load is entirely met by the grid and thermal demand by a natural gas boiler (NGB): this is the baseline configuration. In Scenario S1, the system integrates a hybrid heat pump (HHP), while Scenario S2 incorporates an air-source heat pump (HP) as thermal energy provider.

Alongside these thermal systems, both photovoltaic (PV) and photovoltaic-thermal (PVT) modules are considered, with their operation controlled via a binary switch. Furthermore, battery energy storage systems (BESS) and thermal energy storage (TES) capacities are varied to evaluate their influence on the system's overall performance. For simplification and to ensure feasibility within the MATLAB environment, TES capacity is only present in configurations that include power-to-heat (P2H) conversion.

A parametric analysis was conducted on:

- Installed PV capacity, ranging from o to 1 MW
- TES size, ranging from 0 to 1 MWh
- BESS size, ranging from 0 to 1 MWh

Resulting in 1350 simulations.

The main performance indicators assessed across these scenarios are: self-consumption fraction (f_sc), shared energy fraction (f_sh), self-sufficiency fraction (f_ss), renewable energy fraction (f_REN), avoided CO2 emissions (f_CO2_av), and primary energy savings (PES).

III.1. S0 results analysis

Scenario S0 serves as the baseline configuration of the system. It is important to note that some indicators (f_sc, f_sh, f_ss and f_gp) are primarily driven by the electrical side of the system and are unaffected by the presence or absence of the

thermal contribution from PVT panels in this scenario. In such cases, only one curve is presented, as the result is identical for both PV and PVT configurations.

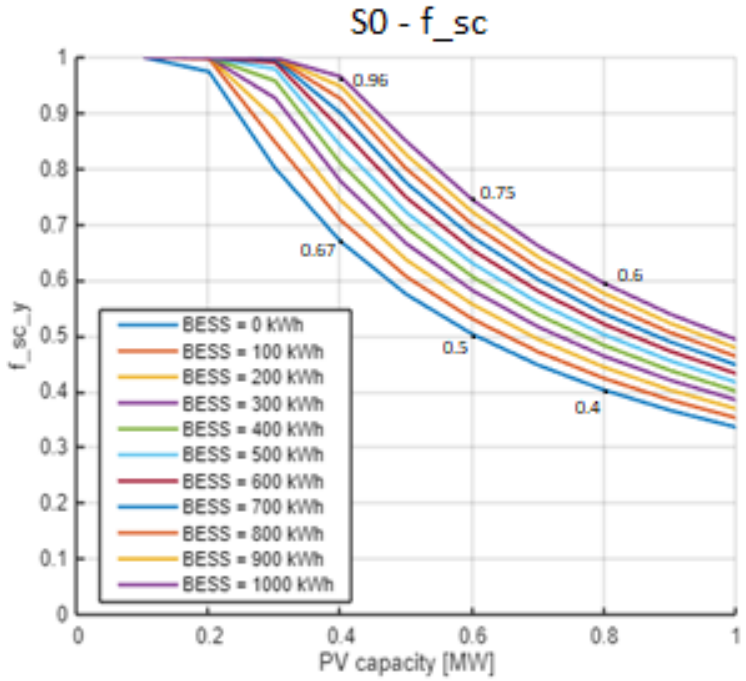

Figure 15: self-consumption fraction vs PV capacity with photovoltaic panels or photovoltaic thermal panels

As the capacity of the PV/PVT system increases, the self-consumption fraction (f_sc) tends to follow a declining trend (figure 14). This behavior can be explained by the fact that, at low installed capacities, nearly all the electricity produced is consumed directly by the building. However, as generation increases, the amount of surplus energy that exceeds immediate demand also grows, leading to a decrease in f_sc.

The starting point at PV capacity= 0.1 can be explained by the system's first input being zero and the second being 0.1.

Considering the curve with BESS=0 and increasing PV capacity from 0.1MW to 1 MW, f_sc decreases from 1 to 0.33 corresponding to a 67% of the self-consumption fraction.

Battery energy storage plays a pivotal role in mitigating this decline. Systems equipped with larger BESS capacities show consistently higher f_sc values, as the batteries store excess generation for use during times when PV/PVT production is low. This results in a vertical shift in the performance curves from blue (smaller

BESS) to purple (larger BESS), extending the system's ability to self-consume even at higher generation levels. Considering a medium PV capacity of 0.6MW, a 1MWh battery allows a 25% f_sc increase with respect to the configuration without storage (0.5-0.75). Gains reduce as PV capacity increases because of saturation of the storage, with a 17% increase at 1 MW.

Interestingly, for certain configurations, f_sc remains close to 1 up to a specific PV size. This plateau phase reflects the balance between generation and consumption, and the turning point—after which surplus begins—depends on the storage capacities available: 0.2MW without BESS and 0.4 with a 1MWh BESS, meaning that employing a high-dimension BESS allows to satisfy electrical loads by more electricity from PV panels effectively.

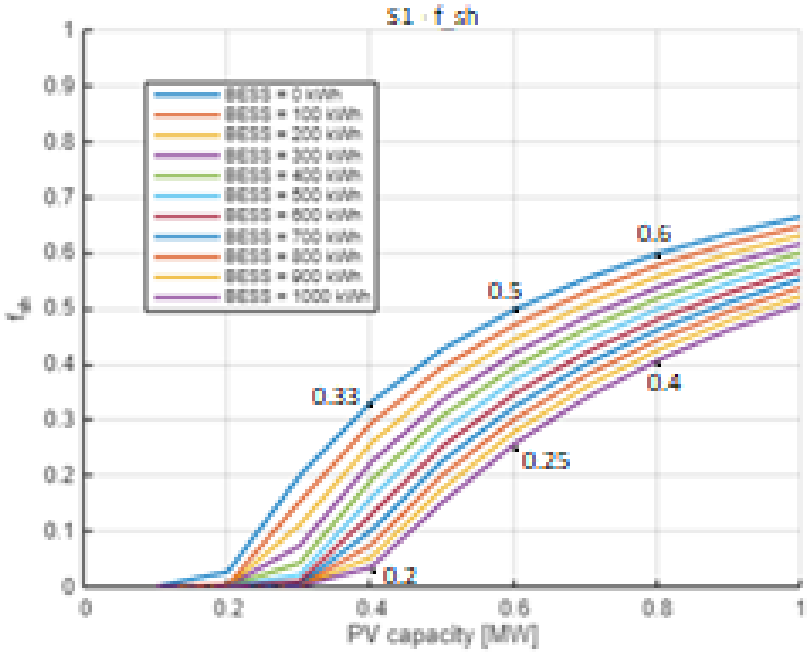

Figure 16: shared energy fraction vs PV capacity with photovoltaic panels

The shared energy fraction (f_sh), defined as the portion of generated energy that is not directly consumed and is therefore fed into the grid, increases with PV/PVT capacity. This behavior complements that of f_sc, as any excess not stored or used onsite is exported.

The increase in f_sh is more gradual when BESS capacity is larger, as more energy is captured and reused internally. Without adequate storage, surplus energy must be exported, resulting in higher f_sh values. The curves clearly show this shift from purple to blue.

With BESS=0, the shared energy fraction is very low until PV capacity reaches ~0.2 MW, where PV starts to produce more than the building's instantaneous load. This changes with a 1MW battery, allowing the system to start feeding energy into the grid only when 0.4 PV capacity is installed. For lower values of the latter the system self consumes most of the electricity.
After this threshold, f_sh increases monotonically with PV size, following a convex shape that tends to plateau around 0.7 at 1 MW with no BESS.
As BESS capacity increases, f_sh curves shift downward and become progressively flatter, especially at high PV: this reflects the fact that more surplus electricity is stored locally rather than shared/exported.
The curves are smooth and regular, with no inflection points; when BESS=0 the slope is highest just after the 0.2 MW mark, then decreases.
No difference is observed between PV and PVT, since only electrical energy is counted in f_sh and their electric output is identical by assumption.

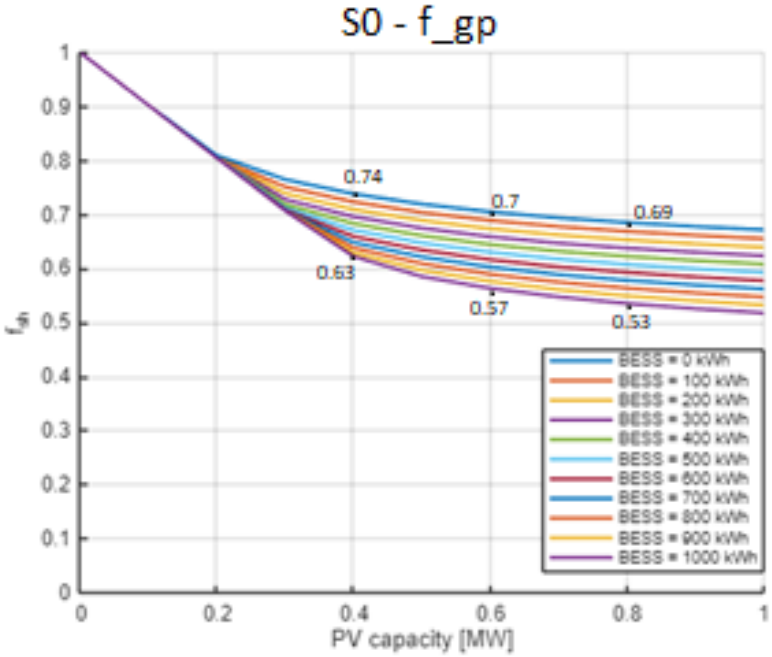

Figure 17: fraction of energy purchased from the grid vs PV capacity with photovoltaic panels

The fraction of electricity purchased from the grid (f_gp) exhibits a clear downward trend as the installed capacity of PV/PVT increases. This trend highlights the growing contribution of local renewable generation in meeting the building's electrical demand. At small PV sizes, f_gp is close to 1, indicating near-total reliance on the grid. As PV capacity expands, this dependency diminishes.

Again, battery storage has a positive effect: higher BESS capacities are associated with steeper declines in f_gp. By storing surplus generation, the batteries allow the building to reduce grid purchases even when solar production is low, such as during the evening or on cloudy days.

The grid purchase fraction (f_gp) decreases as PV capacity increases, from values above 0.9 down to approximately 0.67 at 1 MW with no BESS.
The initial drop is steep (especially between 0.1 and 0.3 MW), showing that a small PV system already displaces a significant portion of grid electricity. Beyond 0.4 MW, the curve begins to flatten, approaching a plateau as the system covers most of the load during daylight.
Adding BESS further reduces f_gp (down to ~0.51 with 1 MWh BESS), thanks to stored surplus being used locally instead of relying on the grid.
No difference between PV and PVT, as only electric energy is considered and PVT thermal contribution reduces NGB fuel consumption in this scenario.

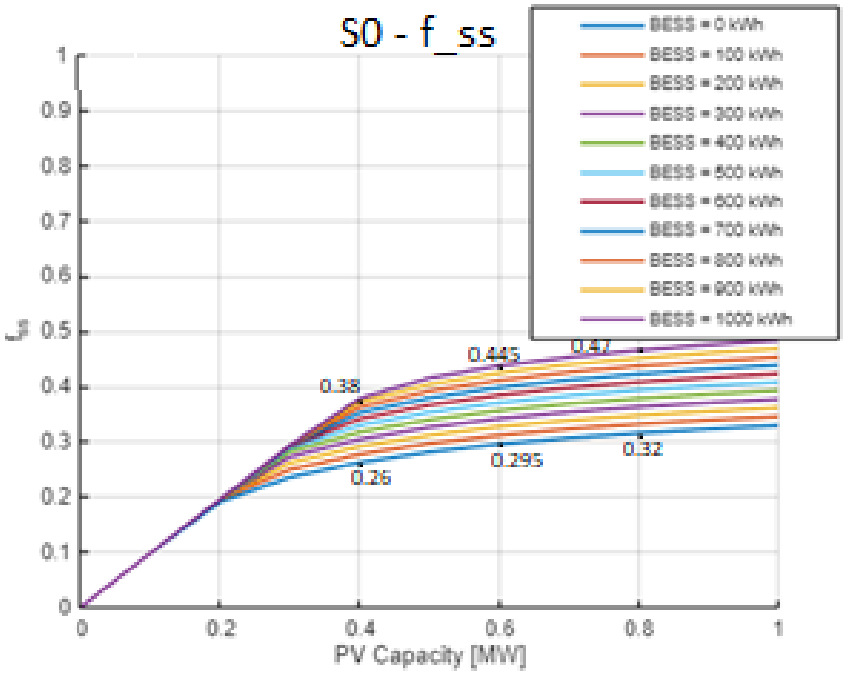

Figure 18 : self-sufficiency fraction vs PV capacity with photovoltaic thermal panels

The self-sufficiency fraction (f_ss) measures the proportion of the building's total electrical energy demand that is satisfied through on-site generation and storage.

In Scenario S0, although PVT panels can provide thermal energy, their contribution does not affect f_ss, as this indicator considers only electrical energy flows.

An increase in PV/PVT capacity or BESS size enhances f_ss, as more electricity can be generated and utilized internally. The performance curves tend to rise gradually, confirming the positive influence of storage in reducing grid reliance and promoting greater energy independence.

For BESS = 0, f_ss increases rapidly up to ~0.2 MW PV capacity. Beyond this point, the slope flattens significantly as PV production starts to exceed on-site demand indicating that most of the load is already met, but the lack of storage limits further improvements.
At 1 MW and no BESS, f_ss reaches ~0.33
With increasing BESS size, the curves continue to grow beyond 0.2 MW PV, up to 0.38MW, as excess electricity can now be stored and reused. The slope becomes smoother and the system benefits from temporal shifting of renewable generation, with diminishing returns at higher capacities.
At 1 MW with 1000 kWh BESS, f_ss reaches around 0.50 . Since thermal energy is not part of the KPI in S0, PV and PV configurations overlap in self-sufficiency fraction.
Overall, in S0 the self-sufficiency improvement is driven exclusively by electrical generation and storage.

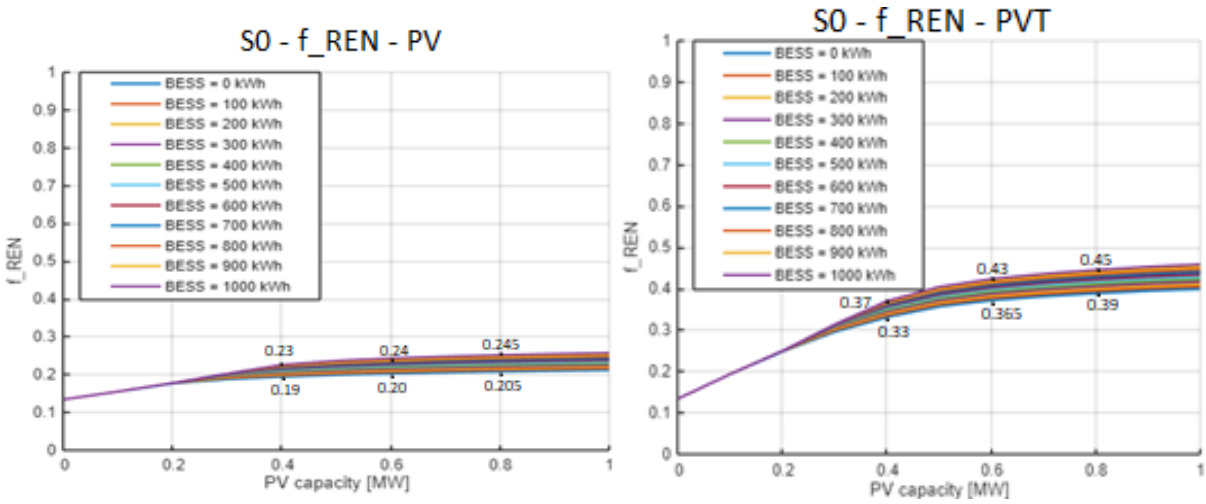

Figure 19: a) reneweable energy share vs PV capacity with photovoltaic panels. B) reneweable energy share vs PV capacity with photovoltaic thermal panels

The renewable energy fraction (f_REN) reflects the proportion of the building's energy demand that is met using renewable sources. As expected, this fraction increases with the expansion of the PV/PVT field. Larger BESS capacities also support this increase by enabling better use of generated electricity.

The difference between the PV and PVT configurations is minimal due to the system architecture, where the thermal contribution of PVT is limited to domestic hot water. As a result, f_REN values are similar across both cases, confirming that the thermal side of PVT does not significantly influence this KPI under the current setup. The shape of the curves tends to rise quickly with early increases in PV capacity, then plateau as saturation effects emerge. This reflects a diminishing return, where further generation adds less to the renewable share due to system limitations in consumption and storage.

- Initial growth: f_REN increases rapidly up to ~0.18–0.22 around 0.4 MW PV capacity. Beyond this threshold, the slope decreases significantly.
- Saturation: After 0.4 MW, the system reaches partial saturation, especially due to the absence of thermal integration—which limits further renewable contributions.
- PV vs PVT: PVT consistently yields higher f_REN values than PV, with differences up to ~0.2 at 1 MW. This occurs because PVT thermal output is counted as renewable.
- Impact of BESS: Increasing BESS size has a limited impact compared to other indicators. The lack of thermal demand matching reduces the ability to store and use excess renewable energy efficiently.

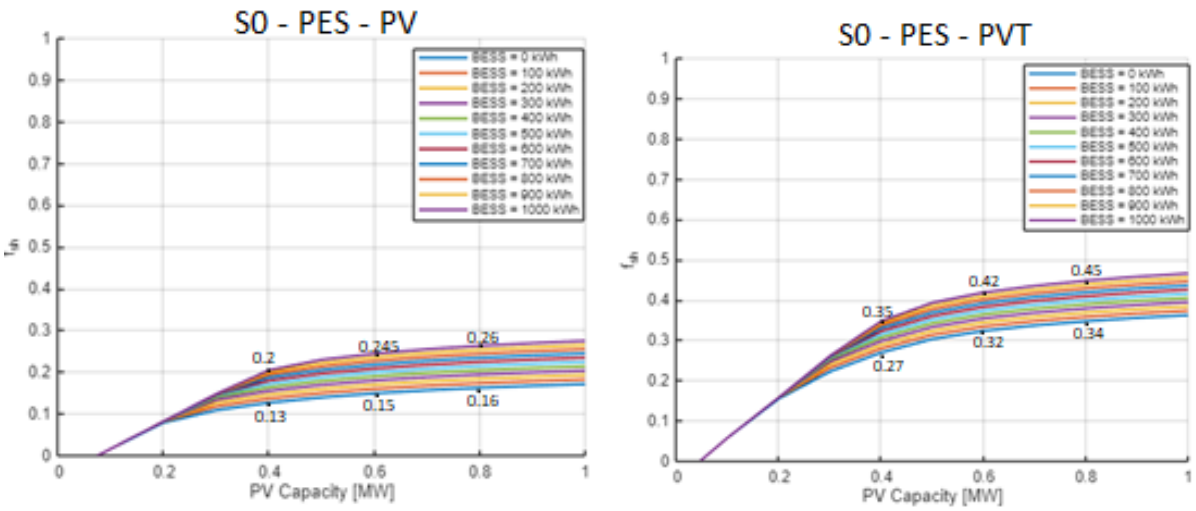

Figure 20: a) Primary Energy Saving vs PV capacity with photovoltaic panels. b)Primary Energy Saving vs PV capacity with photovoltaic thermal panels

The PES indicator reflects the reduction in primary energy demand resulting from the integration of renewable sources with values rising in response to increasing PV or PVT capacity and enhanced BESS storage.

PVT systems generally achieve slightly higher PES values compared to PV-only setups. This can be attributed to the additional thermal contribution provided by the PVT modules, which, although modest in Scenario S0, still offers a small improvement in energy performance.

The curves rise steeply at first, signaling effective primary energy displacement at lower capacities, and then gradually level off due to the system's saturation limits. A consistent yet narrow gap between the PV and PVT configurations is observable, highlighting a marginal benefit from thermal integration. However, this gain remains limited due to the restricted use of thermal energy—only for DHW—in this scenario.

Overall, the data suggest that while PVT provides an incremental boost to primary energy savings, more substantial improvements would require deeper thermal integration through the use of heat pumps and expanded TES capacity.

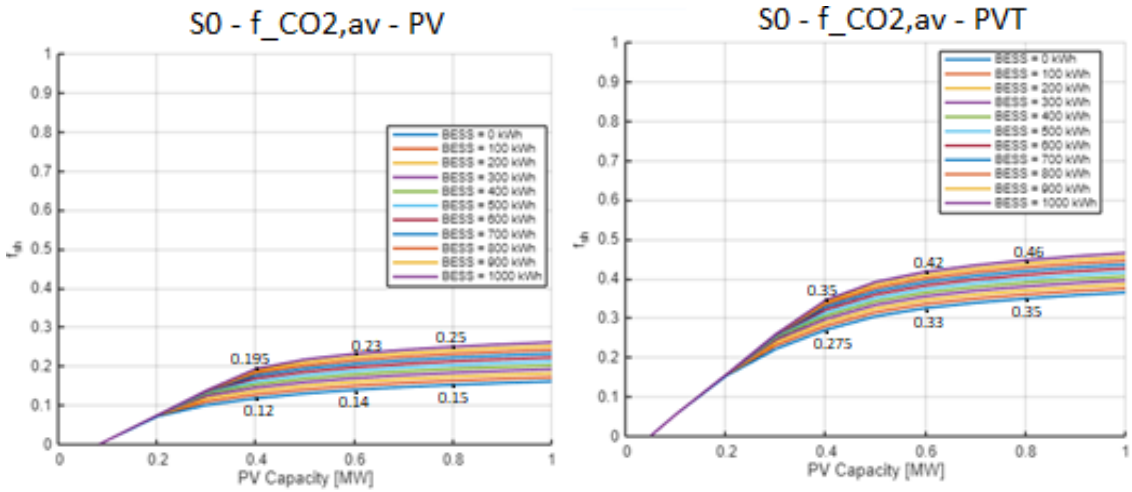

Figure 21: a) fraction of avoided CO2 emissions vs PV capacity with photovoltaic panels. b) fraction of avoided CO2 emissions vs PV capacity with photovoltaic thermal panels

The $f\_CO_2\_av$ index represents the reduction in emissions due to renewable substitution. As expected, its trend closely follows that of PES, it increases with PV/PVT capacity and is reinforced by larger BESS capacities.

The presence of the PVT system introduces a small but consistent improvement in CO_2 savings. This difference stems from the thermal displacement of fossil-based DHW production, though its impact remains limited in this scenario.

The curve shape is quasi-logarithmic: sharp increases are seen at first, followed by a plateau, reflecting the ceiling effect of system limitations in generation or storage.

The CO_2 savings indicator f_CO_2,avg increases with PV capacity, with an initial steep rise up to ~0.4 MW, followed by a noticeable flattening beyond this point, especially without BESS.

At 1 MW with no storage, f_CO_2,avg reaches about 0.18 with PV and about 0.37 with PVT, showing an advantage of PVT. This is due to thermal output of the PVT decreasing the NGB load
Adding BESS gradually improves performance: with 1000 kWh, values reach up to ~0.27 for PV and ~0.48 for PVT.
The improvement from storage is more linear at higher PV sizes but diminishing returns are still visible.
Differences between PV and PVT are consistent across all storage sizes.

III.2. S1 Results analysis

Scenario S1 introduces a hybrid heat pump (HHP) to support the natural gas boiler in meeting thermal demands. The presence of the HHP enables partial electrification of the system and enhances the use of renewable electricity for both space heating and DHW production. In this scenario BESS was varied with a different step (0-100-500-1000kWh), since also the TES capacity was varied.

The f_sc curves in Scenario S1 mirror the overall behavior seen in S0 (fig.14). At low PV/PVT capacities, the system is capable of consuming nearly all the energy produced on-site, resulting in high self-consumption values. As generation capacity increases, the proportion of surplus electricity grows, causing f_sc to gradually decline.

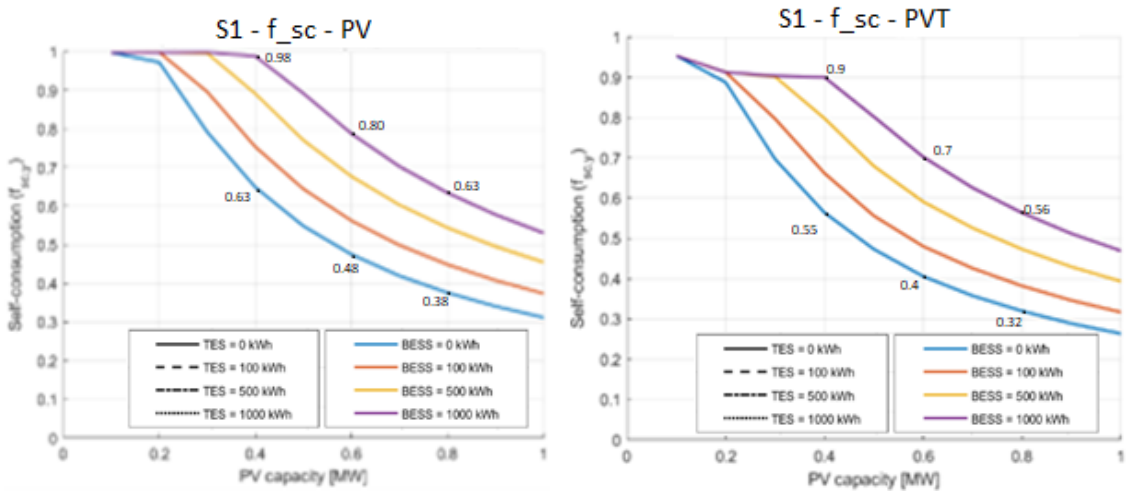

Figure 22:a) self-consumption fraction vs PV capacity with photovoltaic panels. b) self-consumption fraction vs PV capacity with photovoltaic thermal panels

However, with the integration of TES and HHP, the system can absorb part of the excess electricity by converting it into heat. This, combined with the battery's storage capability, contributes to slightly improved f_sc values, especially in PVT cases where thermal output is available. Nonetheless, the thermal component's influence remains secondary, and differences between PV and PVT remain minor.

The transition from blue to purple in the curves reflects increasing BESS capacity, which consistently enhances self-consumption across all generation levels.

when a hybrid heat pump (HHP) is introduced, f_sc still decreases as PV capacity increases, due to the same surplus effect. However, adding battery storage leads

to a notable increase in self-consumption, as excess electricity can be stored and reused later. When comparing PV and PVT configurations, PVT shows a slightly higher f_sc at low PV capacities, as the thermal contribution from the PVT panels supports the HHP, increasing on-site energy use. At higher PV sizes, especially from 0.8 MW onward, the HHP already satisfies the domestic hot water (DHW) demand entirely, meaning the additional heat from the PVT system becomes redundant. As a result, the advantage of PVT over PV diminishes. This highlights that the benefit of PVT systems in Scenario S1 is dependent on whether the thermal demand and the thermal energy storage (TES) system are saturated or not.

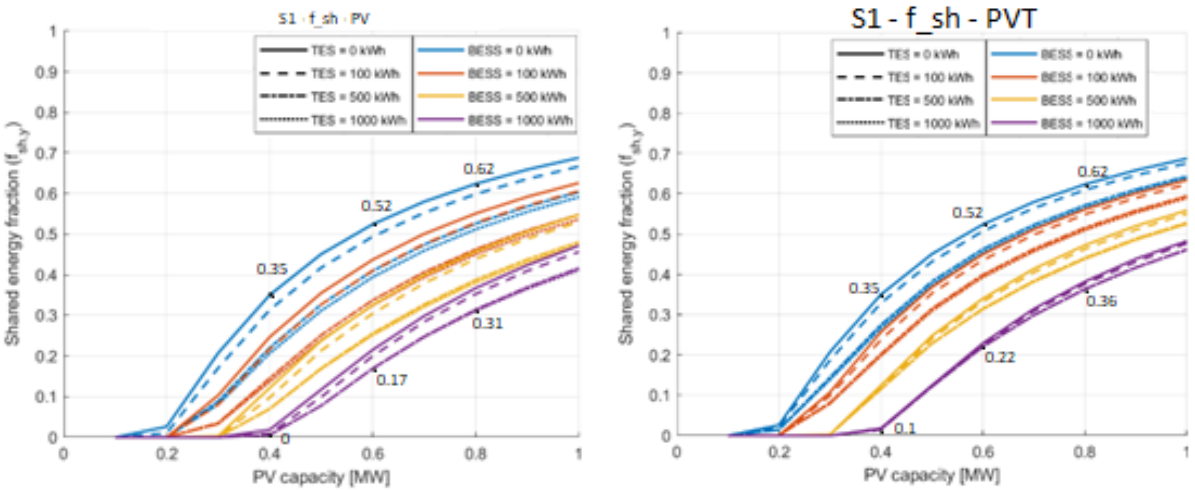

Figure 236: shared energy fraction vs PV capacity with a) photovoltaic panels and b) photovoltaic thermal panels

The shared fraction increases with PV/PVT capacity due to the production of surplus electricity, particularly when BESS capacity is limited. Larger batteries mitigate this by capturing excess energy, reducing the need to export to the grid.

- Although PVT systems can produce additional thermal energy, f_sh focuses on the portion of generated electricity that is not self-consumed and is instead exported to the grid. Although one might expect that PVT systems could increase this surplus by lowering electricity demand through thermal support to the HHP, the actual impact remains negligible in this configuration. This is likely due to the relatively small contribution of thermal energy from PVT modules, which only marginally reduces the HHP's electrical consumption.The threshold for shared energy again

appears around PV = 0.2 MW, after which f_sh increases with PV size, similar to S0.

- At any given BESS size, PVT curves lie slightly above PV curves: a constant ~35% difference between the to consistently along the incrementation of PV capacity; benefits from a larger BESS at high PV capacity installed grow more linearly.
- Enabling PVT systems allow for auxiliary heating power, resulting in higher values of f_sh since the electrical load of the heat pump is lower, and moe energy can be shared. With a 1 MW BESS, f_sh increases by 5% at 0.6 and 0.8 MW of PV capacity installed.
  Without BESS, the potential benefit of thermal support is not reflected in a higher shared fraction, and the curves for PV and PVT overlap more closely, meaning the storage enables a more flexible use of energy.

  Additionally, the thermal energy saved by PVT might be stored in TES, but if the thermal demand is already mostly satisfied or the TES is undersized, this contribution becomes marginal and does not affect the electric sharing fraction significantly. This is reflected by the TES curves reaching only 2/3% better values, with the highest benefit of 0.4% being when a 1 MWh battery is employed

- Increasing BESS lowers f_sh, flattening the curves, especially at higher PV, confirming storage absorbs excess rather than sending it to the grid.
- Curves grow steadily but with reduced slope as PV increases: the initial steepness tapers off, approaching a plateau at higher PV. This behavior is due to the saturation of on-site energy needs: at low PV sizes, each additional kilowatt of PV directly offsets grid consumption, making a significant contribution to shared energy once demand is met. However, as PV capacity continues to rise, more energy is produced during periods when loads are already covered. At that point, additional generation simply adds to surplus without proportionally increasing the fraction of energy that can be shared, especially when BESS capacity is limited. Hence, the marginal gain in shared fraction decreases, causing the curve to flatten out.

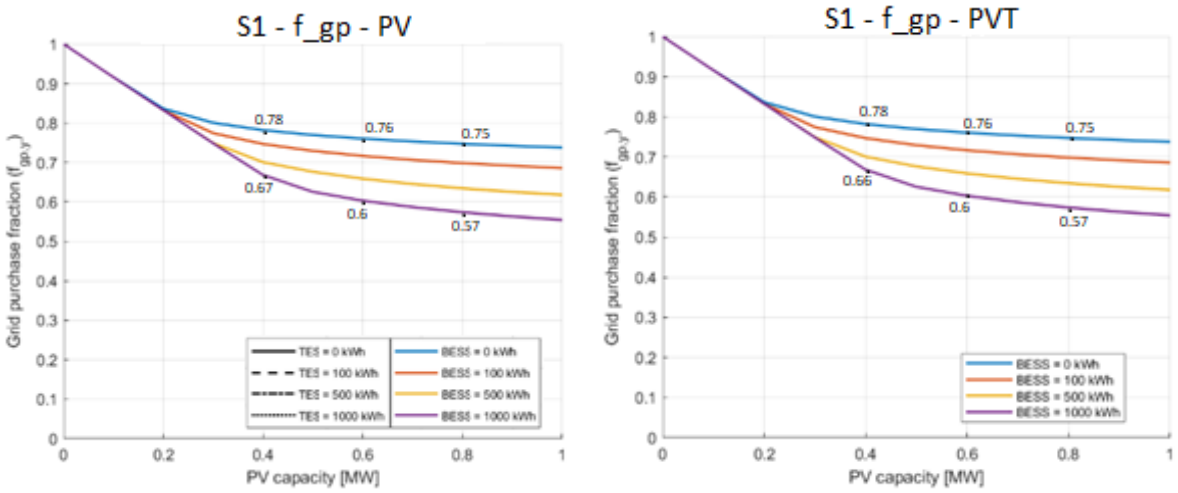

Figure 24: a) grid purchase fraction vs PV capacity with photovoltaic panels. b): grid purchase fraction vs PV capacity with photovoltaic thermal panels

Grid dependency decreases with increasing generation capacity, as more of the load is supplied locally. The inclusion of BESS further reduces reliance on grid electricity by compensating for PV intermittency.

Although f_gp is primarily influenced by the electrical balance of the system, slight differences can be observed between PV and PVT configurations. This is likely due to the marginal reduction in electrical consumption of the HHP when it is thermally assisted by the PVT system. However, since the thermal support provides only a limited benefit under the modeled conditions, the resulting variation in f_gp remains small. As a result, the trends remain largely comparable, but separate graphs for PV and PVT are presented to highlight these subtle distinctions.

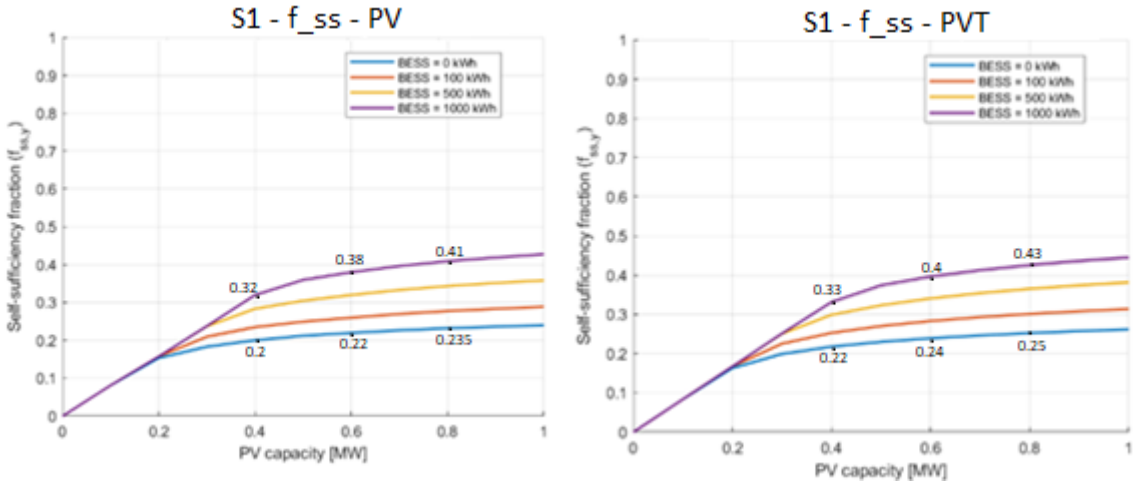

Figure 25: a) self-sufficiency fraction vs PV capacity with photovoltaic panels. b) self-sufficiency fraction vs PV capacity with photovoltaic thermal panels

The integration of the hybrid heat pump makes f_ss a more meaningful metric. As more of the building's total energy demand is met internally—both through direct consumption and storage—the self-sufficiency of the system improves.

PVT configurations exhibit slightly higher values of f_ss due to the additional thermal contribution stored in the TES wich allows the system to effectively utilize P2H strategies.

The curve shape reveals diminishing gains with increasing generation capacity, indicating that beyond a certain threshold, additional PV/PVT capacity offers limited benefits without a proportional increase in storage.

Adding the HHP, which uses both electricity and natural gas, changes the load profile. Electricity demand increases compared to S0, but part of the thermal load is shifted to gas.
f_ss remains close to S0 at low PV capacities, but becomes noticeably higher with large BESS sizes and PVT, as the thermal contribution of PVT reduces electric load on the HHP.
The slope change appears around 0.35–0.4 MW, where production starts to exceed consumption. Without BESS, surplus is lost; with BESS, it is stored and used later, achieving higher values of self-sufficiency fraction and flattening the curves progressively.
PVT performs better than PV in S1, especially with high PV capacity and storage, due to better electric load matching and reduced waste.

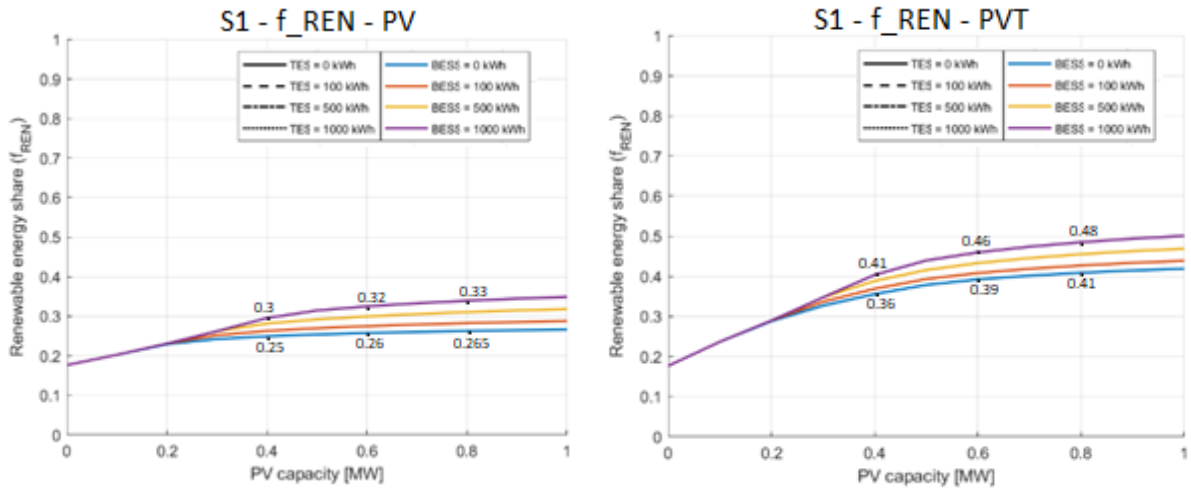

Figure 26:a) Renewable energy share vs PV capacity with photovoltaic panels. b) : Renewable energy share vs PV capacity with photovoltaic thermal panels

In Scenario S1, f_REN increases with both PV/PVT capacity and storage. The influence of TES becomes more significant compared to S0, as the thermal energy generated by PVT panels is no longer limited to immediate DHW use but can now be stored and deployed later to support the hybrid heat pump (HHP) in covering thermal loads.

This enhanced thermal integration grants PVT systems a more distinct advantage over their PV-only counterparts. As a result, the PVT curves tend to rise above those of PV, indicating a higher renewable energy share driven by the combined electrical and thermal contributions. Higher f_REN overall: Electrification of the thermal load through the HHP boosts renewable energy use compared to S0.

PVT advantage remains: PVT continues to perform better than PV, though the gap is slightly narrower than in S0. This is because some thermal demand is met by natural gas in the HHP, partially reducing the effect of thermal energy from PVT.
The thermal storage (TES) starts to play a visible role, especially when coupled with PVT. It enables more renewable heat to be shifted and used, thus raising f_REN.
A noticeable slope reduction occurs around 0.4 MW, but the decline is softer than in S0 due to improved system integration.

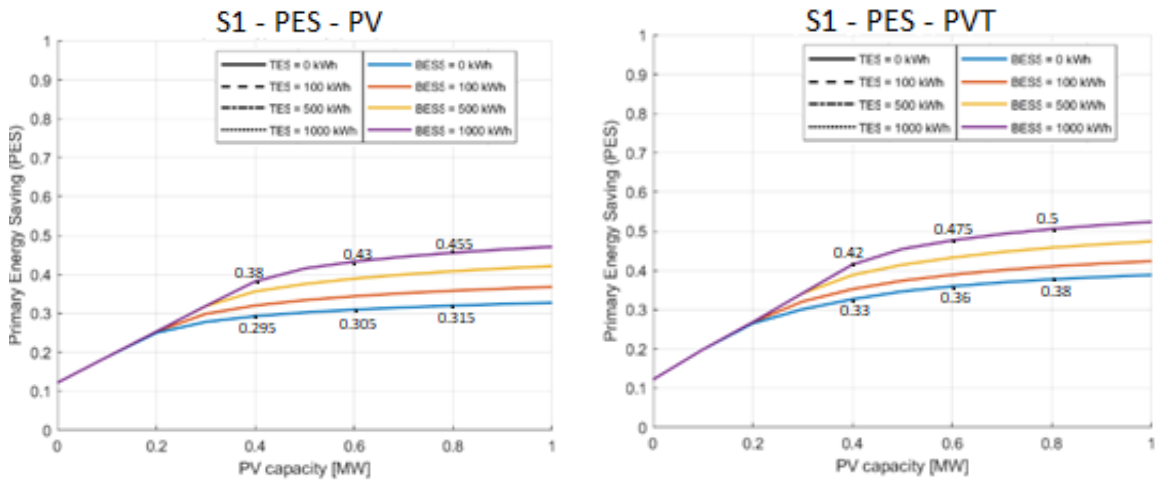

Figure 27: a) Primary Energy Savings vs PV capacity with photovoltaic panels. b) Primary Energy Savings vs PV capacity with photovoltaic thermal panels

PES in Scenario S1 highlights the combined effect of increased renewable generation and improved thermal integration. The system achieves notable energy savings by reducing both electrical imports and fossil fuel use.

PVT configurations again outperform PV-only systems, although the difference remains moderate. The role of HHP and TES is central in achieving higher PES, as these components enable better alignment between generation and demand.

The curves show a steep rise at lower capacities, followed by gradual saturation, suggesting that further improvements would require enhanced control strategies or demand-side management.

The inclusion of HHP (hybrid heat pump using electricity and NG) slightly shifts the energy balance.

- PES is generally higher than in S0 due to partial electrification of heating and the contribution of storage in optimizing electricity usage.
- With PVT, the curves again lie above those with PV, but the difference is slightly less pronounced than in S0. This is likely due to the simultaneous use of NG in the HHP, which limits the primary energy savings achievable via thermal recovery from PVT.
  BESS continues to be a major driver: for example, moving from 0 to 1000 kWh can increase PES by up to 0.15 points at 1 MW PV.
  TES has minimal impact in this scenario, as the thermal load is still partially covered by NG, which reduces the benefits of storing thermal energy

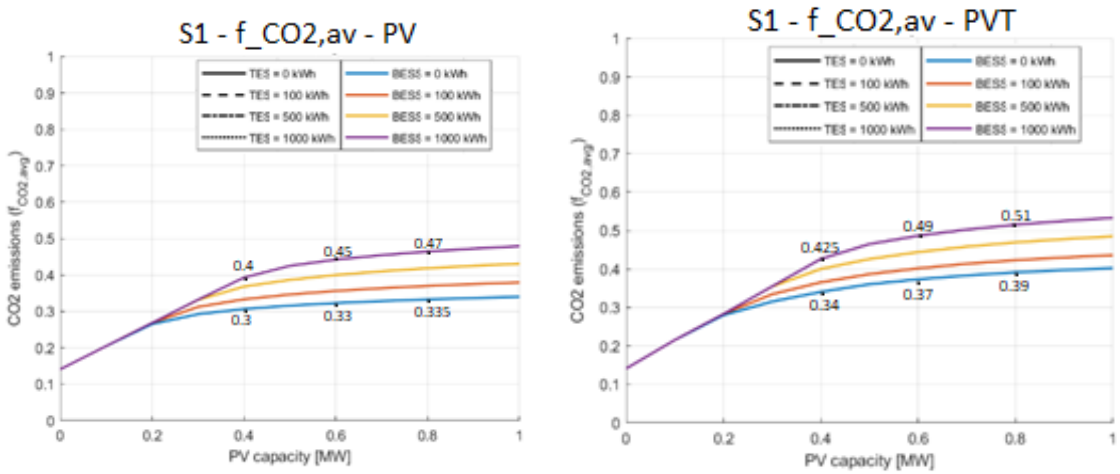

Figure 28:a) fraction of avoided CO2 vs PV capacity with photovoltaic panel. b) fraction of avoided CO2 vs PV capacity with photovoltaic thermal panel

The $f\_CO_2\_av$ indicator demonstrates notable improvements as BESS capacity increases, reflecting the system's enhanced ability to store and utilize renewable electricity. The integration of the hybrid heat pump (HHP) contributes to these

savings by partially electrifying the thermal load and thereby decreasing reliance on natural gas. While the PVT system also contributes thermal energy, its impact on CO_2 savings remains limited under the current simulation setup.

Nonetheless, a small but consistent benefit from the use of PVT over PV is visible across all configurations. This occurs because the thermal energy provided by PVT modules can assist the HHP in satisfying heat demands, leading to reduced consumption of both natural gas and electricity.

The use of TES introduces a new storage dynamic, allowing PVT to partially store and later utilize its thermal output, which benefits f_CO_2,avg clearly.

With PV, CO_2 savings slightly increase compared to S0, but improvements are modest due to limited thermal integration.

With PVT, the benefit is more noticeable. At 1 MW and 1000 kWh of BESS, f_CO_2,avg reaches –0.53, while PV remains below 0.49.

The transition at ~0.4 MW remains a key inflection point for both technologies, but the flattening is slower for PVT, especially thanks to TES since at high PV capacity thermal load is already fulfilled. The combination of TES and BESS creates a synergistic effect for PVT, allowing better matching of generation and thermal demand, especially in winter.

III.3. S2 results analysis

This third configuration includes the integration of an air-source heat pump (HP) to cover the thermal energy demand, both for space heating and domestic hot water. As already observed in the previous sections, the system explores variations in the sizes of the Battery Energy Storage System (BESS), the Thermal Energy Storage (TES), and the photovoltaic (PV) or photovoltaic-thermal (PVT) fields.

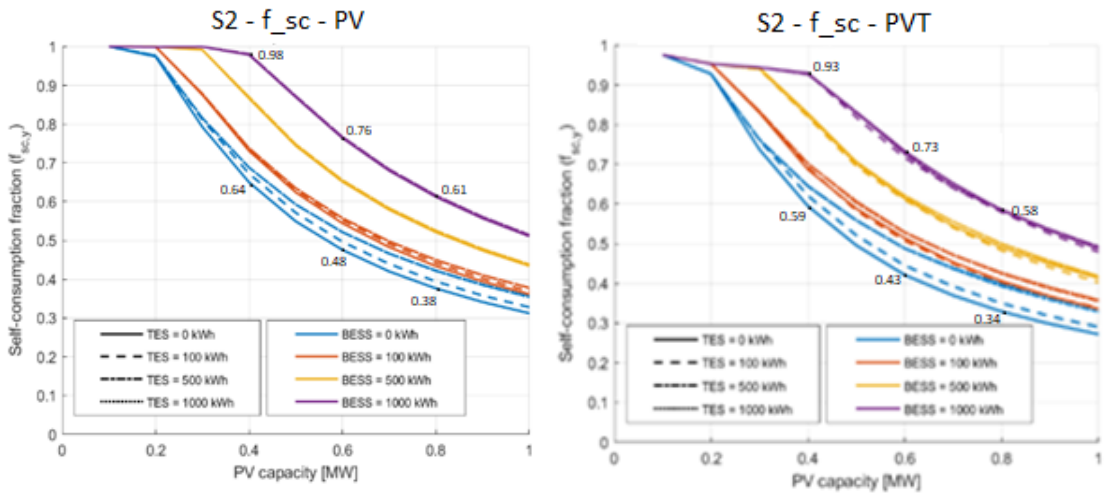

Figure 29: a) self-consumption fraction vs PV capacity with photovoltaic panels. b) self-consumption fraction vs PV capacity with photovoltaic thermal panels

As the PV/PVT capacity increases, the self-consumption fraction (f_sc) initially remains high and then tends to decrease. This is because at low PV capacities, the majority of produced electricity is directly consumed, while increasing production leads to surplus energy that cannot always be absorbed on-site. Conversely, increasing the BESS capacity allows a higher share of self-consumed energy, resulting in upward shifts in the curves from blue to purple. This behavior is consistent with the ability of larger batteries to store excess electricity and make it available during non-generating hours. Notably, the curves often remain constant at values close to 1 until a critical threshold of PV capacity is reached. This threshold represents the point at which the energy produced starts to exceed the building's immediate consumption needs, leading to surplus energy. The exact position of this turning point depends on the sizes of both the battery and the thermal storage: larger storage systems can absorb more excess energy, allowing the system to maintain high self-consumption levels for a wider range of PV capacities.

When an electric heat pump (HP) and TES are both integrated, the larger thermal storage capacity slightly raises the self-consumption curves across all PV sizes. For the PV configuration, f_sc increases from approximately 0.29 to around 0.53 as battery capacity increases from 0 to 1 MWh. For PVT, the same storage range results in an increase from about 0.31 to 0.50. The presence of TES in this scenario enables a more effective absorption of thermal surplus and facilitates power-to-heat (P2H) conversions, thereby reducing the electricity drawn from the grid. The

gap between PV and PVT configurations in terms of f_sc is more noticeable at low to medium PV sizes, where the thermal contribution of PVT is still effectively utilized to support the heat pump before saturation effects occur.

The shared fraction (f_sh) follows an opposite trend to f_sc: it increases with the PV capacity due to the larger amount of excess energy that cannot be used on-site. At fixed BESS capacity, curves shift upward as PV capacity grows. However, increasing battery size results in a downward trend of f_sh, since more energy is stored and consumed locally. Some curves display a plateau at zero before rising, indicating that at low generation levels, nearly all electricity is self-consumed.

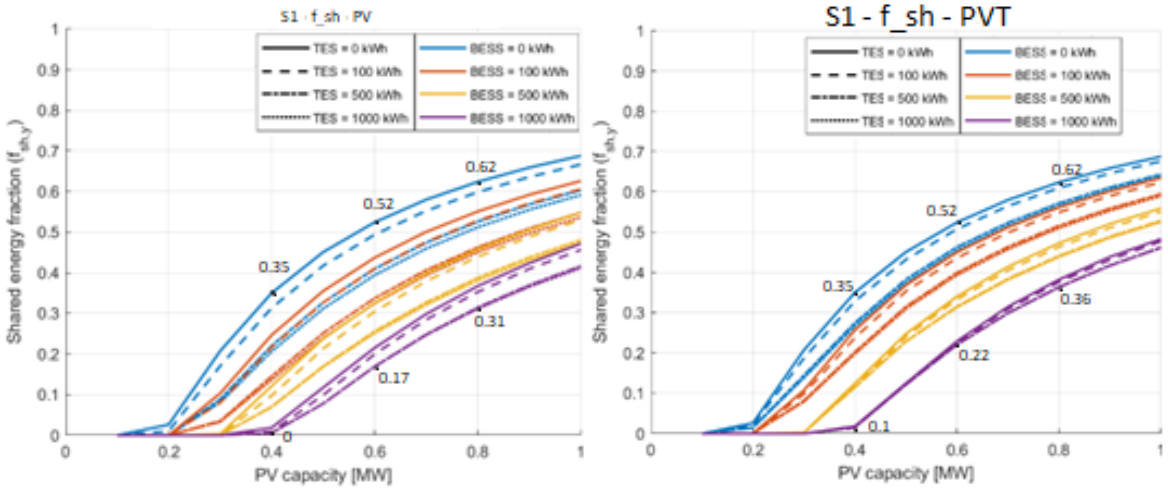

Figure 30: a) shared energy fraction vs PV capacity with photovoltaic panels. b) shared energy fraction vs PV capacity with photovoltaic thermal panels

Interestingly, f_sh curves for PV and PVT are very similar. This is due to the assumption adopted in the model, where the electrical efficiency of PVT panels was approximated to that of standard PV modules. This simplification was necessary to avoid simulation instabilities caused by thermal-electrical coupling. The expected minor gains in efficiency due to PVT cooling were therefore not considered, which constitutes a limitation of the model.

- PVT vs PV: with a 1 MWh BESS, PVT leads to slightly higher f_sh than PV: 0.1% at 0.6MW, o.2% at 0.8 MW, due to part of the electrical output being diverted to the thermal system, increasing exportable energy. The trend PVT > PV is preserved but the effect is negligible. Without BESS the curves converge (both around ~0.7), since the battery absorbs excess energy allowing a better use.

- The TES size has limited effect on f_sh in either case
- The curve shape remains consistent, with f_sh ≈ 0 until PV > 0.2 MW, then steadily increasing. The slope decreases as PV capacity grows, due to saturation of local consumption and storage.

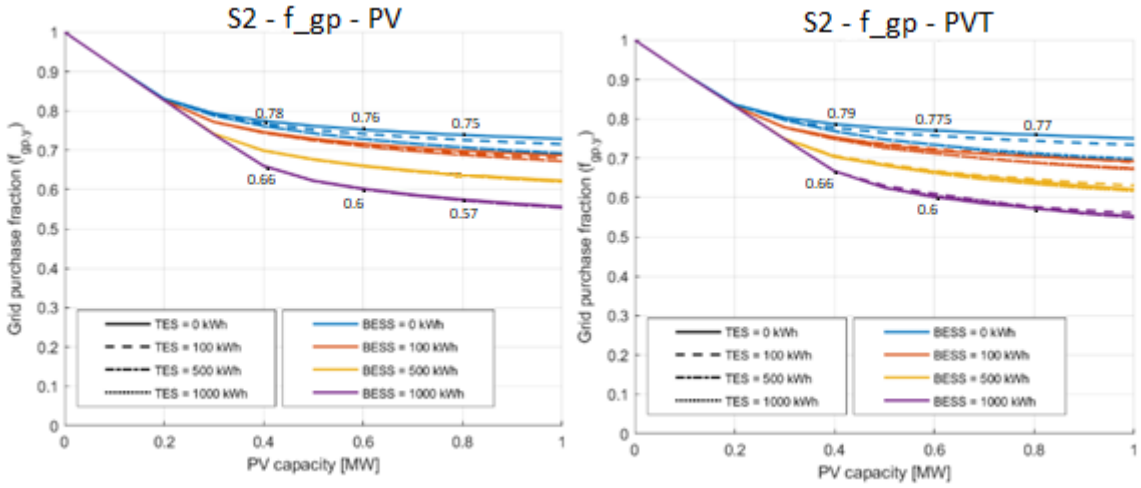

Figure 31:a) fraction of energy purchased from the grid vs PV capacity with photovoltaic panels. b) fraction of energy purchased from the grid vs PV capacity with photovoltaic thermal panels

The grid purchase fraction (f_gp) decreases with increasing PV/PVT capacity, as more of the building's electrical load is met by on-site generation. A higher BESS capacity further reduces the dependency on the grid, evident in the descending curve trends from blue to purple. At low PV sizes, the f_gp is close to 1, meaning that almost all electricity is drawn from the grid. As the PV field grows and storage becomes more effective, the reliance on external supply drops significantly. f_gp is lower than in S1, particularly at high PV capacity and no BESS: e.g., ~0.77 for PV and ~0.73 for PVT at 1 MW. With BESS equal to1 MWh, f_gp drops to 0.57 (PV) and 0.55 (PVT), aligning closely with S1 values.

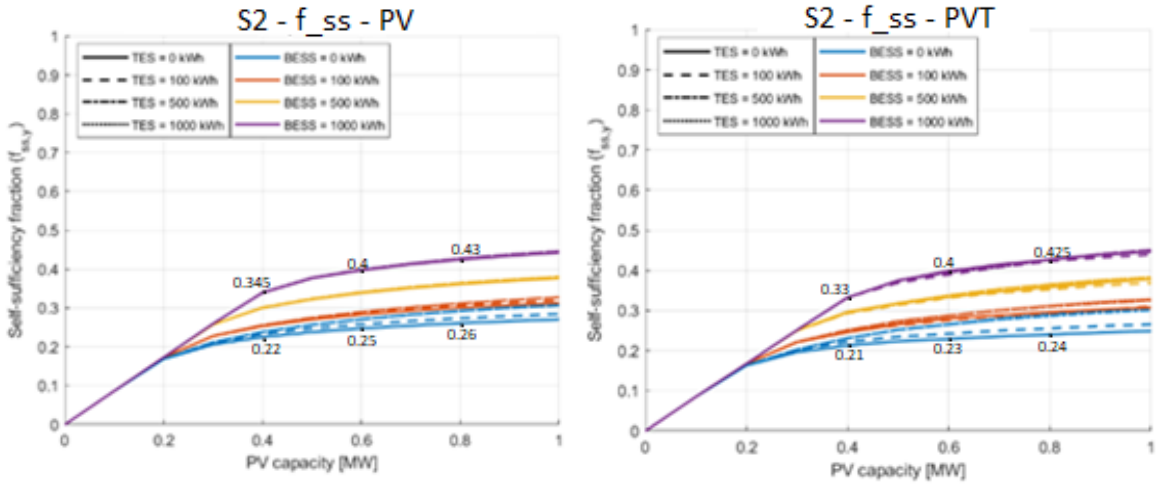

Figure 32: a) self-sufficiency fraction vs PV capacity with photovoltaic panels. b) self-sufficiency fraction vs PV capacity with photovoltaic thermal panels

In both configurations, the self-sufficiency fraction increases with PV capacity, but the influence of storage becomes increasingly significant at higher PV sizes. At low capacities (below ~0.3 MW), all configurations perform similarly, suggesting that storage plays a limited role when PV generation is modest. However, as PV capacity increases, the curves diverge: larger BESS and TES capacities enable the system to store and utilize more surplus energy, resulting in significantly higher self-sufficiency.

This indicates that while initial gains in fss are primarily driven by the generation side, the contribution of storage is critical in harnessing surplus PV energy and shifting it in time—particularly beyond 0.5 MW, where systems with larger storage continue to improve while those with limited or no storage begin to saturate.

The comparison between PV and PVT shows similar trends: differences in the curves are mainly due to thermal contributions via TES, which are more effectively exploited in the PVT scenario.

In conclusion, both BESS and TES are essential for enhancing self-sufficiency at higher levels of PV penetration, with PVT systems offering additional benefits when coupled with appropriate thermal storage.

S2 shows the highest f_ss values among all scenarios. The HP is more efficient than the HHP, consuming less electricity to meet the same thermal demand.

When PVT is used, its thermal output further enhances the performance of the HP, reducing electricity consumption and improving self-sufficiency.

The effect is most visible with large BESS sizes: the gap between PV and PVT increases, as surplus energy can be effectively stored and later used.

Curve slopes change around 0.4 MW, and then start flattening due to saturation. However, the flattening is slower than in S1, due to better synergy between HP and PVT.

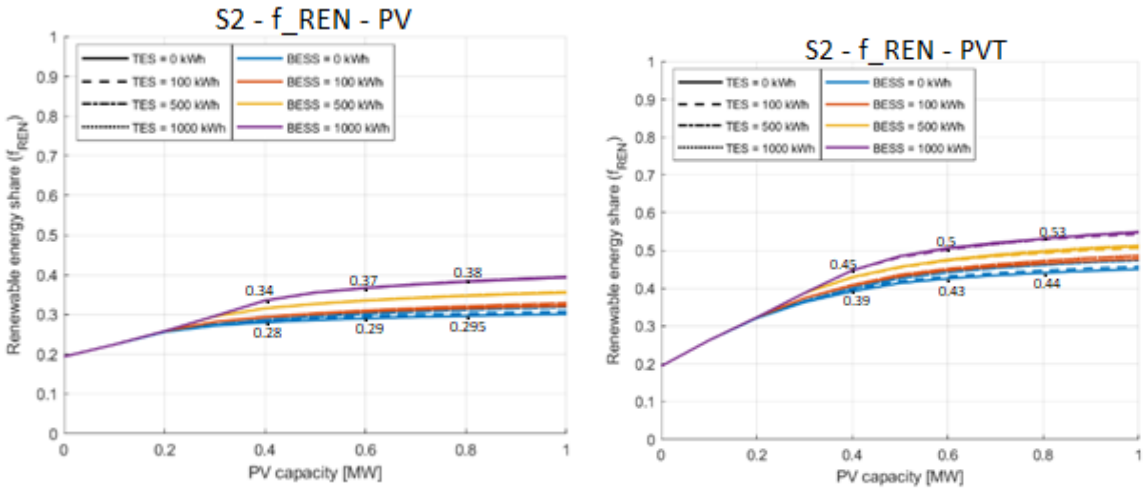

Figure 33: a) reneweable energy share vs PV capacity with photovoltaic panels. b) reneweable energy share vs PV capacity with photovoltaic thermal panels

The renewable energy share f_REN is influenced by both PV generation and the reduction in fossil-based grid imports. At low PV capacities, f_REN remains modest, but it progressively increases with the addition of generation and storage. Larger BESS sizes enhance local renewable electricity use and improve the temporal alignment between production and consumption, contributing significantly to higher f_REN values.

The effect of TES on f_REN is linked to how the stored heat is produced. While TES directly operates in the thermal domain, its contribution to renewable energy share becomes relevant when thermal energy is provided by a heat pump powered by renewable electricity. In this configuration, TES enables the storage and later use of renewable-sourced thermal energy, supporting further displacement of fossil fuel-based heating.

Unlike indicators such as f_sc, which mainly track electrical energy flows, f_REN is directly affected by the electrification of thermal loads. The presence of a heat pump is therefore crucial, as it allows part of the thermal demand to be met using electricity, effectively coupling renewable electricity generation with thermal consumption and increasing the overall renewable share of the system.

S2 shows the highest f_REN values across all configurations: The HP has higher COP than the HHP and fully relies on electricity, making it more suitable for integration with RES.
Thermal energy from PVT directly reduces HP electrical consumption, boosting f_REN, especially when TES is present.
PV vs PVT gap widens: in this scenario, the difference between PVT and PV is more pronounced, especially with large storage sizes, due to better utilization of thermal output.
In this configuration, PES increases linearly up to ~0.3–0.4 MW PV capacity, after which the slope decreases significantly due to limited self-consumption and the absence of thermal optimization (TES is not involved).
At 1 MW, 1000MWh electrical storage, PES reaches ~0.28 with PV and ~0.47 with PVT. The higher PES in PVT is due to the additional thermal energy recovered, which reduces fossil fuel consumption.
Increasing BESS boosts PES, especially in the 0.3–0.6 MW range, where PV production starts to exceed immediate demand.
Threshold effect: After 0.4–0.5 MW, PES gains taper off, indicating saturation of storage or reduced load-matching capability.
The PVT configuration outperforms PV in all cases due to its dual energy output, despite having the same electrical efficiency.
The slope starts to flatten around 0.6 MW, indicating that storage helps delay saturation, particularly when both BESS and TES are well-sized.

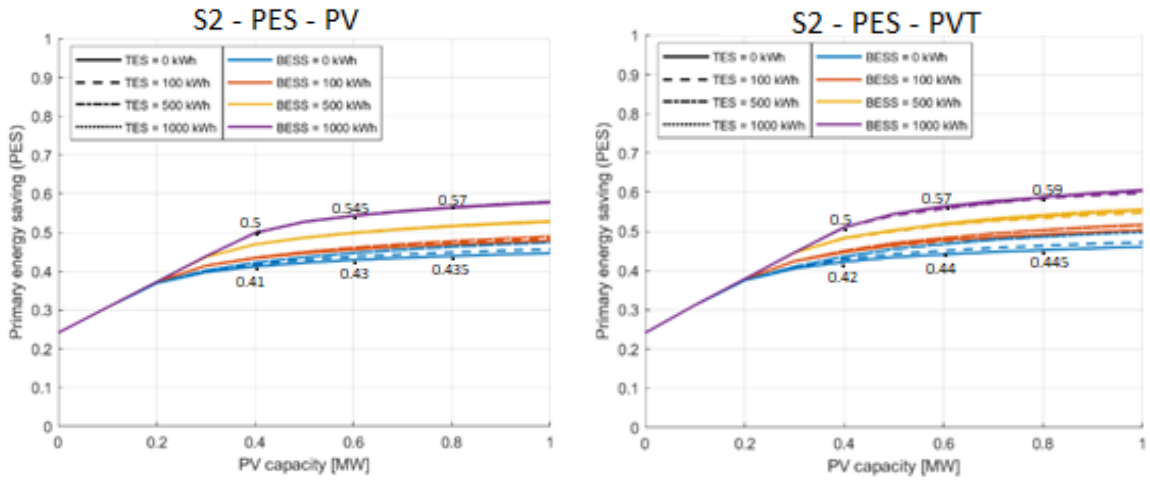

Figure 34:a) Primary Energy Saving vs PV capacity with photovoltaic panels. b) Primary Energy Saving vs PV capacity with photovoltaic thermal panels

The PES increases with both PV capacity and BESS, confirming the improved system efficiency and the reduced reliance on fossil-based primary energy. At low PV sizes, all configurations behave similarly, while the presence of storage becomes increasingly important as generation grows. Larger BESS sizes allow for better use of excess electricity, leading to higher PES values.

The integration of the HP contributes significantly to PES, as it replaces gas consumption with electricity, allowing primary energy savings to reflect both electrical and thermal decarbonization.

Some curves tend to flatten at higher PV capacities, especially when large TES or BESS are present. This reflects the fact that, beyond a certain point, most of the local demand is already covered, and additional renewable energy has limited impact on further primary energy reduction.

The system now relies on an electric-only HP, increasing dependency on electricity but offering higher efficiency compared to the HHP.
This translates into the highest PES values across all scenarios, with clear benefits from both BESS and TES.
PVT reaches PES ≈ 0.62 at 1 MW with maximum storage, compared to PV ≈ 0.58, confirming the complementary role of thermal recovery and TES in reducing primary energy needs.
The slope of the PES curves remains steep up to higher PV sizes (~0.45 MW), indicating more sustained gains thanks to storage and efficient load matching.

Unlike S1, TES has a significant role in S2: thermal energy from PVT can be stored and used efficiently by the HP, reducing both electrical and fossil energy needs.

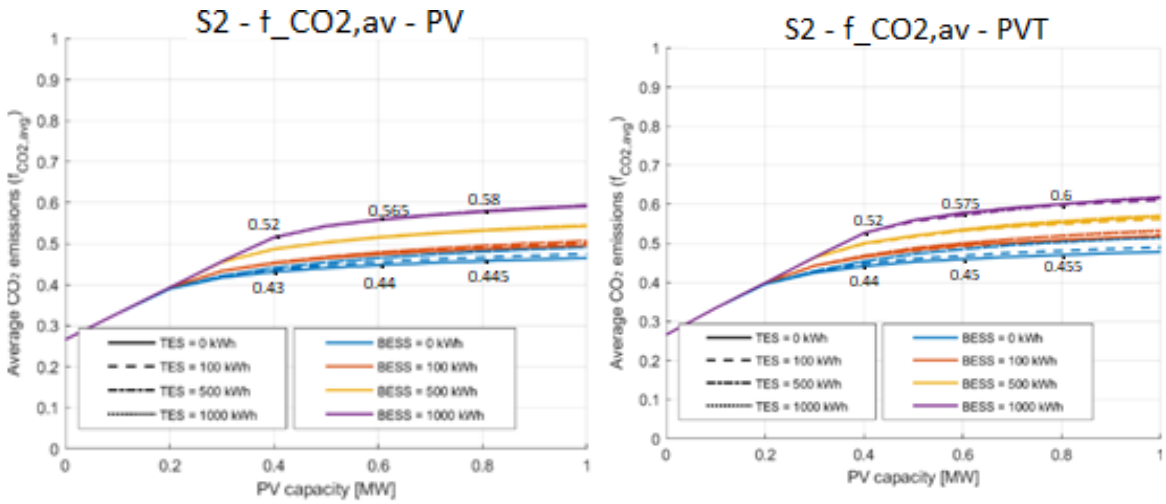

Figure 35:a) fraction of avoided CO2 emissions vs PV capacity with photovoltaic panels. b) fraction of avoided CO2 emissions vs PV capacity with photovoltaic thermal panels

The CO_2 emission reduction follows similar trends to PES, as it is directly tied to the reduction in fossil energy use. A larger PV field and BESS capacity result in significant emissions savings. Again, the HP plays a crucial role: by shifting heating demand from gas boilers to electric heat pumps, it enables a cleaner energy mix. Since the heat pump in this model is used exclusively for space heating to maintain a consistent comparison with the S0 scenario, its contribution becomes particularly relevant during winter, when electricity generated by PV/PVT and stored in the BESS cover thermal loads.

For what regards BESS and TES, there is a visible asymptotic behavior, suggesting that after a certain PV and BESS size, further investments lead to marginal environmental gains.

Scenario S2 shows the highest CO_2 savings overall. This is due to the better performance of the heat pump, which is more efficient than the HHP and uses only electricity (which is decarbonized by RES production), reducing natural gas use.
The gains are especially strong with PVT, which supports the heat pump thermally via TES, further decreasing its electricity consumption and emissions. At 1 MW PV capacity and high storage levels, the fraction of avoided co_2 reaches approximately 0.60 with PV and 0.63 with PVT, the highest values observed across

all configurations. The difference between PV and PVT becomes most visible when no BESS is present, as PVT can exploit its thermal contribution more effectively. Once BESS is introduced, this gap slightly narrows, but not significantly, as the main thermal loads are already satisfied at high PV capacities, and excess energy is increasingly handled electrically. The transition at ~0.4 MW still marks a key inflection point for both technologies. Beyond this threshold, the curves begin to flatten with similar saturation trends, especially under combined BESS and TES configurations. While PVT maintains a performance advantage, the relative improvement decreases as the system approaches full coverage of both thermal and electrical demands.

III.4. Comparative analysis of scenarios and Key Performance Indicators (KPIs)

After analyzing in detail the results of the single scenarios with the different PV/PVT configurations, in this section the comparison between these is presented. To allow for a better understanding, the graphs described above are reported, organized per KPI.

III.4.1. Self-consumption fraction

When a 1 MWh BESS is employed, F_sc is similar between S0 and S1-S2 (around 3-4% difference across different capacities installed).

The difference between S0 and S1/S2 is highest when considering no BESS and PVT configuration: PVT allows for a lower use of electrical energy thanks to the thermal contribution, lowering the amount of energy produced and self-consumed, resulting in lower values of f_sh. This causes a 10% difference between S0 and S1 PVT and a 7% difference between S0 and S2 PVT. Employing PVT allows for higher differences between S1 and S2: without the thermal contribution and no BESS the curves almost overlap, while with this contribution there is a 4% variation at 0.4 MW PV capacity installed, which shrinks to 1% as PV capacity reaches 1MW. With high PV capacity and no BESS it's more difficult to reach high f_sc values even if a HP satisfies the thermal load alone, because of mismatches between generation and consumption.

When a 1MWh BESS is employed, S1 with pure PV results in the best f_sc values overall. BESS introduction allows for a 35% increase if f_sc at low PV capacity

(0.4MW) and for a 25% increase at 0.8 MW. Similar results are founf in S2 PV (34%-23%) attesting the high potential of BESS systems in satisfying loads with renewables.

PV curves lie higher than PVT ones, since PVT allows reduction of the energy that is produced and self- consumed, thus reducing the f_sc factor. The difference is lower when a 1MW BESS is employed and is most noticeable at low PV capacity installed (0.4 MW): 8% for S1 and 5% for S2, meaning that, without this thermal contribution, the self consumption factor remains high for greater PV capacities.

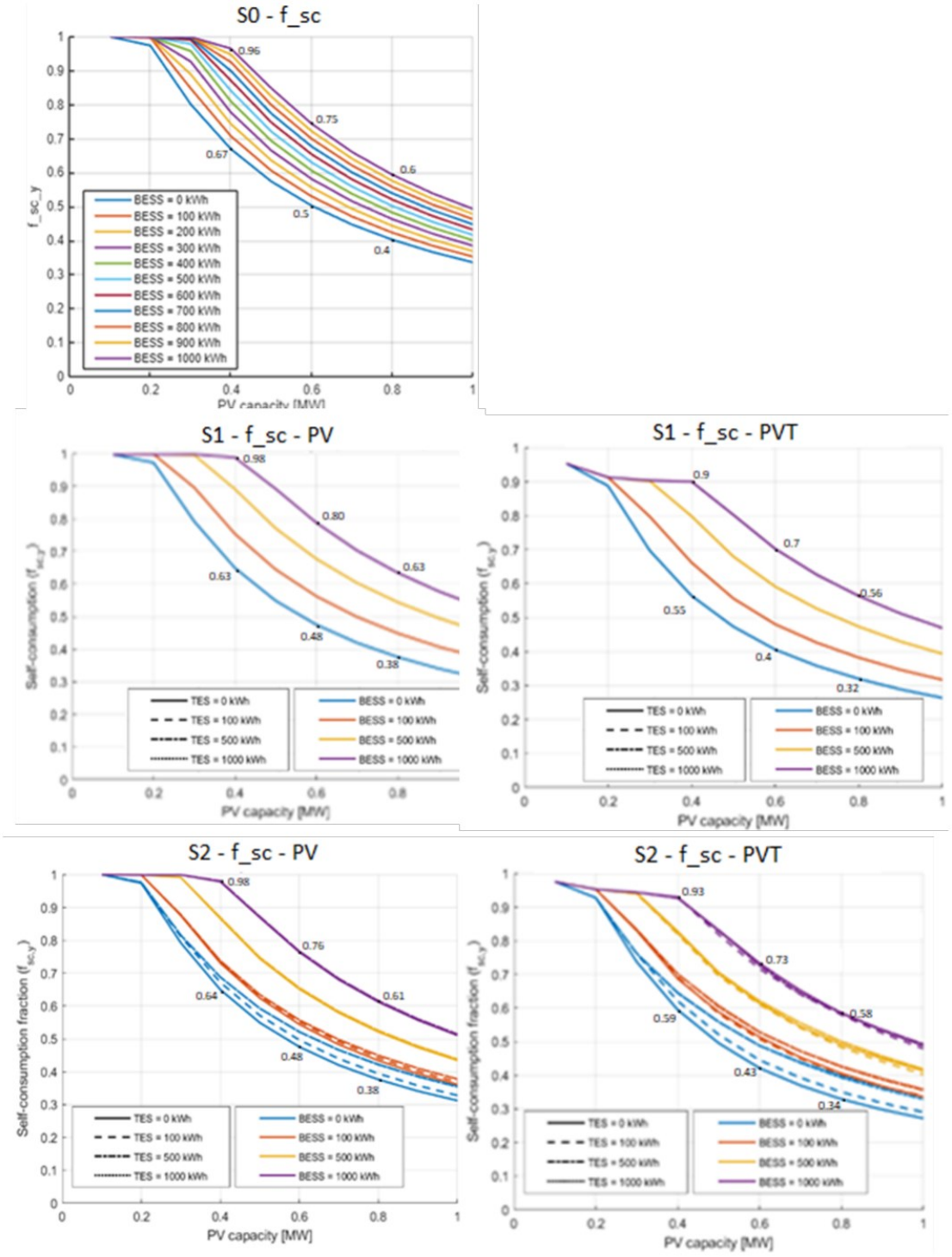

Figure 36: comparison between the different f_sc graphs

III.4.2. Shared energy fraction

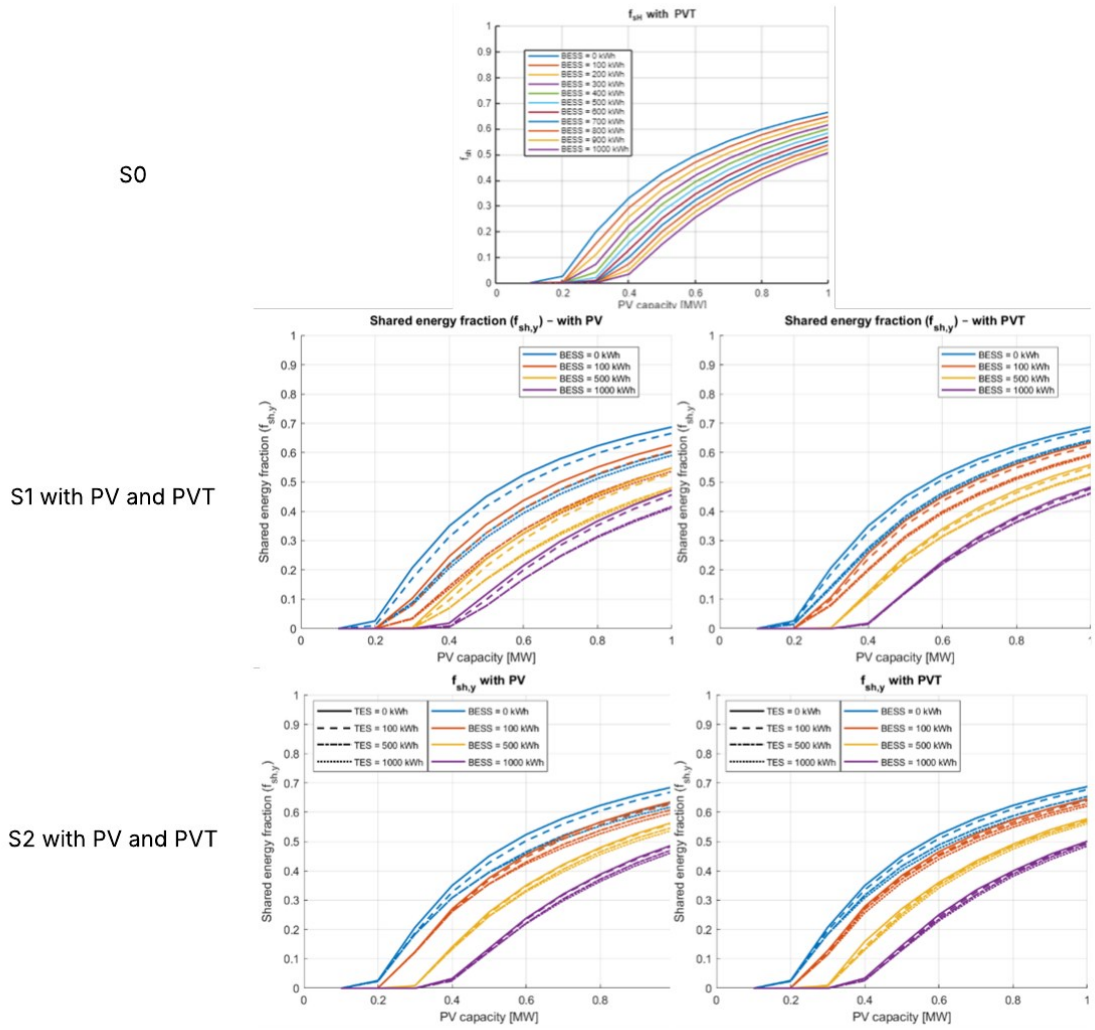

Figure 37: comparison between the different f_sh graphs

The difference between the scenarios is negligible without the support of BESS: S1 and S2 are consistently ~2% higher than S0 across different PV capacities installed. At high PV capacity and no BESS, f_sh values in S1 and S2 are very similar, accounting to 0.7 with 1 MW PV capacity installed. This occurs despite the presence of the gas boiler in S1, because the air-source heat pump (HP) in S2 consumes less electricity than the high-temperature heat pump (HHP) in S1, leaving more PV electricity available to be shared with the grid, so these two contributions balance.

Without BESS, the difference between the two graphs shrinks due to internal consumption and limited excess production at lower PV sizes, the difference in f_sh between S1 and S2 is negligible at medium PV levels (0% at 0.4 MW Pv capacity installed, 0.1% for 0.6 MW).

With BESS=1 MWh, S0 exhibits the highest values of f_sh, since the electrical loads are low in this configuration and much energy can be shared. The difference is highest between S0 and S1 without PVT (~8% at 0.6/0.8 MW capacity installed) but this difference shrinks once PVT is enabled (3-4% difference for the same values). For what regards S2, the case with PV exhibits 3% difference, while with PVT 1-2%, for the same comparison values. This highlights the increasing ability to share energy with increasing technological synergy.

- TES has a negligible impact on f_sh: the highest contribution is seen for S1 with pure PV, when it increase by 2% at 0.6 MW PV capacity installed.
- The shared energy fraction is zero until PV capacity reaches ~0.15–0.2 MW since simulations start from PV capacity=0, where f_sh is null, and the next vlue taken as input is 0.1 MW, leaving the gap between 0-0.1, as already seen in f_sc.

III.4.3. Grid purchase fraction

S0

S1 with PV and PVT

S2 with PV and PVT

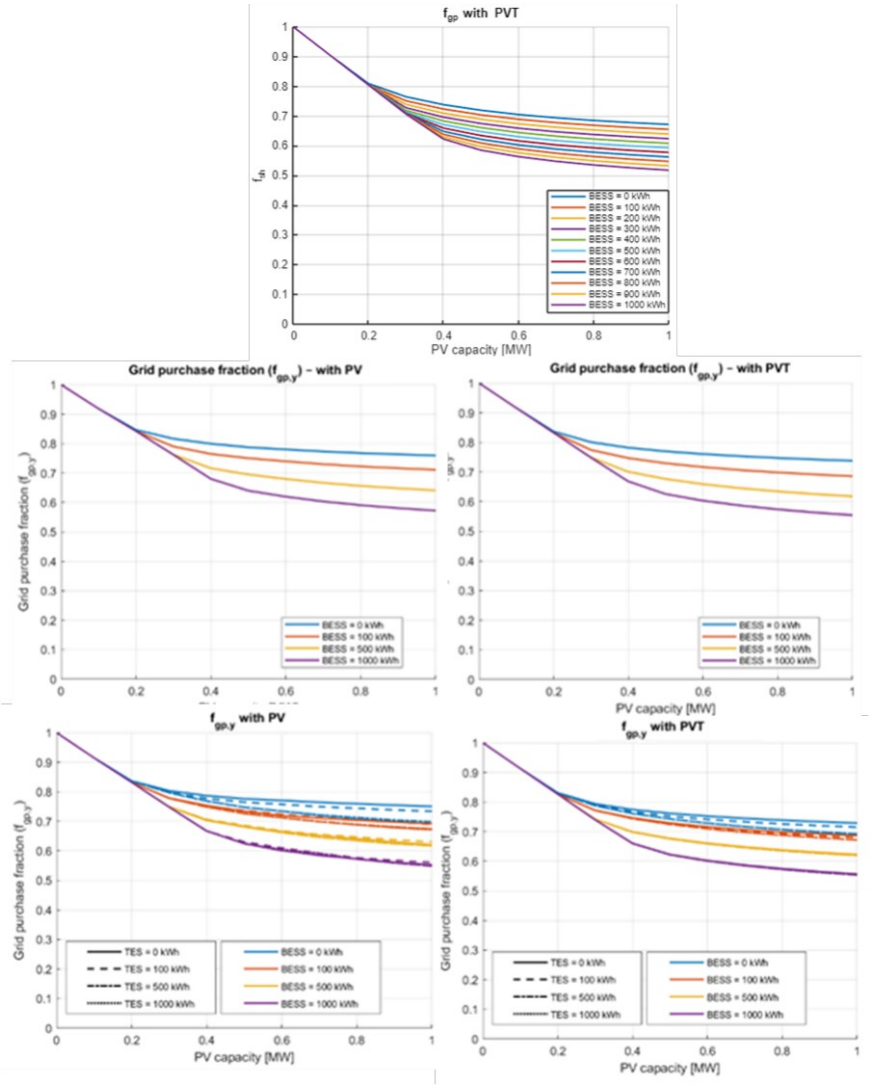

Figure 38: comparison between the different f_gp graphs

In Scenario S1 and S2, the general trend is similar to S0: f_gp decreases with increasing PV capacity, but remains higher than in S0, since less Natural Gas is used to cover thermal load instead of electricity. Without BESS the differences are highest: S0 is 4% lower with PV capacity= 0.4 and 6-7% lower at 0.8 MW installed. This of course is due to the lower electrical loads to be satisfied.

- In S1 very similar values of f_gp are found between PV and PVT; values differentiate slightly only with BESS=1 MWh and PV capacity=1MW: PVT is 1% lower than PV due to the reduced electricity demand for heating.

In S1 and S2, the difference between the PV/PVT configuration is negligible; in the S2 scenario PVT values are even 2% higher than PV at 1 MW PV capacity installed and no BESS; with BESS the curve almost overlap. In S1, they overlap in any case. This can be explained by the lower electrical load to the HP/HHP, which is denominator in f_gp and causes its raise. For thi reason it's difficult to note the benefit from the thermal contribution.
The pure-electric heat pump in S2 does not significantly reduce grid purchases compared to the hybrid in S1. For example, at 1 MW no storage, both f_gp reach 0.74, indicating that reduced electric demand in S2 is balanced by the lack of natural gas input considered in f_gp.

Across all scenarios, f_gp decreases with increasing PV capacity, especially in the low-to-mid range (0–0.4 MW), then approaches a plateau as surplus generation cannot be absorbed or further reduce grid purchases.
BESS consistently lowers f_gp by storing excess energy and reducing dependency on the grid.
The difference between PV and PVT is negligible. Tes impact is also negligible compared to BESS.

In all scenarios, the curves of f_gp exhibit a steep initial decline followed by a flattening trend as PV capacity increases. This behavior is due to a combination of load coverage dynamics and storage behavior:

- Initial steep decline (PV < 0.4 MW):
  -At low PV capacities, most of the electricity is self-consumed.

  -Every additional kW of PV directly offsets grid purchases, so fgpf_{gp}fgp drops rapidly.

  -The slope is steep because electric load is still unmet, and no surplus is produced yet.

- Transition zone (around PV = 0.3–0.5 MW):
  -PV production begins to cover the full load during daylight.

  -Some surplus electricity starts to appear.

  -If BESS is small or absent, surplus energy is not stored and may be curtailed → grid purchases cannot drop further, so the curve slope starts decreasing.

- If BESS is present, surplus can be stored, allowing continued reduction of f_gp, but at a slower rate, due to:
  -Storage limitations (capacity or state of charge).

  -Temporal mismatch between PV generation and load (especially for evening demand).

  -High PV capacity (> 0.6 MW):

  -Most of the load is already covered.

- Additional PV only helps if:
  -The BESS can store and later discharge it efficiently.

  -There is still unmet demand at other times of the day.

  -However, with fixed BESS size, the storage saturates, and its marginal utility decreases.

  -This leads to flattening curves, especially visible with large PV and small BESS.

- Effect of BESS size:
  -Larger BESS delays the onset of saturation.

  -Curves with 1 MWh BESS maintain a steeper slope for longer than those with smaller storage. However, even large BESS cannot eliminate grid purchases entirely, as PV generation and demand mismatch cannot always be bridged.

When comparing S1 (with high-temperature heat pump, HHP) and S2 (with standard air-source heat pump, HP), the f_gp curves are very similar for both PV

and PVT systems across all PV capacities and BESS sizes. However, in most cases, S1 shows slightly higher grid purchase fractions than S2.

This can be explained by two opposing effects:

- On one hand, the HHP in S1 relies more heavily on electricity compared to the HP in S2, which is more efficient and consumes less electric energy for the same thermal output.
- On the other hand, the HHP in S1 uses natural gas as an auxiliary fuel, reducing its dependence on the grid.
  These effects tend to counterbalance each other, resulting in comparable f_gp values in the two scenarios. However, the higher electrical consumption of the HHP slightly prevails, explaining the slightly higher grid reliance in S1.

  This behavior confirms that while the type of heat pump influences the electric load, the overall grid purchase is also shaped by how well PV production and storage match the demand,

III.4.4. Self-sufficiency fraction

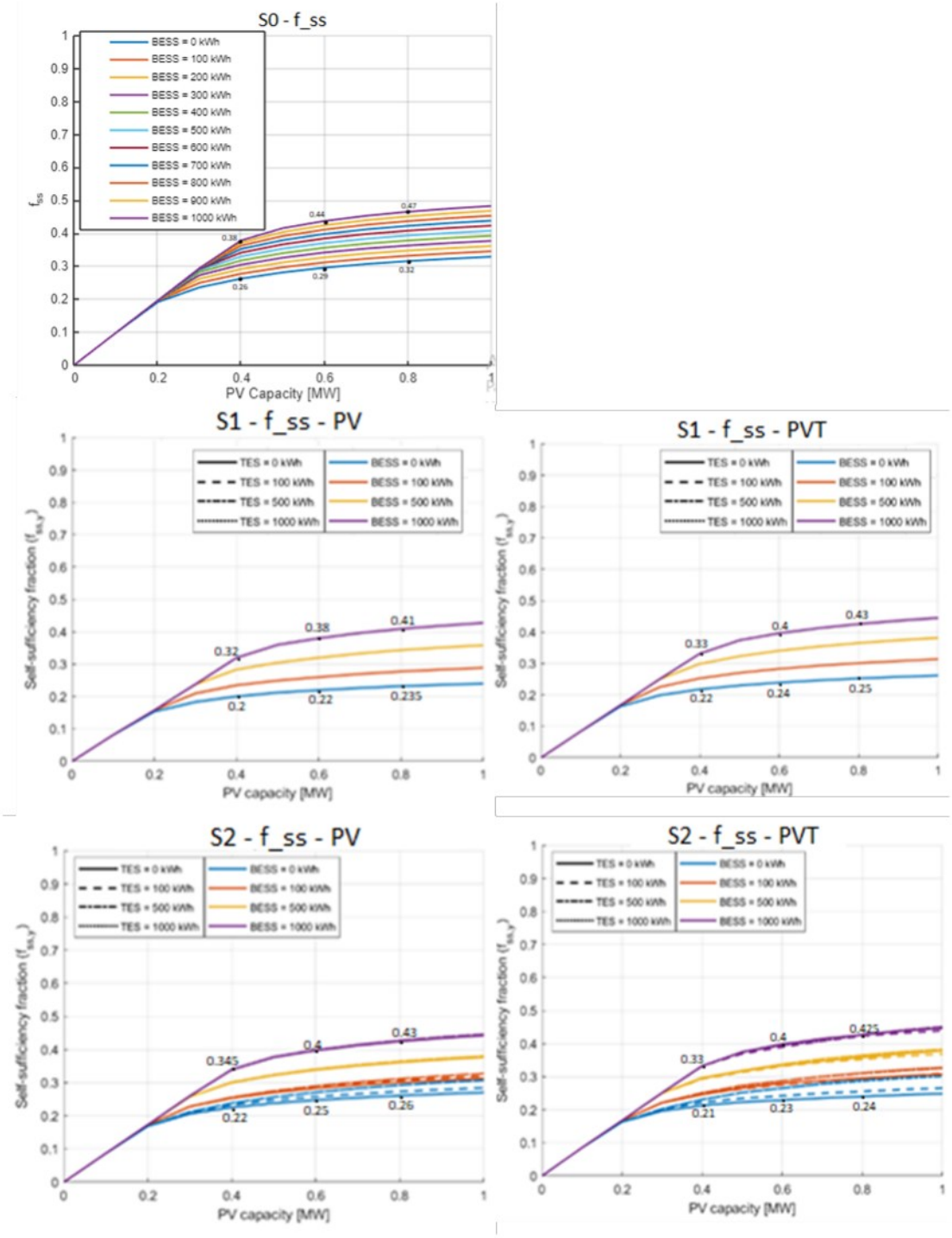

Figure 39: comparison between the different f_ss graphs

Although Scenario S2 shows slightly higher f_{ss} values than S1, the difference is limited: 2% with a 1MWh BESS, 3% without it in the pure PV scenario. In the PVT scenario, differences shrink even more: null without BESS, 1% with a 1 MWh storage.
Therefore, the higher efficiency of the HP in S2 (compared to HHP in S1) is partially balanced out by the dual-fuel operation of the HHP, which this KPI does not account for. As a result, the curves of S1 and S2 remain close, despite their technical differences.

Slope breaks and saturation occur consistently around 0.3 MW PV capacity without BESS and around 0.4 with a 1 MWh BESS in all scenarios, marking the point where production starts exceeding consumption. With BESS, f_ss keeps growing, though with diminishing returns.

BESS size is crucial: gains from 0 to 500 kWh are significant (10% or more), while increasing from 500 to 1000 kWh yields smaller improvements (5%).

Comparing scenarios, S0 shows the highest values of f_ss, since this doesn't account for gas dependance. S1 and S2 have around 5/6.5% lower values than S0.

The intersection of PV capacity, BESS availability, and technology choice (HHP vs HP) strongly determines system self-sufficiency.

III.4.5. Renewable energy fraction

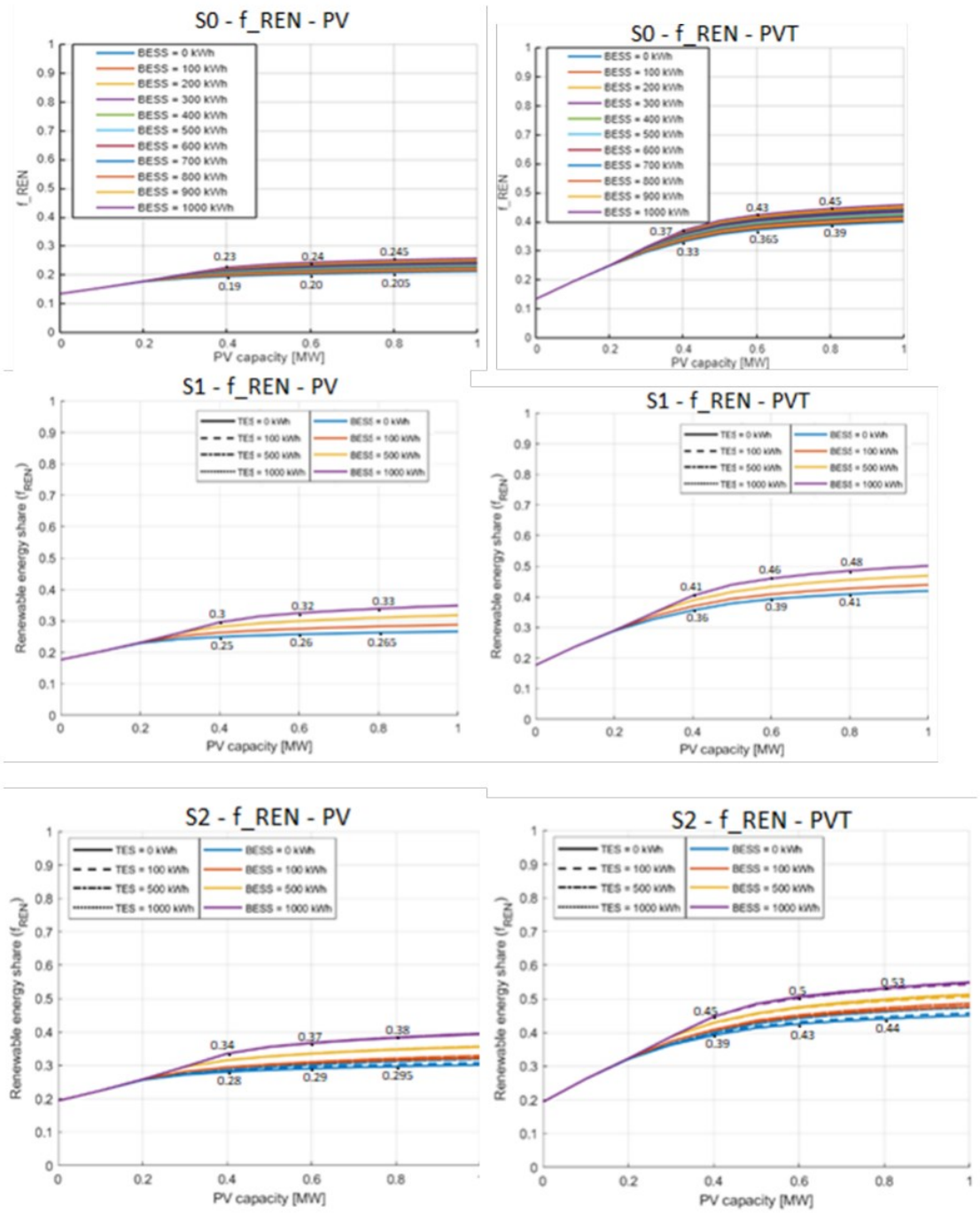

Figure 40: comparison between the different f_REN graphs

PVT consistently outperforms PV in terms of f_REN, as thermal energy is counted and—especially in S1 and S2—actively contributes to demand coverage. The highest difference between the two cases is seen in S0, where 19% increase can be seen with BESS=1 MWh and 17% without BESS. Of course, employing a PVT in a scenario where renewables satisfied only the electrical loads (not the thermal ones) increases the renwable fraction cosiderably. In S1 and S2, adopting the PVT brings similar advantages (14% increase with and without BESS)

BESS enhances f_REN more when combined with flexible thermal systems: S0 increases by 0.15%, S1 by 3% and and S2 by 4% between 0.4-0.8 MW of PV capacity installed, while the advantages increase when PVT are employed: 8% in S0 and S1, 9% in S2. This also shows that, eith PVT employed, BESS brings similar benefits to the three scenarios.

TES allows for a 0.1% performance increase.

Slope changes and flattening points occur later when a battery is employed: curves change slope at 0.2 MW of PV capacity without battery and at 0.4MW with a 1 MW BESS, showing how system design postpones saturation and improves RES integration.

S2 with PVT shows the highest f_REN values across all configurations: 0.55 with Bess=1 MWh and 1MW PV capacity installed, 5% more than S1 and 8% more than S0 for the same conditions. The HP has higher COP than the HHP and fully relies on electricity, making it more suitable for integration with RES.

III.4.6. Primary Energy Savings

PES values increase from S0 to S1 to S2, mainly due to the transition from NG-based systems to more electrified and efficient configurations and to improved synergy between renewables and flexible loads (especially HP in S2).

PVT consistently outperforms PV, with the gap being widest in S0 (8%), since less natural gas is used to meet thermal demands. PVT implementation advantages S1 by 4-6% (with and without BESS) and S2 by 2-1% (with and without BESS). This shows the minor advantages brought to S2, since electrification is already high and it is therefore more difficult to add gains.

TES shows a moderate impact only in S2, where its contribution to thermal recovery is more effectively exploited by the heat pump. However, its overall

influence remains limited (1% increase) compared to the effect of BESS and the integration of PVT.

S2 with PVT shows the highest PES values across all configurations: 0.61 with Bess=1 MWh and 1MW PV capacity installed, 9% more than S1 and 14% more than S0 for the same conditions. The HP has higher COP than the HHP and fully relies on electricity, making it more suitable for integration with RES.

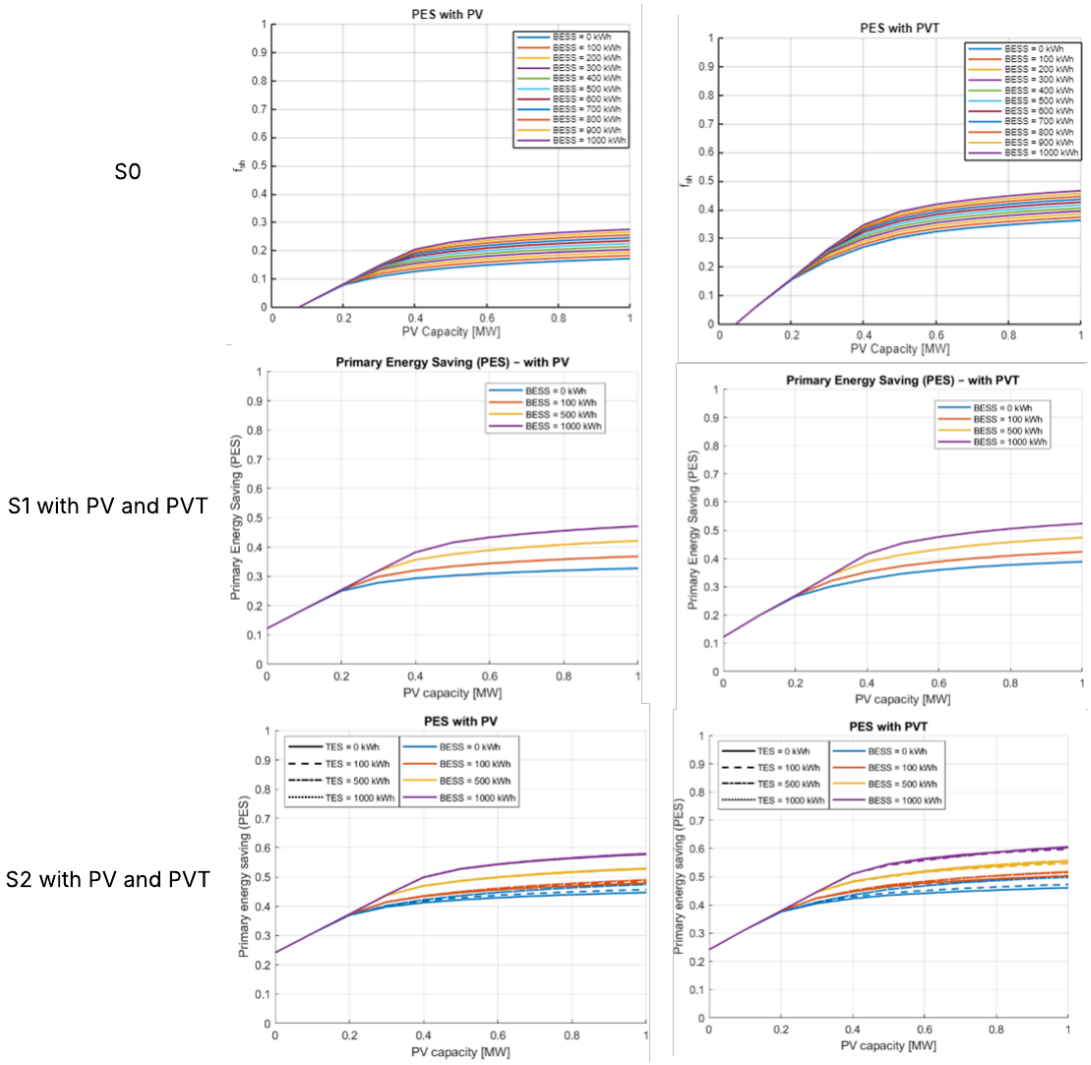

Figure 41: comparison between the different PES graphs

III.4.7. Fraction of avoided CO2

S0

S1 with PV and PVT

S2 with PV and PVT

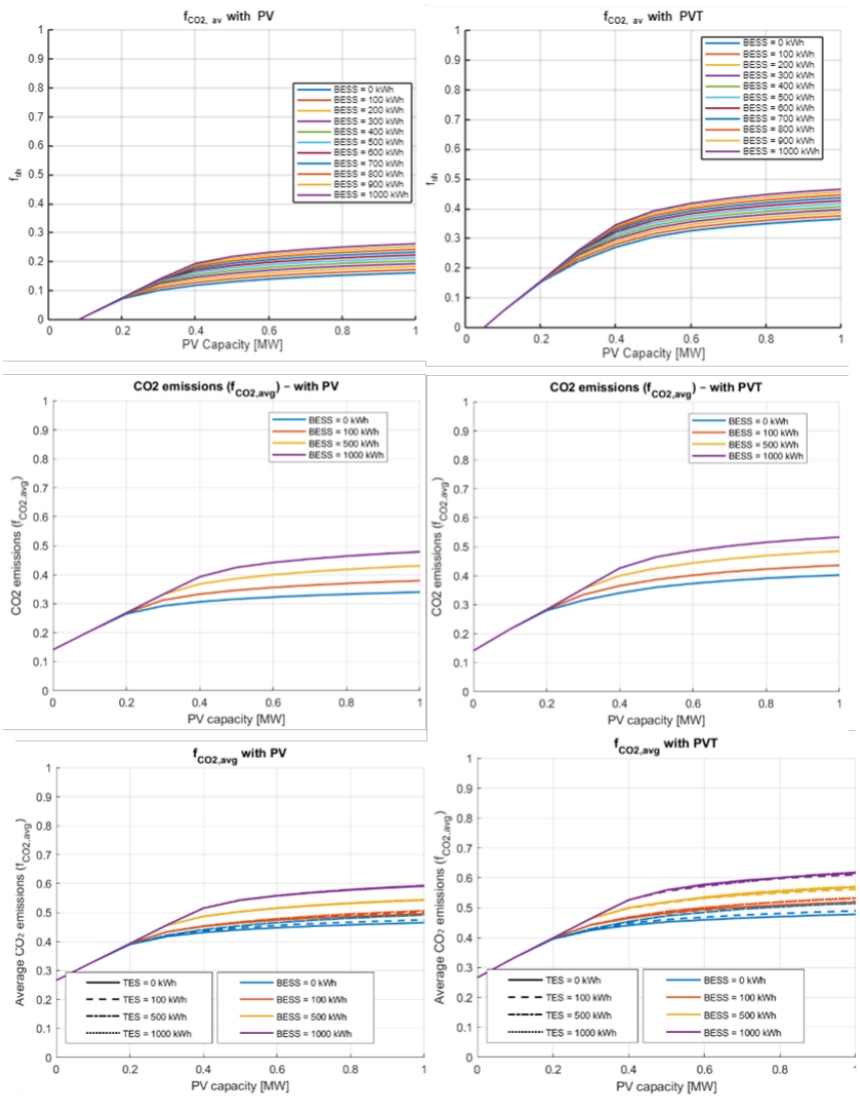

The highest improvement in implementing PVT is seen in S0 (20%). S1 improves by 4.5% and S2 by 1%, confirming what already assessed for f_REN: PVT brings less advantages if the electrification is already high. The differences between the 3 scenarios change a lot based on the presence of the PVT: there's a 20% difference between S0 and S1, and an 11% difference between S1 and S2 without PVT; with the thermal integration the difference decreases to 5% between S0 and S1 and to 8% between S1 and S2, still confirming the trend: it's easier to find gains when starting from a modest electrification, it's more difficult as tecnhology advancement increases.

The difference between not having electrical storage and employing a 1MWh battery are consistent in the three scenario: 10% in S0, 12% in S1, 14% in S2.

It's important to note that in S0 it's easy to gain savings reducing Natural Gas consumption, and this stresses even more how the synergy between different energy systems (HHP/HP, PV/PVT, BESS, TES) allows benefits even when high electrification and already high emission savings are present. This is showed by the different values found: considering PVT and a PV capacity=0.8MW, the fraction of co_2 avoided accounts in S0 to 0.35-0.45 (without electrical storage and with 1 MWh BESS), in S1 to 0.39-0.51 and in S2 to 0.46-0.6, showing a consistent increase with BESS even at high fractions of avoided emissions.

The comparative analysis clearly shows that increasing the integration of renewable and electrical technologies -from the base case S0 to the fully electrified scenario S2-results in consistently better energy performance. S0, which relies mostly on natural gas, benefits significantly even from small PV additions, as it allows to displace gas use; benefits raise by 8% in PES and fraction of avoided co_2 when BESS is employed. However, its potential saturates quickly.

In S1 PV PES increases by 17% compared to S0 and in S1 PVT by 5%; in S2 by 28% in PV case and by 13% in the PVT case.

The adoption of PVT panels brings strong advantages in terms of renewable energy share, thanks to the additional thermal contribution. For instance, switching from PV to PVT can boost the renewable energy fraction by 14–19% in gas-heavy scenarios like S0. S1 and especially S2, by including heat pumps and thermal storage, are able to exploit solar energy more deeply, resulting in 7% (PV) and 5%(PVT) increase in renewable energy share between S1 and S0 and in12% (PV) and 8% (PVT) increase between S0 and S2. This comes at the cost of slightly lower electrical self-consumption, since the reduced electric load satisfied lowers the numerator in f_sc.

The battery storage system (BESS) plays a crucial role: even at high levels of PV penetration (e.g. 0.8 MW), the presence of a 1 MWh BESS can still increase key indicators like CO_2 savings or primary energy savings by 10% for S0, 13% for S1 and 15% for S2, showing that storage enables continued performance improvements even when the system is already highly decarbonized.

Interestingly, the difference between S1 and S2 is not huge in all KPIs, but S2 tends to consistently outperform S1, especially with PVT and BESS: this is due to the higher efficiency of the fully electric heat pump.

In summary, the results demonstrate how systemic integration—combining PV/PVT, HP/HHP, BESS, and TES—delivers synergistic benefits. Even when electrification is already advanced, the combination of thermal and electrical storage and the use of hybrid technologies continue to generate meaningful performance gains. These gains are not only visible in the early stages of PV adoption but persist and grow when moving towards a deeper decarbonization path.

IV. Discussion and conclusions

The analysis of Scenarios S0, S1, and S2 highlights the progressive impact of technological integration in residential, commercial and educational energy systems. The study evaluates key performance indicators (KPIs) such as self-consumption (f_sc), shared energy (f_sh), self-sufficiency (f_ss), renewable energy fraction (f_REN), avoided CO_2 emissions (f_CO_2,av), and primary energy savings (PES), offering a comprehensive perspective on system performance as new components are introduced.

Impact of Technological Integration

Scenario S0, based on a natural gas boiler and renewable electricity generation via PV/PVT, shows limited improvements in thermal KPIs due to the absence of heat pumps or thermal storage. While PV integration improves electrical performance, the thermal contribution of PVT remains marginal, confined to domestic hot water (DHW) production.

Scenario S1 introduces a hybrid heat pump (HHP), marking a significant step forward compared to the baseline configuration (S0) which relies entirely on a natural gas boiler (NGB) for thermal energy supply. The integration of the HHP allows partial electrification of the heating and DHW demands, enabling the system to take greater advantage of on-site renewable electricity. This results in visible improvements across several key performance indicators, including increased self-sufficiency, higher renewable energy share, and reduced CO_2 emissions. While most of the performance gains in Scenario S1 are attributable to the introduction of the HHP, PVT systems provide additional thermal energy, with a modest influence: 4-5% increase in avoided co_2 fraction and Primary Energy Savings.

Scenario S2 represents the full electrification of the residential energy system, replacing the natural gas boiler entirely with an air-source heat pump (HP). This transition eliminates the direct use of fossil fuels for thermal energy, allowing both space heating and DHW to be covered exclusively by electricity—ideally sourced from on-site renewable generation. The configuration enables a deeper synergy between electrical and thermal subsystems, particularly when coupled with appropriately sized battery energy storage systems (BESS) and thermal energy

storage (TES). These storage components play a crucial role in balancing supply and demand, enhancing the system's ability to shift energy use in time and maximize the utilization of renewable electricity.

As a result, Scenario S2 consistently achieves the highest values across all key performance indicators (KPIs), with notable improvements in primary energy savings (PES), renewable energy fraction (f_REN), and avoided CO_2 emissions (f_CO_2,av). Self-consumption (f_sc) also reaches its peak performance when storage is optimally configured, reflecting the system's increased autonomy and efficiency. Although PVT modules continue to provide only marginal thermal benefits, the fully electrified architecture of Scenario S2 allows the greatest overall exploitation of on-site renewable resources, marking it as the most sustainable and forward-looking configuration among those analyzed.

PV vs. PVT Comparison

Across all scenarios, PVT systems demonstrate an advantage over PV in configurations where thermal energy can be meaningfully utilized. In S0, this advantage is negligible due to the lack of TES or thermal integration strategies. In S1 and especially S2, PVT panels contribute both electricity and heat, with the latter reducing the load on the heat pump and improving overall efficiency.

KPI differences between PV and PVT remain small for purely electrical metrics such as f_sc, f_sh, and f_gp. However, KPIs such as f_REN, PES, and f_CO_2_av consistently show slight to moderate improvements in PVT configurations, particularly in S1 where heating is still partially satisfied by Natural Gas.

Importance of Storage

The results emphasize the central role of storage technologies. Increasing battery energy storage (BESS) enhances self-consumption and reduces grid dependency. Similarly, thermal energy storage (TES) allows greater utilization of renewable thermal energy, particularly in scenarios with P2H strategies.

Without appropriate storage sizing, excess energy is either wasted or exported, reducing the effectiveness of on-site generation. Thus, storage enables temporal alignment between generation and consumption, unlocking the full potential of hybrid systems.

Optimization and Diminishing Returns

All scenarios reveal diminishing returns at higher generation capacities. As PV/PVT capacity increases, KPIs tend to plateau unless storage is scaled accordingly. This suggests that system design must balance generation and storage to achieve cost-effective and energy-efficient configurations.

Oversizing the generation system without adequate storage leads to saturation effects and minimal additional gains. Conversely, an optimized balance ensures high performance across a broader range of operating conditions.

Strategic Implications

The study confirms that combining PV, PVT, heat pumps, BESS, and TES in a coordinated system is a promising path toward decarbonizing energy use in buildings. However, the benefits of each technology are maximized only when they are properly integrated and dimensioned within the system.

Dynamic simulation and comparative scenario analysis emerge as essential tools for identifying the most effective configurations. Future development should consider control strategies and demand-side management to further enhance the performance and flexibility of these systems.

Final Remarks

Beyond the detailed KPI trends discussed for each scenario, a few overarching insights emerge. First, the effectiveness of thermal energy storage (TES) is strongly linked to the implementation of power-to-heat (P2H) strategies. Without them, TES remains underutilized. Similarly, while BESS and PV scaling provide clear benefits, several indicators show diminishing returns beyond certain capacity thresholds, underlining the importance of balanced system design rather than oversizing.

The transition from hybrid to fully electric thermal supply not only enhances decarbonization but also eliminates fossil fuel dependency—at the cost of increased reliance on electrical infrastructure. This reinforces the value of integrated storage and smart control systems in future developments.

Finally, the performance gap between PV and PVT systems remains limited under the simulated conditions. This is partly due to the assumed equal electrical

efficiency and the modest thermal contribution in the current system layout. Such differences may become more relevant in scenarios with greater thermal demand or stronger integration between thermal and electrical domains.

Economic Reflections

In conclusion, beyond the technical results, it's crucial to consider the economic performance of the three scenarios (S0, S1, S2). For simplicity and feasibility of our simulation, we assumed standardized costs for equipment and energy (using typical market prices). This means the economic figures are approximate, but they reveal clear trends

- Scenario S0 (Gas Boiler Only): This baseline has the lowest upfront investment. There's essentially no new capital cost beyond a standard gas boiler, so no payback period needs to be recouped. However, S0 incurs the highest ongoing fuel costs (buying all energy as gas) and leaves the system exposed to fossil fuel price volatility. The cost per useful kWh of heat in this scenario is relatively high (given gas prices and boiler efficiency) and of course, CO_2 emissions remain high. In economic terms, S0 avoids large investments but provides no savings and no emissions reduction, which means no "profit" from decarbonization – rather, it's the standard scenario against which the others are compared.
- Scenario S1 (Hybrid Heat Pump – HHP): Introducing a heat pump alongside the gas boiler introduces a moderate upfront investment (for the heat pump unit and system integration, plus PV/PVT panels). This hybrid approach yields significant fuel cost savings: a portion of the heating is supplied by the electric heat pump, which is much more efficient than a boiler (each kWh of electricity yields 3,5 kWh of heat). Even if electricity is more expensive per kWh than gas, the heat pump's high efficiency offsets it – at typical European price ratios (~2.5:1 electricity vs gas), a heat pump can break even with a gas boiler on running costs if it achieves around 3.4 COP (340% efficiency)[77]. In practice, our S1 sees lower fuel cost per useful heat kWh than S0, especially during sunny hours when PV/PVT output supplies the heat pump. The payback time for S1's additional investment is on the order of a decade or more, meaning it may take 10+ years of energy savings to recoup the upfront costs – in line with typical solar payback

periods of ~10–15 years[78]. S1's decarbonization cost (the extra cost per ton of CO_2 avoided relative to S0) is moderate: we spend some money to reduce emissions by using the heat pump when it's efficient to do so. Thanks to the hybrid design, CO_2 emissions are lower than S0 (since a share of heat comes from electricity/PV instead of gas), and the cost per ton of CO_2 avoided is likely lower than in a full electrification scenario because the investment is smaller. In summary, S1 strikes a balance – it reduces gas consumption and emissions with a manageable investment, though it doesn't eliminate carbon emissions entirely. Economically, it offers a middle-ground solution: more up-front cost than S0, but with operating savings and a reasonable payback period, especially if future gas prices rise or carbon taxes kick in.

- Scenario S2 (All-Electric Heat Pump – HP): This scenario requires the highest initial investment. We replace gas entirely with an air-source heat pump, and to maximize renewable usage, S2 typically involves larger PV/PVT installations and potentially battery (BESS) or thermal storage (TES) to store excess solar energy. These additions drive up the capital cost significantly. The upside is minimal ongoing fuel costs – with a high-efficiency heat pump using largely self-generated solar electricity, the effective cost of heat can be very low. In fact, if our PV/PVT covers a good portion of the load, the marginal cost of that solar-derived heat is almost zero, apart from maintenance. Any electricity drawn from the grid for the heat pump is used very efficiently; for example, even if electricity were €0.25/kWh, a COP of 3 brings the effective heating cost to ~€0.08 per kWh heat, comparable to or lower than gas heating costs[77]. Thus, S2 has the lowest fuel cost per useful kWh of all scenarios. Environmentally, S2 achieves the largest CO_2 reduction – potentially near-zero operational emissions if most electricity comes from renewables – making it the greenest option. The trade-off is in economics: due to the high upfront expense, payback times in S2 are typically the longest. Even with energy savings, it can take well over a decade to recover costs; in some configurations with expensive storage, the payback might approach or exceed the system's lifespan. Fully decarbonizing heat through PV-powered heat pumps can come at a high decarbonization cost – possibly

on the order of hundreds of euros per ton of CO_2 avoided when compared to S0[79]. For instance, a recent study found that a nearly 94% emissions reduction via heat pumps and solar in a residential setup cost about €179 per ton of CO_2 abated[80]. This is substantially higher than current carbon market prices (EU ETS permits in 2021 were €32–€80/tCO_2)[79], meaning from a pure market standpoint S2 is not yet cost-effective *solely* for carbon savings. Nonetheless, S2 offers long-term strategic benefits: once the system is paid off, the energy is extremely cheap and shielded from fossil fuel price swings, and the house is essentially "future-proofed" against tightening carbon regulations or fuel shortages. It's an investment in energy autonomy and sustainability. The hope is that as technology costs continue to fall and policies (or future fuel prices) change, the economics of scenarios like S2 will improve further.

One clear trend across S1 and S2 is that the addition of storage systems (both BESS and TES) leads to a substantial increase in capital costs. Batteries and thermal tanks enable greater use of self-generated solar energy during periods of low irradiation, such as evenings or cloudy days. This improves renewable self-consumption and reduces reliance on external sources, thereby lowering emissions. However, from an economic perspective, the return on such investments remains challenging.

In 2025, lithium-ion batteries in Italy typically cost between €500 and €1000 per kWh of installed capacity[81]. Assuming electricity prices around €0.25–0.30 per kWh [82]and a daily cycle, the avoided cost per stored kWh is significant—but not sufficient to offset the initial investment within the battery's useful life, usually 10–15 years. For instance, a 5 kWh battery could generate around €400–€500 in yearly savings, but even in the best-case scenario, the payback period would remain close to or beyond 10 years, often matching or exceeding the battery's the point at which their usable capacity is significantly reduced—typically after 10–15 years.[81].

This aligns with our simplified analysis, which showed that scenarios including BESS or TES (S1 and S2) presented significantly higher upfront costs with only marginal reductions in operating expenses. The result is an increase in the overall lifecycle cost, especially in configurations with oversized storage. Adding a battery often extends the payback period toward or beyond 15 years unless specific

incentives apply[83]. Without such support, many systems may never fully recover their initial cost within the operational lifetime.

Thermal Energy Storage is generally cheaper than battery systems, with costs between €100 and €300 per kWh_th[84]. However, its economic return depends on how much it helps shift renewable thermal energy to useful periods. In many cases, the savings it generates are limited unless the system is carefully sized and operated under dynamic pricing or load-shifting strategies. In our analysis, its contribution to decarbonization was evident, but its financial impact remains moderate, especially when added on top of already efficient systems.

The key conclusion is that while storage improves environmental performance and energy autonomy, it currently delivers limited economic returns under standard conditions. Whether it is worth integrating depends on strategic priorities: if maximum decarbonization, resilience, and grid independence are the primary goals, storage can be justified. But if cost-efficiency is the main driver, its adoption remains difficult without subsidies or further market shifts.

It's important to stress that our cost assumptions were generic; actual project economics can vary. Real-world factors like government incentives, grants, or tax deductions can dramatically improve payback times. (Italy, for instance, has offered Superbonus tax credits, and many countries have rebates for heat pumps or batteries.) With strong incentives, it's possible for solar-plus-battery systems to achieve paybacks around 7–10 years[85], or heat pump retrofits pay back in under a decade[86] – outcomes that are far better than the unsubsidized scenarios. Energy price trends also matter: if gas prices rise or carbon taxes are implemented, scenarios S1 and S2 will save more money each year, effectively shortening their payback. Conversely, if electricity prices rise faster than gas (without green policy adjustments), that could slow down the savings. Our analysis didn't delve into these dynamic factors in depth, but it assumed a stable backdrop for fair comparison. Even so, considering current market data, the average solar PV system in Europe tends to pay back its cost in roughly 10–15 years[78]. Adding a battery often extends that towards or beyond 15+ years, unless special incentives apply. In fact, without incentives, many home batteries may not pay for themselves fully within their lifetime. These context points reinforce why policy support (like upfront subsidies, or pricing carbon emissions) is crucial to make clean energy investments more attractive today. As noted in one study, the

calculated cost per ton of CO_2 for our kind of setups is higher than current carbon prices, highlighting a gap that policy could help bridge[80].

To wrap up, linking the energy, environmental, and economic threads of our results gives a more holistic view of the scenarios:

- S0 is cheapest up front but costliest to run long-term (and emits the most CO_2). It's essentially low investment with later payment, paying for fuel and facing emission costs (direct or indirect).
- S2 is the opposite: expensive up front but cheapest to operate, and dramatically cuts emissions. It's a mechanism that allows to pay now to save later, requiring a long-term vision or supportive policies/incentives to make financial sense. It delivers the strongest environmental benefit and insulates us from future fuel uncertainties, but the economic payoff occures gradually.
- S1 sits in between: it moderates the costs and benefits by blending old and new technology. It demands a higher investment than S0, but lower than S2, and it takes to notable (though not complete) emissions reductions. It can be a pragmatic transitional approach, capturing some efficiency gains and CO_2 savings with a marginally better economic case than S2 in the near term. Essentially, S1 can achieve a significant decarbonization at a lower cost-per-ton than S2, making it an attractive compromise if full electrification isn't immediately feasible.

Overall, our findings suggest that achieving deep decarbonization in buildings is technically feasible (as shown by S2's performance) but economic feasibility is the next obstacle. The technology is available, but to adopt it widely we must consider how to reduce costs or redistribute costs over time. This could be through market evolution (cheaper batteries, cheaper heat pumps, etc.), or through policy (grants, carbon pricing, energy tariffs that favor clean heating). Encouragingly, trends are moving in the right direction: every year we see improvements in efficiency and drops in renewable and storage costs, while planners discuss how to better balance electricity vs gas pricing to favor clean heating. If electricity becomes relatively cheaper (for example, via lower taxes on renewable electricity and higher carbon taxes on gas), the economics of heat pumps improve significantly, as studies have noted [87].

Reassessment of S1, S2 scenarios under current Italian incentives

In the initial assessment without incentives, Scenario S1 — featuring PVT panels, TES, and hybrid heat pumps (HHPs) — was found to offer the best balance among capital cost, environmental performance, and energy independence. The S2 scenario, while more advanced in terms of electrification and decarbonization, suffered from significantly higher investment costs due to the addition of BESS, as well as reliance on electric heat pumps (HPs) instead of HHPs.

However, under current Italian fiscal incentives, this picture changes considerably. Italy currently supports residential and non-residential energy retrofits through the Superbonus, which in its 2025 form offers up to 65% fiscal deduction on energy efficiency improvements such as installation of heat pumps, photovoltaic systems, and energy storage (both BESS and TES).

Given these conditions, Scenario S2 becomes far more economically viable:

- Electric heat pumps (HP): In S2, 40 HPs of 20 kW are deployed (across the residential, commercial, and school buildings). These are fully eligible for the Superbonus as they represent a clean electrification strategy.
- PVT systems: Strongly encouraged under all major incentive schemes, with a 65% detraction on cost.
- Thermal Energy Storage (TES) and Battery Energy Storage Systems (BESS): Both are considered part of the energy efficiency upgrade and can benefit from the same 65% detraction.

Applying these incentives to S2 leads to a substantial reduction in capital costs:

- If we assume a typical installed cost of €1,000/kWh for BESS and a total capacity of 1000 kWh, the net cost after the 65% incentive is only €350,000 instead of €1 million.
- The same applies to TES and PVT systems, which reduces the total upfront investment significantly.

While S1 without storage may still offer a short payback time and low operational costs, S2 becomes increasingly competitive when incentives are included, thanks to the large subsidies covering capital investment. Moreover, S2 has the highest

potential for complete decarbonization and energy independence, as the system is fully electrified and optimized for renewable generation and storage.

Therefore, in light of the current Italian fiscal framework, S2 can now be considered the "best overall scenario" when including available incentives. It offers:

- Full electrification of thermal loads,
- Maximized use of renewable electricity,
- Flexibility and grid support through BESS and TES,
- Access to high subsidies that bring the payback period within a feasible range.

In conclusion, while S1 remains optimal in a subsidy-free context, the structure of Italian incentives strongly favors advanced electrified scenarios like S2, shifting the cost-benefit balance in their favor and making them the most effective choice from both environmental and economic perspectives.

BIBLIOGRAPHY

[1] “https://iea.blob.core.windows.net/assets/5b169aa1-bc88-4c96-b828-aaa50406ba80/GlobalEnergyReview2025.pdf#:~:text=Energy%20sector%20carbon%20emissions%20reached,higher%20than%202023%20and%2050”.

[2] “https://www.iss.europa.eu/publications/briefs/europes-energy-crisis-conundrum#:~:text=The%20balance%20between%20the%20three,market%20all%20the%20more%20imperative”.

[3] “https://www.ipcc.ch/report/ar6/syr/downloads/report/IPCC_AR6_SYR_LongerReport.pdf#:~:text=the%20beginning%20of%202020%20for,due%20in%20part%20to%20mitigation”.

[4] “https://research-and-innovation.ec.europa.eu/system/files/2021-10/ec_rtd_gdce-analysis_report.pdf”.

[5] “https://europeanclimate.org/wp-content/uploads/2022/03/ecf-building-emissions-problem-march2022.pdf#:~:text=finds%20that%20doing%20so%20could,and%20electrifying%20Europe%E2%80%99s%20residential%20buildings1”.

[6] “https://www.ipcc.ch/report/ar6/wg3/chapter/chapter-9/#:~:text=There%20is%20growing%20scientific%20evidence,Mitigation”.

[7] “https://europeanclimate.org/wp-content/uploads/2022/03/ecf-building-emissions-problem-march2022.pdf#:~:text=To%20meet%20the%20EU%E2%80%99s%20climate,of%20CO2%20emissions”.

[8] “https://www.gse.it/documenti_site/Documenti%20GSE/Servizi%20per%20te/AUTOCONSUMO/Gruppi%20di%20autoconsumatori%20e%20comunita%20di%20energia%20rinnovabile/Normative/TESTO%20COORDINATO%20DEL%20DECRETO-LEGGE%2030%20dicembre%202019%20n%20162%20art%2042-bis.pdf”.

[9] “https://energy.ec.europa.eu/topics/renewable-energy/renewable-energy-directive-targets-and-rules/renewable-energy-directive_en”.

[10] X. Masip, E. Fuster-Palop, C. Prades-Gil, J. D. Viana-Fons, J. Payá, and E. Navarro-Peris, “Case study of electric and DHW energy communities in a Mediterranean district,” *Renewable and Sustainable Energy Reviews*, vol. 178, p. 113234, May 2023, doi: 10.1016/j.rser.2023.113234.

[11] “https://commission.europa.eu/strategy-and-policy/priorities-2019-2024/european-green-deal_en”.

[12] “https://www.mimit.gov.it/it/pnrr/progetti-pnrr/pnrr-rinnovabili-e-batterie”.

[13] K. Shafiei, A. Seifi, and M. T. Hagh, “A novel multi-objective optimization approach for resilience enhancement considering integrated energy systems with renewable energy, energy storage, energy sharing, and demand-side management,” *J Energy Storage*, vol. 115, p. 115966, Apr. 2025, doi: 10.1016/j.est.2025.115966.

[14] V. Battaglia and L. Vanoli, “Optimizing renewable energy integration in new districts: Power-to-X strategies for improved efficiency and sustainability,” *Energy*, vol. 305, p. 132312, Oct. 2024, doi: 10.1016/j.energy.2024.132312.

[15] J. Graça Gomes *et al.*, “Maximising sustainability: Planning and optimisation strategies for achieving 100 % renewable energy communities in remote islands - A case study of Corvo Island, Portugal,” *Energy*, vol. 319, p. 134802, Mar. 2025, doi: 10.1016/j.energy.2025.134802.

[16] F. Calise, F. L. Cappiello, L. Cimmino, M. Dentice d’Accadia, and M. Vicidomini, “Thermo-economic analysis and dynamic simulation of a novel layout of a renewable energy community for an existing residential district in Italy,” *Energy Convers Manag*, vol. 313, p. 118582, Aug. 2024, doi: 10.1016/j.enconman.2024.118582.

[17] N. Sandoval *et al.*, “Achieving equitable widespread residential building electrification – examining barriers, strategies, and opportunities using Los Angeles as a case study,” *Appl Energy*, vol. 384, p. 125498, Apr. 2025, doi: 10.1016/j.apenergy.2025.125498.

[18] A. Khosravani, M. DeHaan, B. W. Billings, and K. M. Powell, “Electrification of residential and commercial buildings integrated with hybrid renewable energy systems: A techno-economic analysis,” *Energy*, vol. 302, p. 131893, Sep. 2024, doi: 10.1016/j.energy.2024.131893.

[19] Y. Yang, R. Adhikari, Y. Lou, J. O’Donnell, N. Hewitt, and W. Zuo, “Long-term impact of electrification and retrofits of the U.S residential building in diverse locations,” *Build Environ*, vol. 269, p. 112472, Feb. 2025, doi: 10.1016/j.buildenv.2024.112472.

[20] “https://www.ipcc.ch/report/ar6/wg3/chapter/chapter-9/#:~:text=Total%20GHG%20emissions%20in%20the,of%20global”.

[21] “https://www.iea.org/reports/net-zero-roadmap-a-global-pathway-to-keep-the-15-0c-goal-in-reach”.

[22] “https://energy.ec.europa.eu/topics/energy-efficiency/energy-efficient-buildings/nearly-zero-energy-and-zero-emission-buildings_en#:~:text=The%20recast%C2%A0Energy%20Performance%20of%20Buildings,the%20EU%E2%80%99s%20climate%20neutrality%20goal”.

[23] “https://energy.ec.europa.eu/topics/energy-efficiency/energy-efficiency-targets-directive-and-rules/energy-efficiency-directive_en#:~:text=The%202023%20revised%20directive%20raises,the%20EU%20reference%20scenario%202020.”.

[24] “https://eur-lex.europa.eu/eli/reg/2018/1999/oj/eng”.

[25] “https://makeitright.ca/holmes-advice/hvac/boiler-vs-furnace-which-is-better-for-you/”.

[26] “https://www.microgreening.com/insulating-heating-and-cooling/condensing-boilers.php”.

[27] “https://www.gsa.gov/system/files/GPG_Findings_004-Condensing_Boilers.pdf”.

[28] “https://www.efficienzaenergetica.enea.it/detrazioni-fiscali/ecobonus/vademecum/caldaie-a-condensazione.html”.

[29] “https://www.arera.it/comunicati-stampa/dettaglio/it/com-stampa/23/230103#:~:text=Gas%3A%20bolletta%20in%20aumento%20(%2B,consumi%20di%20dicembre%202022%20%2D%20Arera”.

[30] “https://en.m.wikipedia.org/wiki/File:PV-system-schematics-residential-Eng.png”.

[31] H. Fares, N. Le Pierrès, D. Chèze, and E. Wurtz, “Assessing the energy performance of solar photovoltaic, thermal and hybrid PVT panels in a building context: A systematic study of the criteria’ definitions and studies parameters,” *Solar Energy*, vol. 286, p. 113126, Jan. 2025, doi: 10.1016/j.solener.2024.113126.

[32] “IEA. World Energy Outlook 2020. https://www.iea.org/reports/world-energy-outlook-2020, visited 2024-09-27”.

[33] “http://www.iea-pvps.org/fileadmin/dam/public/report/technical/PVPS_report_-_A_Snapshot_of_Global_PV_-_1992-2014.pdf”.

[34] “https://www.irena.org/-/media/Files/IRENA/Agency/Publication/2019/Oct/IRENA_Future_of_wind_2019.pdf”.

[35] “https://at-source-energy.com/panel/”.

[36] E. Assareh *et al.*, “Enhancing solar thermal collector systems for hot water production through machine learning-driven multi-objective optimization with phase change material (PCM),” *J Energy Storage*, vol. 73, p. 108990, Dec. 2023, doi: 10.1016/j.est.2023.108990.

[37] X. Ma, A. Ghosh, E. Cuce, and S. Saboor, “Building integrated photovoltaic-thermal systems (BIPVT) and spectral splitting technology: A critical review,” *Next Sustainability*, vol. 4, p. 100056, 2024, doi: 10.1016/j.nxsust.2024.100056.

[38] M. Debbarma, K. Sudhakar, and P. Baredar, “Thermal modeling, exergy analysis, performance of BIPV and BIPVT: A review,” *Renewable and Sustainable Energy Reviews*, vol. 73, pp. 1276–1288, Jun. 2017, doi: 10.1016/j.rser.2017.02.035.

[39] A. K. Hamzat, A. Z. Sahin, M. I. Omisanya, and L. M. Alhems, “Advances in PV and PVT cooling technologies: A review,” *Sustainable Energy Technologies and Assessments*, vol. 47, p. 101360, Oct. 2021, doi: 10.1016/j.seta.2021.101360.

[40] “https://www.sciencelearn.org.nz/resources/259-interpreting-representations-heat-pump-cycle”.

[41] “https://nailor.com/resources/news/how-water-source-heat-pump-works-thermodynamics-101”.

[42] “https://airconditioninggoldcoast.com/air-conditioning-eer-and-cop/”.

[43] M. Chesser, P. Lyons, P. O’Reilly, and P. Carroll, “Air source heat pump in-situ performance,” *Energy Build*, vol. 251, p. 111365, Nov. 2021, doi: 10.1016/j.enbuild.2021.111365.

[44] F. Cheng, X.-W. Li, and X.-S. Zhang, “Integral thermal and electrical energy utilization of the capacitive deionization regeneration method for absorption air-conditioning system,” *Renew Energy*, vol. 145, pp. 2233–2244, Jan. 2020, doi: 10.1016/j.renene.2019.07.147.

[45] G. Bagarella, R. Lazzarin, and M. Noro, “Sizing strategy of on–off and modulating heat pump systems based on annual energy analysis,” *International Journal of Refrigeration*, vol. 65, pp. 183–193, May 2016, doi: 10.1016/j.ijrefrig.2016.02.015.

[46] F. Nicoletti, G. Ramundo, and N. Arcuri, “Optimal operating strategy of hybrid heat pump – boiler systems with photovoltaics and battery storage,” *Energy Convers Manag*, vol. 323, p. 119233, Jan. 2025, doi: 10.1016/j.enconman.2024.119233.

[47] F. Schlosser, M. Jesper, J. Vogelsang, T. G. Walmsley, C. Arpagaus, and J. Hesselbach, “Large-scale heat pumps: Applications, performance, economic feasibility and industrial integration,” *Renewable and Sustainable Energy Reviews*, vol. 133, p. 110219, Nov. 2020, doi: 10.1016/j.rser.2020.110219.

[48] A. Khosravani, M. DeHaan, B. W. Billings, and K. M. Powell, “Electrification of residential and commercial buildings integrated with hybrid renewable

energy systems: A techno-economic analysis," *Energy*, vol. 302, p. 131893, Sep. 2024, doi: 10.1016/j.energy.2024.131893.

[49] Y. Tong, T. Kozai, N. Nishioka, and K. Ohyama, "Greenhouse heating using heat pumps with a high coefficient of performance (COP)," *Biosyst Eng*, vol. 106, no. 4, pp. 405–411, Aug. 2010, doi: 10.1016/j.biosystemseng.2010.05.003.

[50] R. Li *et al.*, "Performance of air source heat pump units with different wettability evaporators," *Appl Therm Eng*, vol. 257, p. 124458, Dec. 2024, doi: 10.1016/J.APPLTHERMALENG.2024.124458.

[51] S. Bae, H. Chae, N. Lyu, and Y. Nam, "Development of photovoltaic-thermal using attachable solar collector based on on-site construction," *Appl Therm Eng*, vol. 238, p. 121971, Feb. 2024, doi: 10.1016/J.APPLTHERMALENG.2023.121971.

[52] A. Carella and A. D'Orazio, "The heat pumps for better urban air quality☆," *Sustain Cities Soc*, vol. 75, p. 103314, Dec. 2021, doi: 10.1016/j.scs.2021.103314.

[53] X. Wang, Y. Jia, and D. Zuo, "Study on Optimization of Two-Stage Phase Change Heat Storage Coupled Solar-Air Source Heat Pump Heating System in Severe Cold Region," *Energy Engineering*, vol. 122, no. 4, pp. 1603–1627, 2025, doi: 10.32604/ee.2025.062908.

[54] "https://www.vaillant.it/home/approfondimenti-e-consigli/come-funzionano-le-diverse-tecnologie/pompe-di-calore/pompe-di-calore-acqua-acqua/".

[55] "https://www.researchgate.net/figure/A-typical-diagram-of-a-water-source-heat-pump_fig2_286358619".

[56] H. H. Shin, C. Han, Y. Heo, H. Lee, and Y. Kim, "Optimal partial-load operation strategies of surface water-source centrifugal heat pumps with thermal energy storage for large buildings," *Appl Energy*, vol. 388, p. 125724, Jun. 2025, doi: 10.1016/j.apenergy.2025.125724.

[57] "https://docs.nrel.gov/docs/fy25osti/90324.pdf#:~:text=District%20syste

ms%20enable%20a%20thermal,decarbonization%20and%20reduce%20energy%20bills”.

[58] “https://www.whispervalleyaustin.com/how-our-innovative-geothermal-infrastructure-powers-zero-energy-capable-homes/”.

[59] “https://greenscies.com/”.

[60] “https://www.cibsejournal.com/uncategorized/a-sharing-society-islingtons-greenscies-ambient-loop/#:~:text=Bi”.

[61] “https://www.neatpumps.com/case-studies/queens-quay-water-source-heat-pumps-for-district-heating/#:~:text=Scotland%E2%80%99s%20largest%20water%20source%20heat,local%20carbon%20footprint%20by%2060”.

[62] “https://www.vitalenergi.co.uk/media/kd5fq1v2/queen-s-quay.pdf#:~:text=scheme%20also%20has%20added%20resilience,the%20time%20the%20system%20will”.

[63] “https://www.pv-magazine.com/2024/04/24/solar-assisted-heat-pumps-vs-air-source-heat-pumps/”.

[64] “https://www.researchgate.net/figure/Solar-assisted-heat-pump-concentric-pipe-evaporator_fig4_286474003?__cf_chl_tk=XZ_gXCeS94dpYr25bT8aB1Njar2GcZkv1zfLcRUSOQM-1747134060-1.0.1.1-.CZK5gtpmaOffRd9Q.GX4YQ0td.Pakn_Yb1ZeTcW70c”.

[65] A. Vallati, G. Lo Basso, F. Muzi, C. V. Fiorini, L. M. Pastore, and M. Di Matteo, “Urban energy transition: Sustainable model simulation for social house district,” *Energy*, vol. 308, p. 132611, Nov. 2024, doi: 10.1016/j.energy.2024.132611.

[66] “https://www.mdpi.com/1996-1073/18/2/255#:~:text=MATLAB%20,Toolbox%20and%20Parallel%20Computing%20Toolbox”.

[67] “https://it.mathworks.com/help/simulink/index.html”.

[68] “https://www.mdpi.com/1996-1073/18/2/255#:~:text=TRNSYS%20,of%20complex%20control%20and%20optimal”.

[69] “https://www.trnsys.de/static/d3c3a0e9b3c5aa5d1aeda090f29afc40/250520_Kurzbeschreibung_Trnsys_e.pdf#:~:text=represent%20the%20usually%20complex%20building,between%20room%20surfaces%20and%20the”.

[70] “https://publications.jrc.ec.europa.eu/repository/handle/JRC113779”.

[71] T. Benakopoulos, M. Tunzi, R. Salenbien, D. Vanhoudt, and S. Svendsen, “Low return temperature from domestic hot-water system based on instantaneous heat exchanger with chemical-based disinfection solution,” *Energy*, vol. 215, p. 119211, Jan. 2021, doi: 10.1016/j.energy.2020.119211.

[72] “https://www.irena.org/publications/2021/Jun/Renewable-Power-Costs-in-2020”.

[73] “https://www.vitalenergi.co.uk/media/kd5fq1v2/queen-s-quay.pdf#:~:text=scheme%20also%20has%20added%20resilience,the%20time%20the%20system%20will”.

[74] “https://iea-retd.org/wp-content/uploads/2014/06/RE-PROSUMERS_IEA-RETD_2014.pdf”.

[75] “https://www.iea.org/reports/net-zero-by-2050”.

[76] “https://www.nature.com/articles/s41598-025-96401-z#:~:text=Poland,with%20PHES%20to%20ensure%20continuous”.

[77] “https://www.energy-transitions.org/bitesize/its-in-the-charts-heat-pump-lifetime-cost-electricity-to-gas/#:~:text=times%20more%20than%20gas”.

[78] “https://www.dwellow.co.uk/blog/solar-panel-payback-period#:~:text=The%20average%20payback%20period%20for,15%20years”.

[79] “https://heatpumpingtechnologies.org/heat-pumping-technologies-magazine-vol-42-no-2-2024-2/topical-article-the-cost-of-co2-emissions-

abatement-in-micro-energy-communities/#:~:text=more%20collective%20approach%20lowers%20the,2%7D%20abated".

[80] L. Verleyen, J. Arroyo, and L. Helsen, "The cost of CO2 emissions abatement in a micro energy community in a Belgian context," *Smart Energy*, vol. 16, p. 100162, Nov. 2024, doi: 10.1016/j.segy.2024.100162.

[81] "IRENA (2022). Renewable Power Generation Costs in 2022. International Renewable Energy Agency.".

[82] "ARERA (2024). Prezzi dell'energia elettrica per clienti domestici in Italia. Autorità di Regolazione per Energia Reti e Ambiente".

[83] "https://www.lazard.com/perspective/lcoeplus".

[84] D. A. Elalfy, E. Gouda, M. F. Kotb, V. Bureš, and B. E. Sedhom, "Comprehensive review of energy storage systems technologies, objectives, challenges, and future trends," *Energy Strategy Reviews*, vol. 54, p. 101482, Jul. 2024, doi: 10.1016/j.esr.2024.101482.

[85] "https://www.euro-inox.org/real-solar-battery-backup-costs-in-europe-2024-price-analysis/#:~:text=Current%20market%20trends%20show%20Tesla,prices%20and%20generous%20government%20incentives".

[86] "https://community.openenergymonitor.org/t/heatpump-payback-calculator-total-cost-of-ownership/27091?page=3".

[87] "https://www.energy-transitions.org/bitesize/its-in-the-charts-heat-pump-lifetime-cost-electricity-to-gas/#:~:text=If%20electricity%20and%20gas%20cost,4%20times%20more%20than%20gas".